Investigation of Nitrogen-Doped Pseudo Graphite as an Oxygen Reduction Reaction Electrocatalyst and Robust Electrochemical Sensor

A Dissertation

Presented in Partial Fulfillment of the Requirements for the

Degree of Doctor of Philosophy

with a

Major in Chemistry

in the

College of Graduate Studies

University of Idaho

by

Kailash Hamal

Approved by

Major Professor: I. Francis Cheng,

Ph.D. Committee Members: Kristopher V. Waynant, Ph.D.; Dean B. Edwards, Ph.D.;

Peter B. Allen, Ph.D.

Department Administrator: Ray von Wandruszka, Ph.D.

December 2021

Abstract

This dissertation discusses the nitrogen modification of GUITAR (Pseudo-Graphite from the University of Idaho Thermalized Asphalt Reaction). Different methods for selectively doping a variety of nitrogen moieties and their characterization are presented in various chapters. Chapter one introduces the material 'GUITAR' and presents the motivation for these works. Chapter two discusses the method for selectively doping pyridinic- and pyrrolic-nitrogen groups (with 0.0 % graphitic nitrogen) onto the GUITAR surface. It is herein referred to as N'-GUITAR. Physical and electrochemical characterization revealed that this material makes the robust electrode for oxygen reduction reaction (ORR) via four-electron pathways, which is desirable for fuel cell applications. The material exhibited high performance and excellent stability than any other carbon materials reported in the literature. Chapter three presents the method for synthesis of N-GUITAR, which comprises predominantly graphitic nitrogen (72.6%). Like N'-GUITAR, this material retains basic characteristic features of GUITAR but demonstrated robustness toward electrode fouling by air aging and polymerization of matrix components during dopamine detection. Application of later form of selectively nitrogen-doped GUITAR (N-GUITAR) for ORR is discussed in chapter four. This material efficiently reduces oxygen to hydrogen peroxide via two-electron pathways. It exhibited higher current efficiency (up to 96%) for H_2O_2 generation with a significant production rate. This experimental result, along with the results from chapter two, suggests that graphitic nitrogen moieties are responsible for two-electron ORR to hydrogen peroxide. In contrast, pyridinic- and pyrrolic- nitrogen moieties are responsible for four-electron ORR to water. The ability to selectively dope different nitrogen moieties is unique to this GUITAR material. This investigation, along with the resistance behavior of the N-GUITAR electrode, is summarized

in chapter five. Chapter five further reveals the possibilities of this material as an excellent electrocatalyst and robust electrochemical sensor for numerous applications.

Acknowledgments

I would like to express my gratitude and sincerity to my supervisor Prof. Dr. I. Francis Cheng, for his regular supervision, guidance, and mentorship throughout my Ph. D. study. I am forever grateful for his help to shape my career and professional life. I would also like to appreciate my graduate committee members Dr. Dean B. Edwards, Dr. Kristopher V. Waynant, and Dr. Peter B. Allen, for their time and comments, which helped shape my research.

I am grateful to the department chair, Dr. Ray von Wandruszka, and the whole Chemistry department faculty and staff who have created a friendly research environment at the University of Idaho in a diverse way.

Many thanks go to my current and former lab mates, especially Jeremy May, Dipak Koirala, Forrest Delbec, and Dr. Hayou Zhu. It was a great experience working together and helping each other.

Dedication

This dissertation is dedicated to my wife, Babita Budhathoki, and my brother Subash Hamal.

Thank you so much for your countless support.

Table of Content

List of Tables

List of Figures

Chapter 1: Introduction

1.1 Introduction of Carbon Materials

Carbon is one of the most abundant elements on earth, and its versatility lies in the diversity of its chemical bonds. Diamond and graphite are two widely known carbon materials that are composed of 100 % sp^3 and sp^2 carbon bonds, respectively. The mixture of sp^2 and sp^3 hybridized carbon atoms forms amorphous carbon. [1] The dangling bond in amorphous carbon sometimes contains hydrogen atoms and becomes hydrogenated amorphous carbon. Based on the relative percent of sp^2-sp^3 content, along with the portion of the hydrogen atoms, the carbon materials can be categorized in according to Figure 1.1, known as a sp^2-sp^3-H ternary phase diagram.[2]

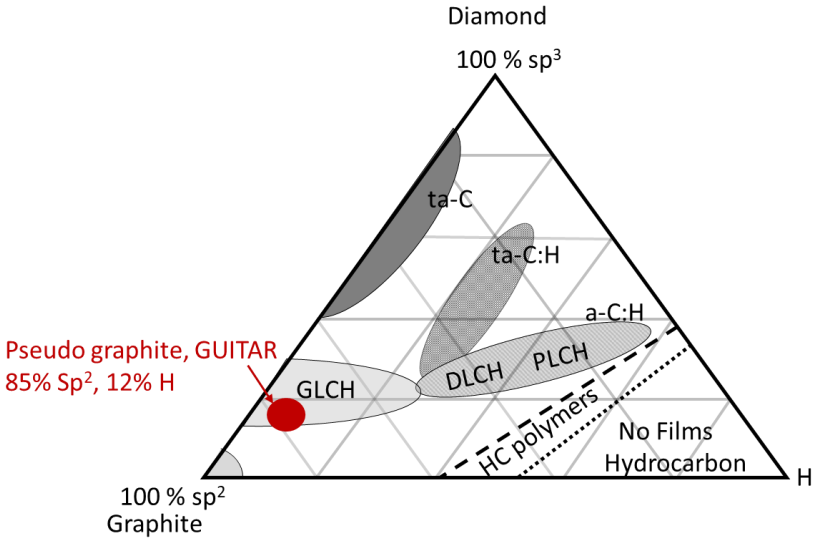

Figure 1.1 sp^2-sp^3-H ternary phase diagram for carbon materials. The red circle shows GUITAR, which contains 85% sp2, 15% sp3, and 12% H by mole. Abbreviation: a-C: H is Hydrogenated Amorphous Carbon, ta-C is Tetrahedral Amorphous Carbon, ta-C:H is Tetrahedral Hydrogenated Amorphous Carbon, GLCH is Graphite like Hydrogenated Amorphous Carbon, DLCH is Diamond-like Hydrogenated Amorphous Carbon, and PLCH is Polymer like Hydrogenated Amorphous Carbon.

The electrode materials most often used in literature are graphitic type carbons (graphene, pyrolytic graphite, carbon nanotubes, and glassy carbon). Pure diamond (100% sp^3) cannot be used as an electrode material due to its high band gap and electrical resistivity. However, the introduction of boron enhances conductivity and electron transfer, making it useful as an electrode and known commonly as boron-doped diamond (BDD).

1.2 Introduction To GUITAR: A Unique Carbon Material from The University of Idaho

GUITAR (pseudo-Graphite from the University of Idaho Thermalized Asphalt Reaction) is a unique thin-film carbon material in literature. GUITAR was discovered in 2010 and characterized in detail in recent publications.[3,4] In general, GUITAR is a nanocrystalline graphite-like hydrogenated amorphous carbon consisting of 88% carbon (85 %/15 % sp^2/sp^3) and 12% H by mole. GUITAR's position in the ternary phase diagram is identified by the red circle in Figure 1.1. GUITAR has a multilayer structure with a d-spacing of 0.350 nm (vs. 0.334 nm for graphite), an average crystallite grain size of 1.5 nm (vs. μm to mm range for CVD grown graphene/graphite), and a Raman I(D)/I(G) ratio of 1.16 (indicating a high density of defects). It is referred to as pseudo graphite as its visual and microscopic appearances are similar to highly oriented pyrolytic graphite (HOPG) (see Figure 1.2) but with divergent electrochemical characteristics. Both possess edge/ basal plane configuration with a layered structure and visually look black, shiny, and metallic (see Figure 1.2 insets). HOPG is well known to have an atomically flat basal plane with characteristic step defects; however, these structural features are missing on GUITAR's basal plane.

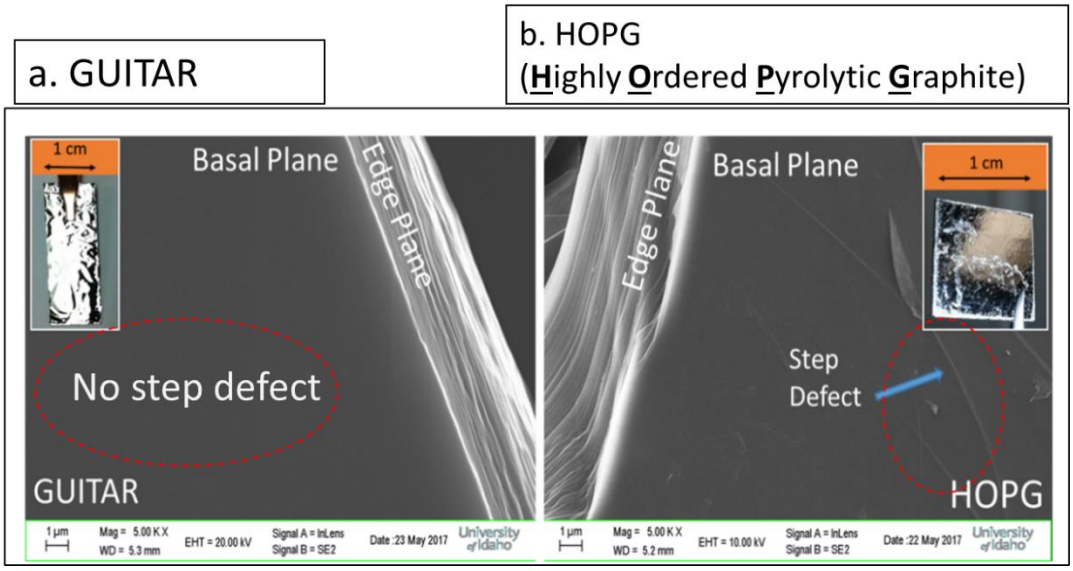

Figure 1.2 SEM micrographs of (A) GUITAR and (B) Highly oriented pyrolytic graphite (HOPG). Both materials have the basal and edge plane configurations with a layered structure, but the characteristic step defects are missing in GUITAR. Insets are photographs of the respective materials.

Despite the superficial similarities between HOPG and GUITAR, there are significant differences in electrochemical properties. These differences include (i) a heterogeneous electron transfer (HET) rate with the $Fe(CN)_6^{4-/3-}$ probe that is equally fast at both the basal and edge planes of GUITAR surface, (ii) resistance to corrosion that equals sp^3 carbon electrodes, and (iii) GUITAR has a high hydrogen overpotential that is 500 mV greater than pure sp^2 C materials.[5] Figure 1.3 summarizes the general trend of the first two characteristics for all carbon electrodes. The literature trend on these indicates that increasing sp^2 content increases the HET rate constant while decreasing corrosion resistance behavior. In this aspect, GUITAR is an outlier in this trend and has the best combination of resistance to corrosion and fast heterogeneous electron transfer of any known carbon material.[4] These properties, and the low cost of the synthesis, lend GUITAR well to electrochemical applications, including energy

conversion (oxygen reduction in fuel cells), energy storage (battery, super capacitor), and electrochemical sensor applications.[6,7,8]

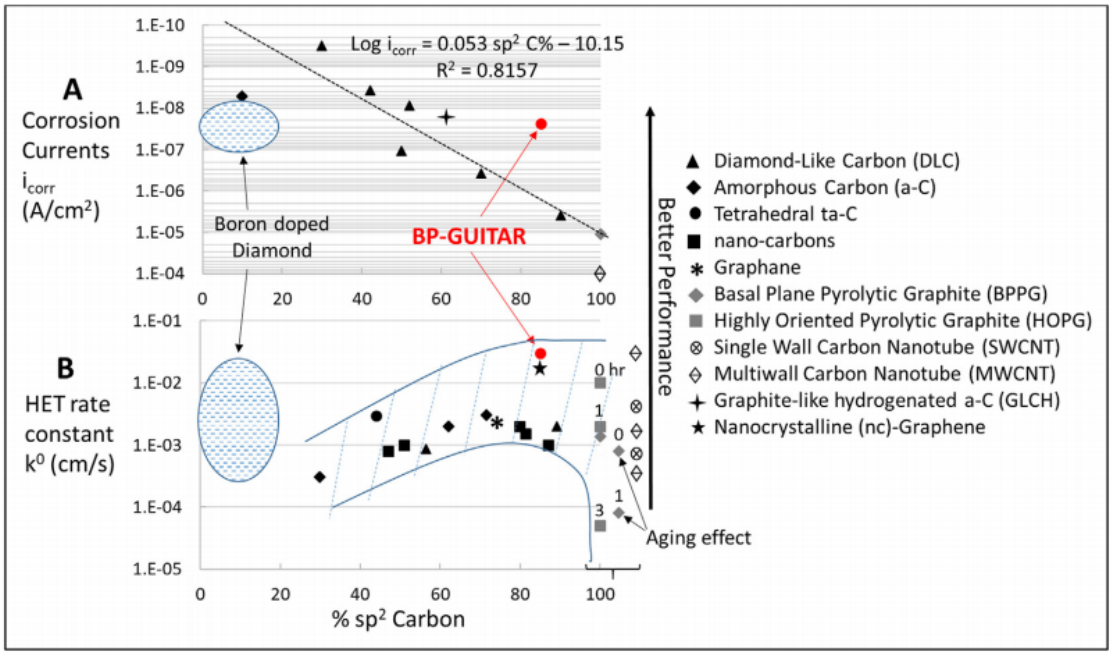

Figure 1.3 (A) Corrosion currents (i_{corr}) vs. sp^2 -C content for carbon electrodes. A linear trend for log (i_{corr}) vs. % sp^2 -C in amorphous carbon is noted. GUITAR is an outlier in that trend. (B) HET rates for $Fe(CN)_6^{3-/4-}$ expressed as k^0 (cm/s). The outlined region is the observed trend for amorphous (with 85% sp^2) and graphitic (100% sp^2) carbons. HOPG and BPPG age over time in air or solution, which eventually lowers the HET rates.

Previous investigations on GUITAR proved that GUITAR has HET rates 2–10 orders of magnitude faster than other carbon materials for a variety of inner- and outer-sphere redox couples.[6,8,9,10] Apart from GUITAR's excellent electrochemical properties, GUITAR electrodes can be grown in a variety of shapes and sizes without the use of metal catalysts (graphene and carbon nanotubes need metal catalysts during CVD synthesis). It is expected that GUITAR's highly defective surface has the viability of modification by nitrogen doping.

1.3 Nitrogen-Doped Carbon Material

Recent advancements in the literature suggest that the functionalization of carbon materials with nitrogen can increase interfacial and electronic properties and improve their use in a wide range

of applications. Such applications include fuel cells, batteries, supercapacitors, electrochemical sensors, and many more.[11] Among possible techniques for carbon modification, nitrogen doping has been extensively studied for the oxygen reduction reaction.[11] Doping nitrogen (electronegativity of nitrogen is 3.06 vs. 2.55 for carbon) atoms in the carbon matrix cause charge polarization in the C-N bond, facilitating the adsorption of oxygen and hence in reduction.[12,13] Nitrogen-doped vertically aligned CNT showed the change in chemisorption of oxygen from the usual end-on adsorption (Pauling model) to side-on adsorption (Yeager model), which effectively weakens the O-O bond and thus enhance the ORR process.[14] A similar effect has been observed in nitrogen-doped graphene. It has been demonstrated that the introduction of N-atoms into the matrix of an sp^2 bonded graphitic framework can lead to three different N-moieties (i) pyridinic-N, (ii) pyrrolic-N, and (iii) graphitic-N (or quaternary-N) as shown in Figure 1.4.[15] The pyridinic and pyrrolic N species are edge plane functionalities and coordinated with two adjacent carbon atoms, whereas graphitic N species are coordinated with three adjacent carbon atoms. Determining the exact role of each nitrogen species is challenging due to the difficulties of achieving a selectively doped material with purely pyridinic, pyrrolic, or graphitic nitrogen. However, most of the trends in the literature where this has been achieved (combined with this work) indicates that graphitic N is responsible for ORR through the 2 electron mechanism while pyridinic and pyrrolic N is responsible for the 4 electron mechanism.[14]

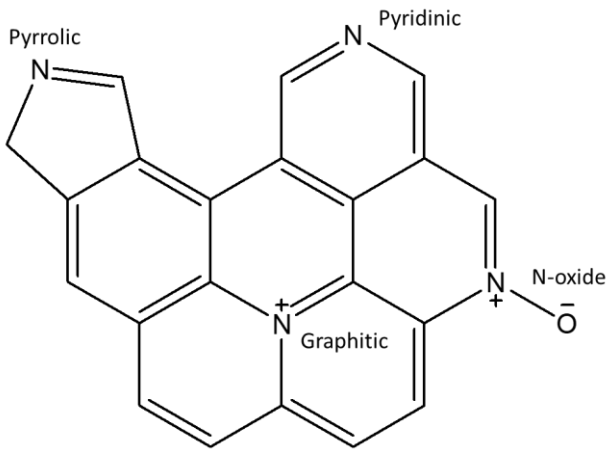

Figure 1.4 Possible N-moieties on the nitrogen-doped carbon surface.

In this dissertation, two different forms of nitrogen-doped GUITAR are synthesized and tested for the oxygen reduction reaction. The emphasis is placed towards selective nitrogen doping and their role in ORR ($4e^-$ vs. $2e^-$).

1.4 References

(1) Muzyka, K.; Sun, J.; Fereja, T. H.; Lan, Y.; Zhang, W.; Xu, G. Boron-Doped Diamond: Current Progress and Challenges in View of Electroanalytical Applications. *Anal. Methods* **2019**, *11* (4), 397–414. https://doi.org/10.1039/C8AY02197J.

(2) Casiraghi, C.; Ferrari, A. C.; Robertson, J. Raman Spectroscopy of Hydrogenated Amorphous Carbons. *Phys. Rev. B* **2005**, *72* (8), 085401. https://doi.org/10.1103/PhysRevB.72.085401.

(3) Cheng, I. F.; Xie, Y.; Allen Gonzales, R.; Brejna, P. R.; Sundararajan, J. P.; Fouetio Kengne, B. A.; Eric Aston, D.; McIlroy, D. N.; Foutch, J. D.; Griffiths, P. R. Synthesis of Graphene Paper from Pyrolyzed Asphalt. *Carbon* **2011**, *49* (8), 2852–2861. https://doi.org/10.1016/j.carbon.2011.03.020.

(4) Kabir, H.; Zhu, H.; May, J.; Hamal, K.; Kan, Y.; Williams, T.; Echeverria, E.; McIlroy, D. N.; Estrada, D.; Davis, P. H.; Pandhi, T.; Yocham, K.; Higginbotham, K.; Clearfield, A.; Cheng, I. F. The Sp2-Sp3 Carbon Hybridization Content of Nanocrystalline Graphite from Pyrolyzed Vegetable Oil, Comparison of Electrochemistry and Physical Properties with Other Carbon Forms and Allotropes. *Carbon* **2019**, *144*, 831–840. https://doi.org/10.1016/j.carbon.2018.12.058.

(5) Gyan, I. O.; Wojcik, P. M.; Aston, D. E.; McIlroy, D. N.; Cheng, I. F. A Study of the Electrochemical Properties of a New Graphitic Material: GUITAR. *ChemElectroChem* **2015**, *2* (5), 700–706. https://doi.org/10.1002/celc.201402433.

(6) Kabir, H.; Gyan, I. O.; Foutch, J. D.; Zhu, H.; Cheng, I. F. Application of GUITAR on the Negative Electrode of the Vanadium Redox Flow Battery: Improved V3+/2+ Heterogeneous Electron Transfer with Reduced Hydrogen Gassing. *C* **2016**, *2* (2), 13. https://doi.org/10.3390/c2020013.

(7) Francis Cheng, I.; Xie, Y.; Owusu Gyan, I.; W. Nicholas, N. Highest Measured Anodic Stability in Aqueous Solutions: Graphenic Electrodes from the Thermolyzed Asphalt Reaction. *RSC Advances* **2013**, *3* (7), 2379–2384. https://doi.org/10.1039/C2RA23103D.

(8) Gyan, I. O.; Cheng, I. F. Electrochemical Study of Biologically Relevant Molecules at Electrodes Constructed from GUITAR, a New Carbon Allotrope. *Microchemical Journal* **2015**, *122*, 39–44. https://doi.org/10.1016/j.microc.2015.04.002.

(9) Kabir, H.; Ma, P. Y.; Renn, N.; Nicholas, N. W.; Cheng, I. F. Electrochemical Determination of Free Chlorine on Pseudo-Graphite Electrode. *Talanta* **2019**, *205*, 120101. https://doi.org/10.1016/j.talanta.2019.06.101.

(10) Kabir, H.; Zhu, H.; Lopez, R.; Nicholas, N. W.; McIlroy, D. N.; Echeverria, E.; May, J.; Cheng, I. F. Electrochemical Determination of Chemical Oxygen Demand on Functionalized Pseudo-Graphite Electrode. *Journal of Electroanalytical Chemistry* **2019**, *851*, 113448. https://doi.org/10.1016/j.jelechem.2019.113448.

(11) Wood, K. N.; O'Hayre, R.; Pylypenko, S. Recent Progress on Nitrogen/Carbon Structures Designed for Use in Energy and Sustainability Applications. *Energy Environ. Sci.* **2014**, *7* (4), 1212–1249. https://doi.org/10.1039/C3EE44078H.

(12) Ma, R.; Lin, G.; Zhou, Y.; Liu, Q.; Zhang, T.; Shan, G.; Yang, M.; Wang, J. A Review of Oxygen Reduction Mechanisms for Metal-Free Carbon-Based Electrocatalysts. *npj Comput Mater* **2019**, *5* (1), 1–15. https://doi.org/10.1038/s41524-019-0210-3.

(13) Nitrogen-modified carbon-based catalysts for oxygen reduction reaction in polymer electrolyte membrane fuel cells - ScienceDirect https://www.sciencedirect.com/science/article/abs/pii/S0378775308022325 (accessed 2021 -10 -13).

(14) Nitrogen-Doped Carbon Nanotube Arrays with High Electrocatalytic Activity for Oxygen Reduction https://www.science.org/doi/full/10.1126/science.1168049 (accessed 2021 -10 -13).

(15) Wang, H.; Maiyalagan, T.; Wang, X. Review on Recent Progress in Nitrogen-Doped Graphene: Synthesis, Characterization, and Its Potential Applications. *ACS Catal.* **2012**, *2* (5), 781–794. https://doi.org/10.1021/cs200652y.

Chapter 2: "A Highly Stable, Low-Cost Metal-Free Oxygen Reduction Reaction Electrocatalyst Based on Nitrogen-Doped Pseudo-Graphite." *Energy & Fuels*, 2021, 35 (12), 10146–10155.

2.1 Abstract

There have been many advancements in the search for an oxygen reduction reaction (ORR) catalyst that exhibits strong performance and exceptional durability using low-cost materials. Although recent advancements have focused on matching or surpassing the ORR performance of Pt/C, exploring ways to improve the durability of electrocatalysts on longer time scales has not been adequately addressed. In this work, a high-performing and stable ORR electrocatalyst was produced using a simple nitrogen-doping protocol on GUITAR (pseudo-Graphite from the University of Idaho Thermolyzed Asphalt Reaction)-coated Ketjen black (N´-GUITAR/KB). X-ray photoelectron spectroscopy indicates selective doping of pyridinic and pyrrolic moieties (total N abundance of 0.9%). Voltammetric experiments in O_2-saturated 0.1 M KOH indicate that the electrocatalyst is exceptionally stable and one of the highest performers regarding overvoltage and current density. The system maintained its electrocatalytic performance throughout the Department of Energy (DOE) stress protocol, which consists of 30,000 convective Cyclic voltammetry cycles in O_2-saturated 0.1 M KOH. This remarkable stability, along with the low-cost synthesis, represents an important milestone in overcoming the challenges that prevent the wide-scale adoption of fuel cell technology.

Keywords: Electrocatalysis, Fuel Cells, N-doping, Selective doping, Oxygen Reduction Reaction, Pseudo-graphite

2.2 Introduction

The material, GUITAR (pseudo-Graphite from the University of Idaho Thermalized Asphalt Reaction), was discovered in 2010 and characterized in detail in recent publications.[1–5] It is a graphite-like hydrogenated amorphous carbon (GLCH) in Stage 2 of the Ferrari amorphization trajectory.[1,6] Specifically, it consists of 85%/15% sp^2/sp^3 hybridized carbon, with a d-spacing of 0.350 nm and a crystallite grain size of 1.5 nm.[1] A computational study of amorphous carbon with this same composition predicted a graphite-like layered structure with interconnected molecular planes.[7] These are features observed with GUITAR.[1] It is pseudo-graphitic, having similar visual and microscopic appearances with graphite but with diverging electrochemical characteristics. These differences include electron transfer with the $Fe(CN)_6^{4-/3-}$ probe that is equally fast at both the basal and edge planes, the resistance to corrosion that equals sp^3 carbon electrodes, and a hydrogen overpotential that is 0.5 V greater than other pure sp^2 C materials.[1,4] It has the best combination of resistance to corrosion and fast heterogeneous electron transfer (HET) of any electrode material.[1] These properties lend themselves well to electrochemical energy applications, including fuel cells.[8]

While fuel cells function at high rates of efficiencies, their wide-scale adoption is tempered by several barriers, notably the sluggishness of the oxygen reduction reaction (ORR) at the cathode.[9–11] The ORR kinetics are fastest in alkaline media where the following half-reactions are relevant.[11,12]

$$O_2 + 2H_2O + 4e^- \rightarrow 4OH^- \qquad E^0 = 0.401 \text{ V vs SHE} \qquad (1)$$

$$O_2 + H_2O + 2e^- \rightarrow HO_2^- + OH^- \qquad E^0 = -0.076 \text{ V vs SHE} \qquad (2)$$

$$HO_2^- + H_2O + 2e^- \rightarrow 3OH^- \qquad E^0 = 0.878 \text{ V vs SHE} \qquad (3)$$

The $4e^-$ mechanism (Reaction 1) is preferred as it maximizes fuel cell voltage without creating corrosive byproducts. The $2e^-$ reduction (Reaction 2) is less energy efficient and produces corrosive hydroperoxides.[11,13] Reaction 3 is the $2e^-$ consumption of the hydroperoxide ion to water.

Commercial ORR catalysts consist of nano-Pt on carbon black (Pt/C), which has drawbacks of high costs and poor stability, experiencing a ~ 10% loss in current after 10 hours.[14–19] This loss is attributed to aggregation or loss of Pt and corrosion of the carbon substrate.[20–22] Recent efforts have examined non-precious metals-based as well as a variety of metal-free N-doped carbon materials, which have a competitive ORR performance with lower costs. However, all experience performance losses under various stress regimens.[14–19,23–25] For this contribution, a nitrogen-doped form of GUITAR (N´-GUITAR) was examined for ORR electrocatalysis and durability. It is expected that GUITAR's resistance to corrosion and fast HET rates will give stable ORR electrocatalysis. This investigation was based on the guidelines offered by the U.S. Department of Energy and a recent editorial on the best practices for reporting the electrocatalytic performance of nanomaterials.[26,27] A previous study of another form of N-doped GUITAR (N-GUITAR) indicated a predominance of graphitic nitrogen groups.[28] This differs from the material of this study (N'-GUITAR) which produced pyrrolic and pyridinic groups with an absence of graphitic N.

2.3 Experimental

2.3.1 Chemicals.

The electrode components consisting, 20% Pt on Vulcan CX 72 carbon black (Fuel Cell Store, Texas, USA) and KFD graphite felt (SLG Carbon Company, St. Marys, PA, USA) were used as received. Ketjen black was obtained from eBay and ball milled for 24 hours before use. The reagents in this investigation were compressed N_2(g) and O_2(g) (>99.5 %, Oxarc, WA, USA), soybean oil (Walmart), clear silicone sealant (Momentive Performance Materials Inc. Huntersville, NC), 1,3,5-triazine-2,4,6-triamine or melamine (99%, Sigma-Aldrich, USA), 5% Nafion perfluorinated resin solution (Sigma-Aldrich, USA), KOH (97%, EMD Chemicals, USA) and ethanol (99.5%, Pharmaco, CT, USA) were used without further purification. House deionized water was further purified through an activated carbon cartridge (Barnstead, model D8922, Dubuque, IA) and was used to prepare solutions. Silica gel sorbent (35-70 mesh, Fisher Scientific) was used for BET analysis.

2.3.2 Synthesis of nitrogen-doped GUITAR on Ketjen black (N´-GUITAR/KB).

As received Ketjen black (KB) was ball milled for 24 hours, and the GUITAR coating (GUITAR/KB) was done following a previously reported chemical vapor deposition method.[1] The Ketjen black was treated with a 15-minute GUITAR deposition using a soybean oil precursor under nitrogen flow at 900ºC. Afterwards, the coated particles were dried at 125 ºC for 24 hours. Nitrogen doping proceeded by mixing the GUITAR/KB particles with melamine in a 1:10 mass ratio and placing in a tube furnace under N_2 flow (1.4 L min^{-1}). The temperature was increased at a rate of 10°C min^{-1} from room temperature to 800°C, where it was annealed for 1 hour.[29] The resulting N´-GUITAR/KB particles were cooled to room temperature under

N_2 atmosphere. Nitrogen-doped Ketjen black (N´-KB) was also synthesized as a control using the same process.

2.3.3 Physical Characterization.

The XPS (x-ray photoelectron spectroscopy) apparatus was built in-house at Oklahoma State University. Spectra were recorded and performed in a vacuum chamber with a base pressure of 1×10^{-9} torr, with the Al Kα emission line (1486.6 eV) and a hemispherical energy analyzer with a resolution of 0.025 eV at room temperature. Deconvolved C1s and N1s XPS peaks were fitted to Gaussian curves with Shirley background subtraction and with the full width at half maximum kept constant. Brunauer–Emmett–Teller (BET) surface area measurements of the samples were conducted using a Micrometrics, Flowsorb II 2300. Two runs on standard silica gel sorbent were carried out before analyzing N´-GUITAR/KB and KB. Measured values for standard silica gel were 536 ± 13 m^2 g^{-1} (vs. 512 m^2 g^{-1} as reported by the manufacturer). Scanning electron microscope (SEM) images were obtained with a Zeiss Supra 35 SEM (Carl Zeiss, Germany). The electrochemically active surface area (ECSA) of N´-GUITAR/KB was determined by measuring the non-faradaic current density between the scan rates of 0.005 and 0.3 V s^{-1} in 0.1 M KOH. The ECSA was calculated by dividing the double-layer capacitance (C_{dl}) of particles electrode with that of flat GUITAR ($C_{dl,\ flat}$) $\left(ECSA = \frac{C_{dl,}}{C_{dl,flat}}\right)$. [27] The GUITAR coated quartz slides (flat GUITAR) were sealed using a clear silicone sealant, leaving an exposed area of 0.1–0.2 cm^2 (as described in a previous publication).[1] Raman spectra were taken with a 532 nm laser.

2.3.4 Electrochemical Analysis.

The ORR electrode was prepared by a drop cast method. The catalyst ink solution consisted of 450 µL of deionized water, 450 µL of ethanol, 100 µL of 5 wt.% Nafion solution, and 10 mg of N´-GUITAR/KB particles. A 7.5 µL aliquot of the catalyst ink was carefully deposited on a micro-polished glassy carbon surface, then dried at room temperature for 2 hours prior to use. The particle loading for N´-GUITAR/KB, GUITAR/KB, KB, and N´-KB in the Nafion films was 1.0 mg per cm^2 of geometric surface area. Figure S2.1 shows the performance of other loading levels for N´-GUITAR/KB that ranged from 0.6 to 2.0 mg/cm^2. The control Pt/C (20%) films in this study had 0.2 mg cm^{-2}, a typical loading in literature.[16,24,30] All electrochemical experiments were performed in an undivided three-electrode cell, with a Ag/AgCl (3 M KCl, aq) reference electrode, a 15 cm x 10 cm KFD graphite felt counter electrode in 0.1 M KOH using a Bioanalytical Systems CV-50W Potentiostat (West Lafayette, IN, USA). Electrode potential conversions to the reversible hydrogen electrode (RHE) were done using the Nernst relationship, $E_{RHE} = E_{Ag/AgCl} + 0.977$ at pH 13.[31] Cyclic stability tests were carried out using a Gamry instruments interface 1000 Potentiostat and a Pine Instruments glassy carbon rotating disk electrode (RDE) (Grove City, PA, USA). The cyclic stability test was carried out based on the DOE test protocol, which includes a 30,000 cycle test between +0.025V and -0.375V vs. Ag/AgCl at 0.05 V s^{-1}at 800 rpm in O_2 saturated 0.1 M KOH.[26] The cycling was paused after every 5,000 cycles, during which a CV at quiescent conditions and RDE LSV at 1600 rpm were recorded to measure any performance losses. Oxygen or nitrogen gases were purged through the 0.1 M KOH solution for an hour to produce saturated solutions prior to testing.

2.4 Results and Discussion.

2.4.1 X-ray Photoelectron Spectroscopy.

The extent of N-doping in the N'-GUITAR/KB particles was examined by X-ray photoelectron spectroscopy (XPS). Results are shown in Figure 2.1. The wide-scan spectrum in s 2.1A and D and high-resolution XPS spectra of the N1s peak in Figures 2.1C and F indicate that the control GUITAR/KB particles lack the N1s peak observed in the N´-GUITAR/KB particles. Based on peak areas, the relative atomic percentages for C (C1s, 284.1eV) and O (O1s, 532.4 eV) in GUITAR/KB are 94.7% and 5.3%, respectively. With N´-GUITAR/KB, the C, O, and N (N1s, 398.2 eV) abundances are 97.0%, 2.1%, and 0.9%, respectively. The deconvolved C1s peaks of N´-GUITAR/KB and GUITAR/KB are shown in Figure 2.1B and Figure 2.1E, respectively. The peak assignments and relative abundances are labeled in that diagram and are based on recent XPS literature.[32–37] The peaks at 288.7 eV and 290.6 eV in Figure 2.1E are assigned to C-O and C=O, respectively. Slight increases in those peaks on N´-GUITAR/KB in Figure 2.1B can be attributed to C=N and C-N from the doping process.[38] The sp^2/sp^3 (85%/15%) ratio in Figure 1B & E is in agreement with a previous study on GUITAR.[1] Figure 2.1A shows an N abundance of 0.9% in N´-GUITAR/KB. In the literature, N-doped carbon materials typically range from 1.2 to 11.3 atomic %.[16,19,23,24,30,38–42] The N´-GUITAR/KB XPS indicates the presence of pyridinic (398.2 eV), pyrrolic (400.4 eV) and N-oxides (404.3 eV) (see Figure 2.1C), however graphitic nitrogen (401.5 eV) is notably absent. It is unusual to find such selectively nitrogen-doped carbon materials in literature. The XPS analysis on KB and N´-KB samples show that N´-KB contains 0.6 atomic % of nitrogen (Figure S2.8), compared to the 0.9% abundance in N´-GUITAR/KB (Figure 2.1A). N´-KB also contains 17.2 % graphitic nitrogen (Figure S2.2), whereas N´-GUITAR/KB contains none. A previous study using an alternative method for nitrogen doping gave a predominance of graphitic nitrogens.[28]

Only two other N-doped carbon materials were located in the literature that also lacks quaternary (graphitic) N.[41,42]

A Raman study of N´-GUITAR/KB gave a D and G band position of 1349 and 1585 cm^{-1}, respectively, with a I(D)/I(G) ratio of 1.14. These are essentially unchanged compared with undoped GUITAR. This behavior has been observed with other N-doped carbon materials with undoped starting materials.[43]

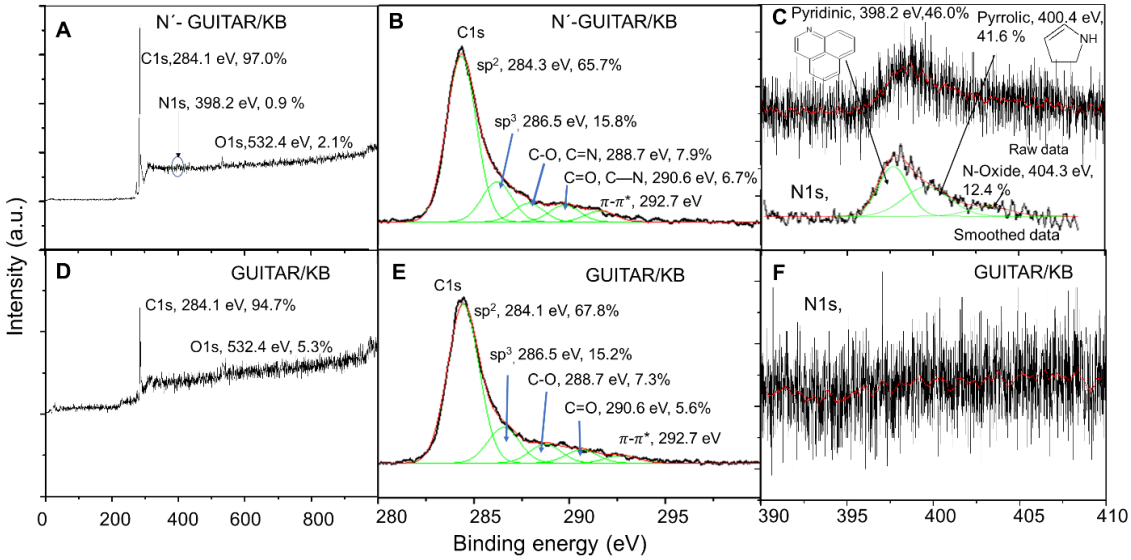

Figure 2.1. (A) Wide-scan XPS spectra of N´-GUITAR/KB. The C1s, N1s, and O1s peaks are labeled. (B) High-resolution XPS spectra of the C1s peak of N´-GUITAR/KB with deconvolved functional group peaks. (C) High-resolution XPS spectra of N1s peak of N´-GUITAR/KB indicating pyridinic (398.2 eV), pyrrolic (400.4 eV), and N-oxide (404.3 eV) peaks. (D) Wide-scan XPS spectra of GUITAR/KB. (E) High-resolution XPS spectra of the C1s peak of GUITAR/KB and (F) High-resolution XPS spectra indicating the lack of N1s peak (398.2 eV) of GUITAR/KB. Deconvolution was carried out after data smoothing using the Savitzky-Golay method.

2.4.2 Surface Area Analyses Measurements.

Coating KB with N´-GUITAR increases the average particle diameter from 30 ± 10 nm (n = 25) to 61 ± 17 nm (n = 25), as shown in the SEM images of Figure 2.2. These measurements were conducted with ImageJ software.

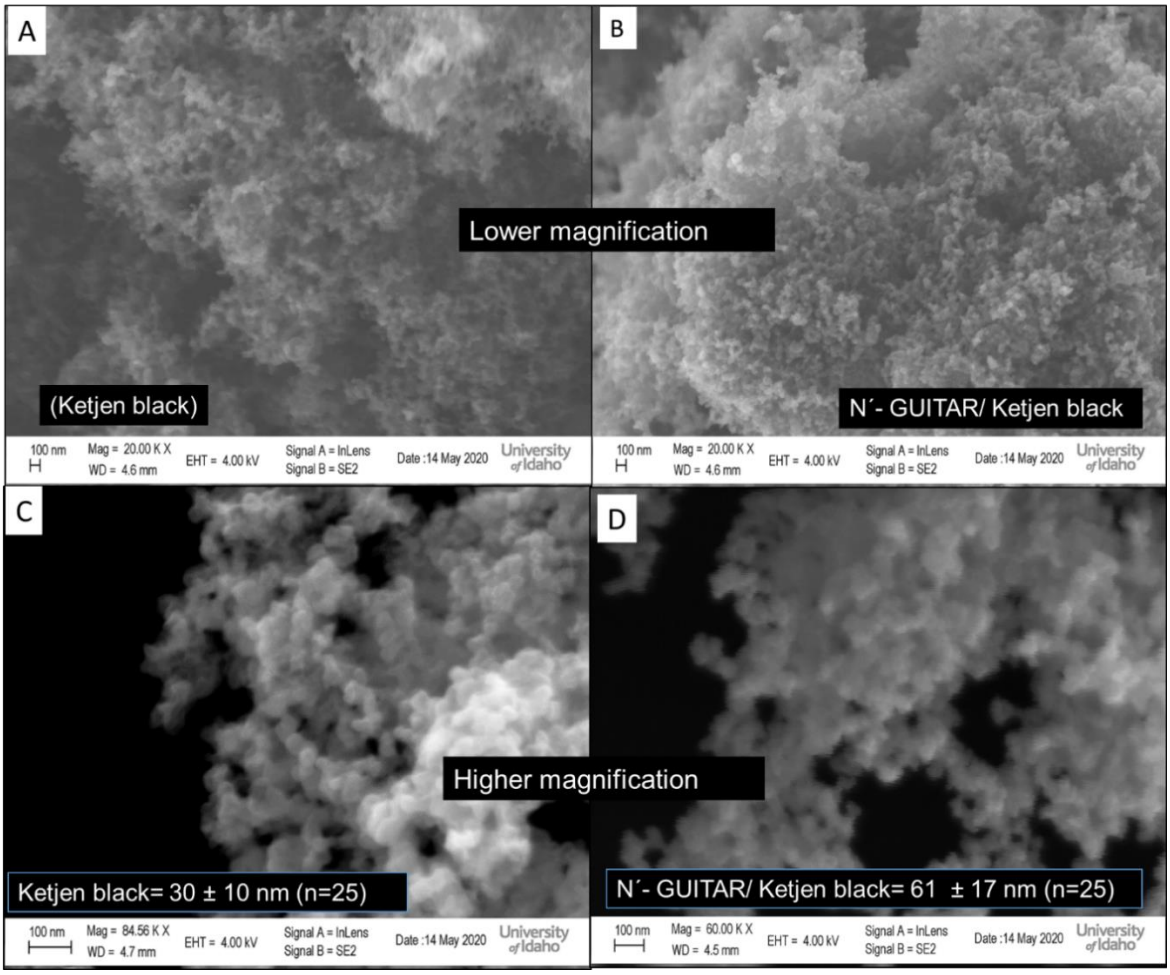

Figure 2.2. SEM micrographs of Ketjen black (A) and (C), diameter (d) = 30 nm with a standard deviation (s) = 10 nm over 25 samples (n = 25) and, (B) and (D) N´-GUITAR/KB, d = 61 ± 17 nm (n = 25).

Surface area measurements of the particles were estimated by Brunauer, Emmett, and Teller (BET) analysis and for the electrochemically active surface area (ECSA) by cyclic

voltammetry (CV) as discussed in the Supplementary information (SI) Figure S2.3 and S2.4. A recent editorial for reporting electrocatalytic performance recommends normalizing with ECSA rather than the BET area, as the latter may include areas that are not-entirely utilized.[27] The data are summarized in Table 1. The reduction in BET surface area from KB to N´-GUITAR/KB indicates that the GUITAR coating fills in the pores of the substrate.[8] The N´-GUITAR/KB surface area lies within the range of literature ORR electrocatalysts.[16,17,23,24,38,44–47] For the N-doped electrocatalyst, the ECSA is based on non-faradaic capacitive current in 0.1 M KOH. This was measured with CV at 0.005-0.3 V $s^{-1,}$ with capacitive current measured at 0.1 V vs. Ag/AgCl.[27] For the Pt/C electrocatalyst, the ECSA measured by hydrogen desorption methods is described in the SI (Figure S10).[26,48,49] The ratio of ECSA/BET area is 25% for N´-GUITAR/KB and 31% for Pt/C. For the latter, this is similar to what is observed in the literature (~20%).[48] In both cases, this is probably caused by the limited access of the aqueous electrolyte in the nanopores of the composite electrocatalyst.

Table. 2-1. BET and electrochemically active (ECSA) surface areas of materials used in this study.

Material	BET ($m^2 g^{-1}$)	ECSA ($m^2 g^-$	References
Ketjen Black (KB)	1230	N/A	This Work
N´-GUITAR/KB	340	84.7	
Pt/C	180* given by vendor	57.9	
Literature	101-3092	N/A	16,17,23,24,38,44–47

2.4.3 Electrocatalyst Performance.

2.4.3.1 Cyclic Voltammetric Experiments.

Figure 2.3A shows the CVs at 0.05 V s^{-1} in 0.1 M KOH under O_2 and N_2 saturated conditions for N´-GUITAR/KB and GUITAR/KB. The importance of N-doping of GUITAR for the ORR is evident in the comparison of the CVs of this electrocatalyst with the controls consisting of GUITAR/KB, N-doped KB, and KB. The CV, peak current density (j_p), and peak potential (E_p) of these materials are compared in Table 2. Among all catalysts in this study, N´-GUITAR/KB has the highest current density at the lowest overpotential.

Table 2-2. ORR performance as evaluated from cyclic voltammetry at 0.05 V s^{-1} under O_2 purged 0.1 M KOH. ORR CV for GUITAR/KB and N´-GUITAR/KB are in Figure 2.3A. ORR CV for KB and N´-KB are in Figure S2.5.

Catalyst	Current density at -0.2 V (mA cm^{-2})	CV Ep for ORR (V)	Background subtracted j_p at E_p (mA cm^{-2})
N´-GUITAR/KB	3.9	-0.270	6.2
GUITAR-KB	0.4	-0.303	3.0
Ketjen black (KB)	0.2	-0.295	2.5
N´-KB	0.6	-0.335	3.8

The two reduction peaks observed for GUITAR/KB at -0.3V and -0.81 V are consistent with the 2-step 2e^- reduction of O_2 with HO_2^- as the intermediate (Equations 2 and 3). This is typical for undoped carbon electrodes.[16,29,41,50,51] The single peak of N´-GUITAR/KB is consistent with a 4e^- reduction directly to water (Equation 1). The N´-GUITAR/KB ORR electrocatalyst demonstrates the best performance based on current density, and only Pt/C has

a lower overpotential of the electrodes tested in this study (Figure 2.3C). The Pt/C electrocatalyst before the cycling stress test (dashed line) has an E_p of -0.14 V and j_p of 2.1 mA cm^{-2}. This value lies within the literature range of -0.12 to -0.15 V and 1.1 to 2.30 mA cm^{-2}, respectively.[52,53]

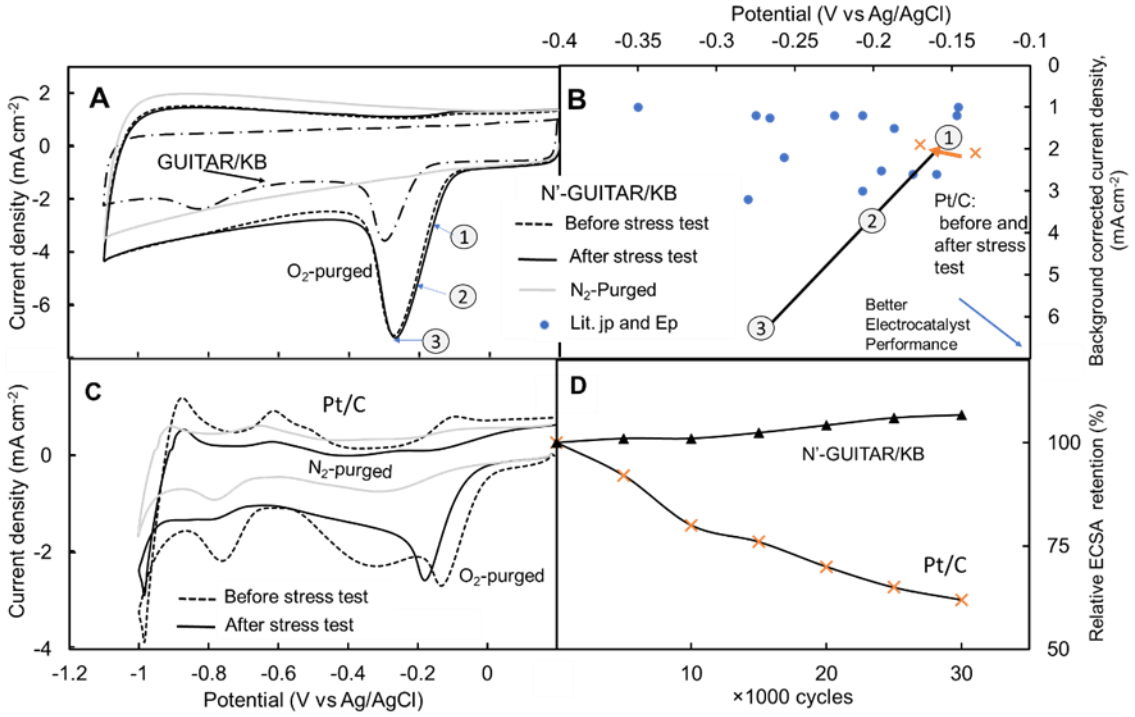

Figure 2.3. (A) ORR cyclic voltammogram for N´-GUITAR/KB and GUITAR/KB. (B) Comparison of ORR peak potentials and background subtracted current densities with literature (values are listed in Table S2.1).[16,18,23,24,30,38,45,47,54–59] The Pt/C before and after the DOE-based stress test are shown (X). (C) ORR cyclic voltammograms at 0.05 V s^{-1} for Pt/C before (dashed) and after (solid) the DOE stress test. (D) Electrochemical active surface area (ECSA) retention during the DOE stress test. The experimental conditions for all CVs in this figure are taken from the literature (unless otherwise labeled) are at 0.05 V s^{-1} in O_2 saturated 0.1 M KOH.

The N´-GUITAR/KB j_p of 6.2 mA cm^{-2} (geometric area) is the highest reported in the literature. These range from 1–3 mA cm^{-2} at the potential sweep rate of 0.05 V s^{-1} in 0.1M KOH.[16,18,23,24,30,38,45,47,54–59] However, the E_p for N´-GUITAR/KB is more negative relative to

these studies and Pt/C results.[23,24,30,38,54] For comparison with literature, Figure 2.3B plots the CV current densities of N´-GUITAR/KB at -0.15, -0.20, and at its E_p of -0.27 V vs Ag/AgCl (labeled as points 1-3, respectively). At point 2 of Figure 2.3A, the CV current density of N´-GUITAR/KB at -0.2 V is 3.9 mA cm^{-2}. This would be at the top end of typical ORR CV performances for recent ORR electrodes if considering their respective E_p and j_p. Despite having a relatively low nitrogen content, the N´-GUITAR/KB ORR electrocatalyst is one of the top performers compared to other modified carbon materials. This adds to the evidence that pyridinic and pyrrolic groups enhance ORR kinetics.[19] This selective doping may be due to the relatively high degree of disorder within the lattice of GUITAR, which minimizes graphitic N.[1–5,8]

2.4.3.2 Rotating Disk Electrode Experiments.

Rotating disk electrode voltammetry (RDE) further confirmed the exceptional performance of the ORR electrocatalyst. Figure 2.4A shows the RDE-linear sweep voltammograms (LSV) at 0.005 V s^{-1} at 1600 rpm in 0.1M KOH. The RDE-LSV obtained before the stress tests are in the dashed lines. As with the CV j_p's, the limiting current density (j_{lim}) of N´-GUITAR/KB achieves a higher current density than Pt/C, however, at a more negative (less favorable) half-wave potential ($E_{1/2}$). The $E_{1/2}$ values for Pt/C and N´-GUITAR/KB are 0.103 and 0.053 V vs SHE, respectively. Figure 2.4B highlights this comparison with N´-GUITAR/KB (black triangle) with Pt/C (brown X). The combination of more positive $E_{1/2}$ and higher j_{lim} gives a better overall performance. Using this consideration, the literature values for other electrocatalyst systems are represented in Figure 2.4B. The carbon-based electrocatalysts are in triangle and the metal-based systems in squares.[14,24,54,56,60–73] N´-GUITAR/KB (black triangle) is highly competitive in these considerations especially with Pt/C (X). The $E_{1/2}$ of

N´-GUITAR/KB is only 0.05 V negative of Pt/C, but with a higher limiting current density of 6.3 mA cm^{-2} vs., 5.3 mA cm^{-2} at -0.6 V. A Tafel study conducted at 1600 rpm for the N´-GUITAR/KB and Pt/C gave slopes of 0.098 V dec^{-1} and 0.110 V dec^{-1}, respectively in the potential region above -0.15 V (Figure S2.6). The slopes indicate that the two electrocatalysts have similar electrode kinetics values in this potential region.

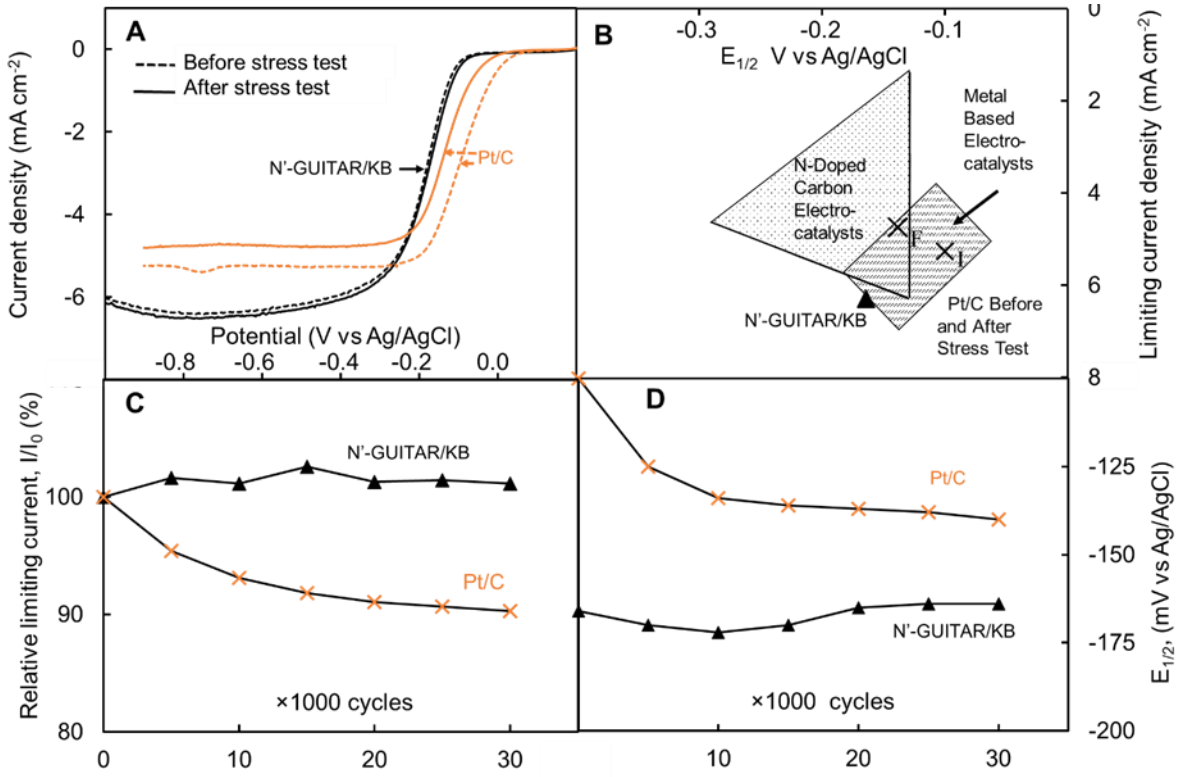

Figure 2.4. (A) Linear sweep voltammogram (RDE-LSV) recorded at 0.005 V s^{-1} at 1600 rpm in O_2 saturated 0.1M KOH with N´-GUITAR/KB in black and Pt/C in orange lines. The voltammograms obtained before the DOE stress tests are dashed (---). (B) Comparison of half-wave potential ($E_{1/2}$) and limiting current densities of ORR catalysts of this study with literature, see Table S2.2 for tabulation.[14,24,54,56,60–73] (C) Plots of relative limiting currents for N´-GUITAR/KB and Pt/C during the DOE stress test. (D) Plots of $E_{1/2}$ shifts during stress test for N´-GUITAR/KB and Pt/C.

2.4.4 Electrocatalyst Durability.

The durability of the ORR electrocatalyst was examined by CV methods as recommended by the Department of Energy (DOE) and a recent commentary.[26,27] The DOE test protocol for ORR catalysts specifies 30,000 CV scans at 0.05 V s^{-1} under convection between +0.025 V and -0.375 V vs Ag/AgCl. In this study, the N´-GUITAR/KB and commercial Pt/C electrocatalyst Nafion films were drop cast on an RDE and stressed by cycling using the DOE protocol in 0.1 M KOH under continuous O_2 purging and 800 rpm.

The stability of the electrocatalysts was assessed by pausing the stress test every 5,000 cycles and conducting an RDE-LSV and a CV under quiescent conditions. The N´-GUITAR electrocatalyst remained stable under both voltammetric assessments. In Figure 2.4C and 4D**,** the RDE voltammetric analyses show no shift in $E_{1/2}$ or j_{lim} for N-doped material, whereas Pt/C experienced a 9% loss in j_{lim} (5.3 to 4.8 mA cm^{-2}) and 0.038 V cathodic shift in $E_{1/2}$ (-0.100 V to -0.138 V). The overall loss in performance for Pt/C of this study is typical for literature.[41,46,55,74,75]

The CVs (Figure 2.3A and C) obtained during the pauses are able to estimate losses in ECSA along with E_p and j_p**.** The nitrogen-doped material exhibits complete stability as the CVs are identical before and after the stress tests. Evidence for the performance degradation of the Pt/C electrocatalysts is with the shifts of initial E_p and j_p of -0.140 V and 2.1 mA $cm^{-2,}$ respectively, to -0.170 V and 1.9 mA cm^{-2} after 30,000 CV cycles in Figure 2.3C. Figure 2.3D highlights the changes in ECSA during CV stressing. The commercial Pt/C electrocatalyst experienced losses of 38% of the ECSA (35.8 vs. 57.9 m^2 g^{-1}) at the end of cycling; this is typical of what is observed in the literature.[41,75] The N´-GUITAR/KB catalyst maintains and slightly increases by 3% its ECSA throughout the stress test as estimated from capacitive

currents. This increase is not understood but might arise from increases from surface activation from continued use. [76]

Other ORR electrocatalysts degrade under similar test protocols, typically ranging between 1,000 and 10,000 CV cycles. The estimated losses in ECSA and current density were 5% to 15%. There is also an $E_{1/2}$ shift of -0.003 to -0.022 V with these materials (Table S2).[14,24,45,46,54,56,60–73,77,78] A notable exception in the literature was composed of a vertically aligned nitrogen-doped carbon nanotube array, that was stable through 100,000 CV cycles.[41] No other ORR electrocatalysts could be located in the literature that demonstrates complete stability. It is important to note that many investigations were ambiguous in descriptions of their convection conditions.

The stability of the N´-GUITAR system (Figure 2.3A and Figure 2.4A) indicates the robustness of both the active ORR electrocatalytic sites and the surface of this material. Also, note that the $E_{1/2}$ for N´-GUITAR/KB is only 0.024 V negative of Pt/C with a higher limiting current density (6.3 mA cm^{-2} vs. 4.8 mA cm^{-2}) at the end of the durability test (see Figure 2.4A). This is also apparent with the CV experiments in Figure 2.3A-C, as discussed above. Given the apparent stability of the N´-GUITAR/KB, it is expected to be an excellent ORR catalyst for long-term applications. This stability may be attributed to the corrosion resistance of GUITAR. Such attack may be from the peroxides formed by partial consumption of O_2 by the electrocatalyst (see Equation 2). Recent publications elaborate on the corrosion stability of GUITAR relative to other carbon materials.[1] GUITAR has corrosion rates 2–3 orders of magnitude lower than other sp^2 carbon allotropes, which likely contributes to its stability as ORR catalyst.

2.4.5 Estimation of Number of Electron Transferred in Electrocatalytic Reduction of Oxygen.

Complete consumption of O_2 is a four-electron pathway to water (Reaction 1). This is the preferred process to maximize fuel cell voltage output and minimize corrosive intermediates. Hydrodynamic studies allow for the estimation of n, the number of electrons transferred per O_2, for the electrocatalysts of this investigation through the Koutecky-Levich (K-L) equation below.

$$\frac{1}{J} = \frac{1}{J_k} + \frac{1}{\boldsymbol{B}\omega^{1/2}} \quad (4)$$

The variable J is the measured current density, J_k is kinetic current density, and ω is the angular velocity of the disk electrode in radians per second. The factor, B is $0.62\, nFv^{\frac{1}{6}}C_{O_2}D_{O_2}^{\frac{2}{3}}$, F is Faraday's constant, ν is the kinematic viscosity of the electrolyte (0.01 $cm^2\ s^{-1}$), C_{O_2} is the bulk concentration of oxygen in 0.1 M KOH at room temperature (1.20×10^{-6} mol cm^{-3}), and D_{O_2} is the diffusion coefficient of O_2 in 0.1 M KOH (1.90×10^{-5} $cm^2\ s^{-1}$). All studies were conducted at 0.005 V s^{-1} sweep rate with an RDE.[16,23,24,30,39,46]

Background corrected LSV-RDE at various rotation rates are shown in Figure 2.5A for N´-GUITAR/KB and SI for GUITAR/KB and Pt/C (Figure S2.7 and S2.8).[16,31,79] The K-L plot are also shown for N´-GUITAR/KB, with n = 3.6 to 3.7 within the potential range of -0.4 V to -0.7 V. This is consistent with other N-doped carbon materials observed in the literature, which range from 3.1 to 4.1 electrons per O_2.[16,17,31,38,39,46,55,59,80] Unmodified GUITAR/KB has a predominantly 2-electron pathway, with n = 2.6 to 2.8. The commercial Pt/C used in this study ranges from n = 3.6 to 3.7, which is consistent with the literature (Figure 2.5B).[16,17]

The change from a predominantly 2-electron pathway with GUITAR/KB to a predominantly 4-electron pathway with N´-GUITAR/KB is attributed to the presence of pyridinic nitrogen and the absence of quaternary nitrogen (see the XPS results above and Figure 2.1C).[19,24,29,81–84] The 4-electron and 2-electron ORR pathways are associated with pyridinic and quaternary nitrogen functionalities, respectively.[32,41,85]

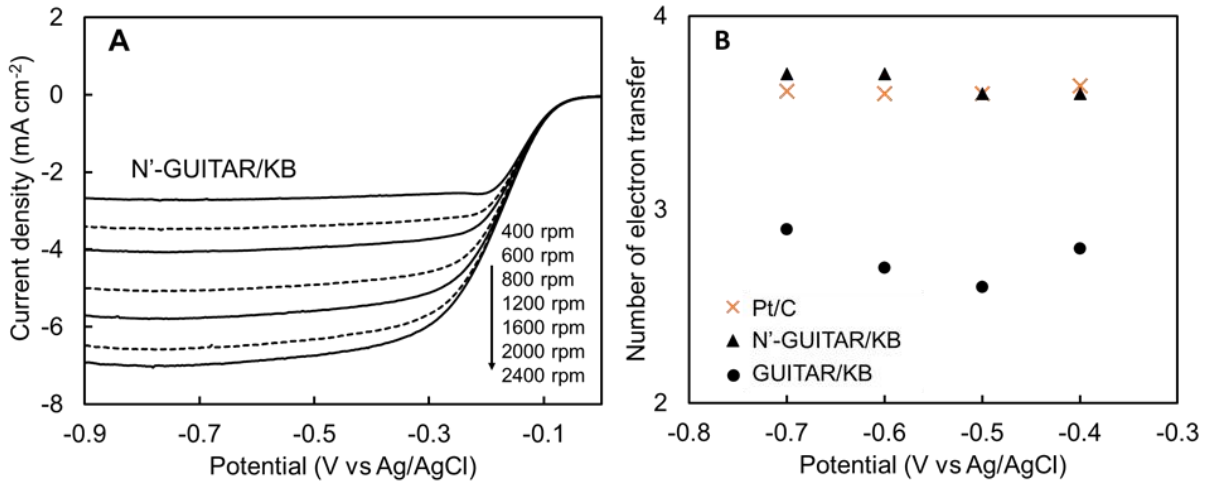

Figure 2.5. (A) Background corrected RDE-LSV in O_2 saturated 0.1 M KOH at 0.005 V s^{-1} at different rotation speeds (rpm-rotations per minute) with N´-GUITAR/KB. (B) Number of electron transfer vs. potential as obtained from Koutecky-Levich (K-L) plots derived from respective RDE LSV shown in Figure S2.7 and S2.8

2.4.6 The ORR Electrocatalyst is not Affected by Methanol Crossover.

Crossover of methanol into the cathodic compartment poisons Pt-based ORR catalysts.[86,87] To assess the tolerance of the N´-GUITAR/KB system to methanol, chronoamperometric RDE responses were recorded at -0.45 V (vs. Ag/AgCl) at 800 rpm in O_2 saturated 0.1 M KOH before and after introducing 3.0 M methanol. As seen in Figure 2.6, the ORR current remained constant for N´-GUITAR/KB, while a sharp decrease of approximately 60% in ORR current

was observed for Pt/C after the introduction of 3.0 M methanol at 240 sec. This steep decline in performance by Pt/C is consistent with the literature. In general, nitrogen-doped carbon ORR catalysts are known to be tolerant in the presence of methanol.[16,23–25]

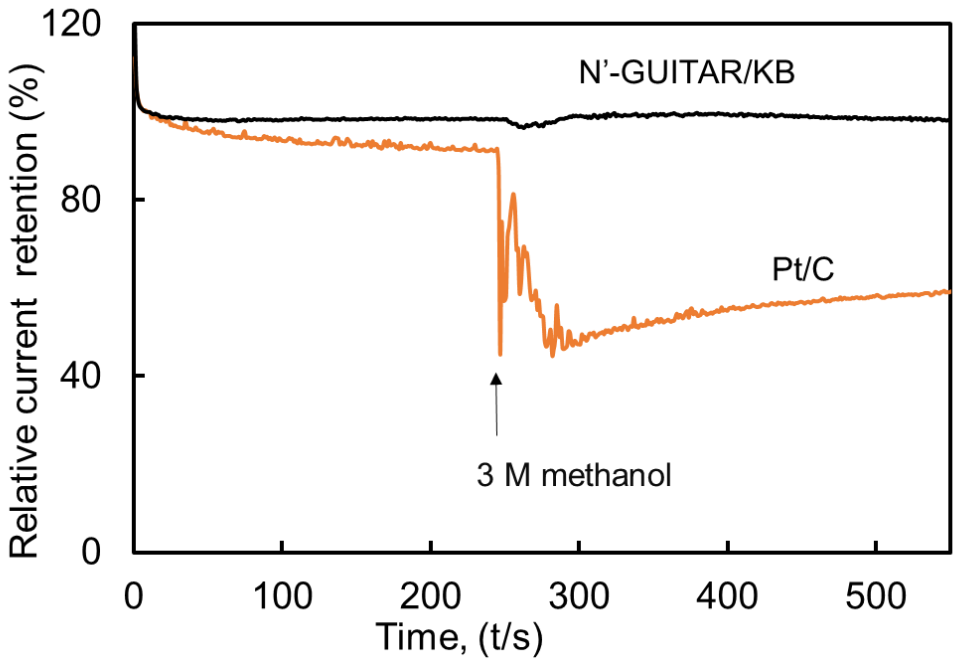

Figure 2.6. Methanol interference studies with N´-GUITAR/KB and Pt/C ORR electrocatalysts using RDE (800 rpm) at -0.45V vs. Ag/AgCl in O_2 saturated 0.1 M KOH. Methanol was injected at 240 sec, the relative current for N´-GUITAR/KB remained constant in the post-injection time period.

2.5 Conclusion

In this contribution, N´-GUITAR was synthesized, characterized, and found to be a stable and high-performing ORR electrocatalyst. N´-GUITAR exhibited no loss in current density, no E_p shift, and no reduction in capacitive current throughout the DOE recommended 30,000 cycle stress test in O_2 saturated 0.1 M KOH. It is worth noting that despite being a significant

benchmark for fuel cell development, the durability testing observed in literature is often much less rigorous than the protocol employed in this study. The remarkable stability of this catalyst is most likely related to several underlying properties of N´-GUITAR. It was found that annealing GUITAR with melamine will result in the selective doping of pyridinic and pyrrolic nitrogen. These moieties are more selective to the 4-electron process, which makes it a more efficient ORR catalyst and reduce the production of reactive oxygen species (a possible source or catalyst degradation). GUITAR also possesses a high degree of anodic stability and resistance to corrosion by reactive oxygen species (as mentioned in the introduction). The competitive ORR performance is rooted in the fast-heterogeneous electron-transfer (HET) rate of GUITAR. Previous studies indicate that GUITAR has HET rates 2-10 orders of magnitude faster than other carbon materials for a variety of inner and outer-sphere redox couples.[1–5,8] The sum of these features, along with the low cost of synthesis, make N´-GUITAR/KB a practical candidate for widespread use in fuel cell technology.

2.6 References

(1) Kabir, H.; Zhu, H.; May, J.; Hamal, K.; Kan, Y.; Williams, T.; Echeverria, E.; McIlroy, D. N.; Estrada, D.; Davis, P. H.; Pandhi, T.; Yocham, K.; Higginbotham, K.; Clearfield, A.; Cheng, I. F. The Sp2-Sp3 Carbon Hybridization Content of Nanocrystalline Graphite from Pyrolyzed Vegetable Oil, Comparison of Electrochemistry and Physical Properties with Other Carbon Forms and Allotropes. *Carbon* **2019**, *144*, 831–840. https://doi.org/10.1016/j.carbon.2018.12.058.

(2) Cheng, I. F.; Xie, Y.; Allen Gonzales, R.; Brejna, P. R.; Sundararajan, J. P.; Fouetio Kengne, B. A.; Eric Aston, D.; McIlroy, D. N.; Foutch, J. D.; Griffiths, P. R. Synthesis of Graphene Paper from Pyrolyzed Asphalt. *Carbon* **2011**, *49* (8), 2852–2861. https://doi.org/10.1016/j.carbon.2011.03.020.

(3) Francis Cheng, I.; Xie, Y.; Owusu Gyan, I.; W. Nicholas, N. Highest Measured Anodic Stability in Aqueous Solutions: Graphenic Electrodes from the Thermolyzed Asphalt Reaction. *RSC Advances* **2013**, *3* (7), 2379–2384. https://doi.org/10.1039/C2RA23103D.

(4) Gyan, I. O.; Wojcik, P. M.; Aston, D. E.; McIlroy, D. N.; Cheng, I. F. A Study of the Electrochemical Properties of a New Graphitic Material: GUITAR. *ChemElectroChem* **2015**, *2* (5), 700–706. https://doi.org/10.1002/celc.201402433.

(5) Gyan, I. O.; Cheng, I. F. Electrochemical Study of Biologically Relevant Molecules at Electrodes Constructed from GUITAR, a New Carbon Allotrope. *Microchemical Journal* **2015**, *122*, 39–44. https://doi.org/10.1016/j.microc.2015.04.002.

(6) Casiraghi, C.; Ferrari, A. C.; Robertson, J. Raman Spectroscopy of Hydrogenated Amorphous Carbons. *Phys. Rev. B* **2005**, *72* (8), 085401. https://doi.org/10.1103/PhysRevB.72.085401.

(7) Galli, G.; Martin, R. M.; Car, R.; Parrinello, M. Structural and Electronic Properties of Amorphous Carbon. *Phys. Rev. Lett.* **1989**, *62* (5), 555–558. https://doi.org/10.1103/PhysRevLett.62.555.

(8) Kabir, H.; Gyan, I. O.; Foutch, J. D.; Zhu, H.; Cheng, I. F. Application of GUITAR on the Negative Electrode of the Vanadium Redox Flow Battery: Improved V3+/2+

Heterogeneous Electron Transfer with Reduced Hydrogen Gassing. *C — Journal of Carbon Research* **2016**, *2* (2), 13. https://doi.org/10.3390/c2020013.

(9) Sharaf, O. Z.; Orhan, M. F. An Overview of Fuel Cell Technology: Fundamentals and Applications. *Renewable and Sustainable Energy Reviews* **2014**, *32*, 810–853. https://doi.org/10.1016/j.rser.2014.01.012.

(10) Wang, Y.; Chen, K. S.; Mishler, J.; Cho, S. C.; Adroher, X. C. A Review of Polymer Electrolyte Membrane Fuel Cells: Technology, Applications, and Needs on Fundamental Research. *Applied Energy* **2011**, *88* (4), 981–1007. https://doi.org/10.1016/j.apenergy.2010.09.030.

(11) Ge, X.; Sumboja, A.; Wuu, D.; An, T.; Li, B.; Goh, F. W. T.; Hor, T. S. A.; Zong, Y.; Liu, Z. Oxygen Reduction in Alkaline Media: From Mechanisms to Recent Advances of Catalysts. *ACS Catal.* **2015**, *5* (8), 4643–4667. https://doi.org/10.1021/acscatal.5b00524.

(12) Ramaswamy, N.; Mukerjee, S. Influence of Inner- and Outer-Sphere Electron Transfer Mechanisms during Electrocatalysis of Oxygen Reduction in Alkaline Media. *J. Phys. Chem. C* **2011**, *115* (36), 18015–18026. https://doi.org/10.1021/jp204680p.

(13) Zhao, Y.; Chu, Y.; Ju, X.; Zhao, J.; Kong, L.; Zhang, Y. Carbon-Supported Copper-Based Nitrogen-Containing Supramolecule as an Efficient Oxygen Reduction Reaction Catalyst in Neutral Medium. *Catalysts* **2018**, *8* (2), 53. https://doi.org/10.3390/catal8020053.

(14) Yang, H. B.; Miao, J.; Hung, S.-F.; Chen, J.; Tao, H. B.; Wang, X.; Zhang, L.; Chen, R.; Gao, J.; Chen, H. M.; Dai, L.; Liu, B. Identification of Catalytic Sites for Oxygen Reduction and Oxygen Evolution in N-Doped Graphene Materials: Development of Highly Efficient Metal-Free Bifunctional Electrocatalyst. *Sci Adv* **2016**, *2* (4), e1501122. https://doi.org/10.1126/sciadv.1501122.

(15) Lin, X.; Wang, Y.; Liu, T.; Chen, H.; Jiang, Z.; Chen, Y.; Liu, J.; Huang., J.; Liu, M. Hierarchically Porous Co and N-Codoped Carbon Hollow Structure Derived from PS@ZIF-67 as an Electrocatalyst for Oxygen Reduction. *ChemistrySelect* **2018**, *3* (17), 4831–4837. https://doi.org/10.1002/slct.201800979.

(16) Panomsuwan, G.; Saito, N.; Ishizaki, T. Nitrogen-Doped Carbon Nanoparticle–Carbon Nanofiber Composite as an Efficient Metal-Free Cathode Catalyst for Oxygen Reduction Reaction. *ACS Appl. Mater. Interfaces* **2016**, *8* (11), 6962–6971. https://doi.org/10.1021/acsami.5b10493.

(17) Pan, T.; Liu, H.; Ren, G.; Li, Y.; Lu, X.; Zhu, Y. Metal-Free Porous Nitrogen-Doped Carbon Nanotubes for Enhanced Oxygen Reduction and Evolution Reactions. *Science Bulletin* **2016**, *61* (11), 889–896. https://doi.org/10.1007/s11434-016-1073-3.

(18) Qin, L.; Yuan, Y.; Wei, W.; Lv, W.; Niu, S.; He, Y.-B.; Zhai, D.; Kang, F.; Kim, J.-K.; Yang, Q.-H.; Lu, J. Graphene-Directed Formation of a Nitrogen-Doped Porous Carbon Sheet with High Catalytic Performance for the Oxygen Reduction Reaction. *J. Phys. Chem. C* **2018**, *122* (25), 13508–13514. https://doi.org/10.1021/acs.jpcc.7b12327.

(19) Zhong, H.; Wang, J.; Zhang, Y.; Xu, W.; Xing, W.; Xu, D.; Zhang, Y.; Zhang, X. ZIF-8 Derived Graphene-Based Nitrogen-Doped Porous Carbon Sheets as Highly Efficient and Durable Oxygen Reduction Electrocatalysts. *Angewandte Chemie International Edition* **2014**, *53* (51), 14235–14239. https://doi.org/10.1002/anie.201408990.

(20) Meier, J. C.; Galeano, C.; Katsounaros, I.; Topalov, A. A.; Kostka, A.; Schüth, F.; Mayrhofer, K. J. J. Degradation Mechanisms of Pt/C Fuel Cell Catalysts under Simulated Start–Stop Conditions. *ACS Catal.* **2012**, *2* (5), 832–843. https://doi.org/10.1021/cs300024h.

(21) Liu, Z. Y.; Zhang, J. L.; Yu, P. T.; Zhang, J. X.; Makharia, R.; More, K. L.; Stach, E. A. Transmission Electron Microscopy Observation of Corrosion Behaviors of Platinized Carbon Blacks under Thermal and Electrochemical Conditions. *J. Electrochem. Soc.* **2010**, *157* (6), B906–B913. https://doi.org/10.1149/1.3391737.

(22) Katsounaros, I.; Cherevko, S.; Zeradjanin, A. R.; Mayrhofer, K. J. J. Oxygen Electrochemistry as a Cornerstone for Sustainable Energy Conversion. *Angewandte Chemie International Edition* **2014**, *53* (1), 102–121. https://doi.org/10.1002/anie.201306588.

(23) Men, B.; Sun, Y.; Liu, J.; Tang, Y.; Chen, Y.; Wan, P.; Pan, J. Synergistically Enhanced Electrocatalytic Activity of Sandwich-like N-Doped Graphene/Carbon Nanosheets Decorated

by Fe and S for Oxygen Reduction Reaction. *ACS Appl. Mater. Interfaces* **2016**, *8* (30), 19533–19541. https://doi.org/10.1021/acsami.6b06329.

(24) Lv, Y.; Yang, L.; Cao, D. Nitrogen and Fluorine-Codoped Porous Carbons as Efficient Metal-Free Electrocatalysts for Oxygen Reduction Reaction in Fuel Cells. *ACS Appl. Mater. Interfaces* **2017**, *9* (38), 32859–32867. https://doi.org/10.1021/acsami.7b11371.

(25) Tao, G.; Zhang, L.; Chen, L.; Cui, X.; Hua, Z.; Wang, M.; Wang, J.; Chen, Y.; Shi, J. N-Doped Hierarchically Macro/Mesoporous Carbon with Excellent Electrocatalytic Activity and Durability for Oxygen Reduction Reaction. *Carbon* **2015**, *86*, 108–117. https://doi.org/10.1016/j.carbon.2014.12.102.

(26) Kocha, S. S.; Garsany, Y.; Myers, D. Testing Oxygen Reduction Reaction Activity with the Rotating Disc Electrode Technique. 44. Technical Report; U.S. Department of Energy: Washington, DC, 2013 (https://www.energy.gov/eere/fuelcells/downloads/testing-oxygen-reduction-reaction-activity-rotating-disc-electrode

(27) Voiry, D.; Chhowalla, M.; Gogotsi, Y.; Kotov, N. A.; Li, Y.; Penner, R. M.; Schaak, R. E.; Weiss, P. S. Best Practices for Reporting Electrocatalytic Performance of Nanomaterials. *ACS Nano* **2018**, *12* (10), 9635–9638. https://doi.org/10.1021/acsnano.8b07700.

(28) Hamal, K.; May, J.; Zhu, H.; Dalbec, F.; Echeverria, E.; McIlroy, D. N.; Aston, E.; Cheng, I. F. Electrochemical Aspects of a Nitrogen-Doped Pseudo-Graphitic Carbon Material: Resistance to Electrode Fouling by Air-Aging and Dopamine Electro-Oxidation. *C* **2020**, *6* (4), 68. https://doi.org/10.3390/c6040068.

(29) Sheng, Z.-H.; Shao, L.; Chen, J.-J.; Bao, W.-J.; Wang, F.-B.; Xia, X.-H. Catalyst-Free Synthesis of Nitrogen-Doped Graphene via Thermal Annealing Graphite Oxide with Melamine and Its Excellent Electrocatalysis. *ACS Nano* **2011**, *5* (6), 4350–4358. https://doi.org/10.1021/nn103584t.

(30) Sun, T.; Xu, L.; Li, S.; Chai, W.; Huang, Y.; Yan, Y.; Chen, J. Cobalt-Nitrogen-Doped Ordered Macro-/Mesoporous Carbon for Highly Efficient Oxygen Reduction Reaction. *Applied Catalysis B: Environmental* **2016**, *193*, 1–8. https://doi.org/10.1016/j.apcatb.2016.04.006.

(31) Seredych, M.; Szczurek, A.; Fierro, V.; Celzard, A.; Bandosz, T. J. Electrochemical Reduction of Oxygen on Hydrophobic Ultramicroporous PolyHIPE Carbon. *ACS Catal.* **2016**, *6* (8), 5618–5628. https://doi.org/10.1021/acscatal.6b01497.

(32) Qiu, S.; Yu, L.; Tang, D.; Ren, W.; Chen, K.; Sun, J. Rapidly Enhanced Electro-Fenton Efficiency by in Situ Electrochemistry-Activated Graphite Cathode. *Ind. Eng. Chem. Res.* **2018**, *57* (14), 4907–4915. https://doi.org/10.1021/acs.iecr.7b05380.

(33) Ratso, S.; Kruusenberg, I.; Vikkisk, M.; Joost, U.; Shulga, E.; Kink, I.; Kallio, T.; Tammeveski, K. Highly Active Nitrogen-Doped Few-Layer Graphene/Carbon Nanotube Composite Electrocatalyst for Oxygen Reduction Reaction in Alkaline Media. *Carbon* **2014**, *73*, 361–370. https://doi.org/10.1016/j.carbon.2014.02.076.

(34) Kumar, M. P.; Kesavan, T.; Kalita, G.; Ragupathy, P.; Narayanan, T. N.; Pattanayak, D. K. On the Large Capacitance of Nitrogen Doped Graphene Derived by a Facile Route. *RSC Adv.* **2014**, *4* (73), 38689–38697. https://doi.org/10.1039/C4RA04927F.

(35) Mosch, H. L. K. S.; Höppener, S.; Paulus, R. M.; Schröter, B.; Schubert, U. S.; Ignaszak, A. The Correlation of the Binding Mechanism of the Polypyrrole–Carbon Capacitive Interphase with Electrochemical Stability of the Composite Electrode. *Phys. Chem. Chem. Phys.* **2015**, *17* (20), 13323–13332. https://doi.org/10.1039/C5CP01406A.

(36) Park, M.; Ryu, J.; Kim, Y.; Cho, J. Corn Protein-Derived Nitrogen-Doped Carbon Materials with Oxygen-Rich Functional Groups: A Highly Efficient Electrocatalyst for All-Vanadium Redox Flow Batteries. *Energy & Environmental Science* **2014**, *7* (11), 3727–3735. https://doi.org/10.1039/C4EE02123A.

(37) Ariharan, A.; Viswanathan, B.; Nandhakumar, V. Nitrogen Doped Graphene as Potential Material for Hydrogen Storage. *Graphene* **2017**, *6* (2), 41–60. https://doi.org/10.4236/graphene.2017.62004.

(38) Zhong, H.; Zhang, S.; Jiang, J.; Li, D.; Tang, P.; Alonso-Vante, N.; Feng, Y. Improved Electrocatalytic Performance of Tailored Metal-Free Nitrogen-Doped Ordered Mesoporous Carbons for the Oxygen Reduction Reaction. *ChemElectroChem* **2018**, *5* (14), 1899–1904. https://doi.org/10.1002/celc.201700910.

(39) Liu, M.; Song, Y.; He, S.; Tjiu, W. W.; Pan, J.; Xia, Y.-Y.; Liu, T. Nitrogen-Doped Graphene Nanoribbons as Efficient Metal-Free Electrocatalysts for Oxygen Reduction. *ACS Appl. Mater. Interfaces* **2014**, *6* (6), 4214–4222. https://doi.org/10.1021/am405900r.

(40) Wu, J.; Ma, L.; Yadav, R. M.; Yang, Y.; Zhang, X.; Vajtai, R.; Lou, J.; Ajayan, P. M. Nitrogen-Doped Graphene with Pyridinic Dominance as a Highly Active and Stable Electrocatalyst for Oxygen Reduction. *ACS Appl. Mater. Interfaces* **2015**, *7* (27), 14763–14769. https://doi.org/10.1021/acsami.5b02902.

(41) Gong, K.; Du, F.; Xia, Z.; Durstock, M.; Dai, L. Nitrogen-Doped Carbon Nanotube Arrays with High Electrocatalytic Activity for Oxygen Reduction. *Science* **2009**, *323* (5915), 760–764. https://doi.org/10.1126/science.1168049.

(42) Qu, L.; Liu, Y.; Baek, J.-B.; Dai, L. Nitrogen-Doped Graphene as Efficient Metal-Free Electrocatalyst for Oxygen Reduction in Fuel Cells. *ACS Nano* **2010**, *4* (3), 1321–1326. https://doi.org/10.1021/nn901850u.

(43) Zahoor, A.; Christy, M.; Hwang, Y. J.; Lim, Y. R.; Kim, P.; Nahm, K. S. Improved Electrocatalytic Activity of Carbon Materials by Nitrogen Doping. *Applied Catalysis B: Environmental* **2014**, *147*, 633–641. https://doi.org/10.1016/j.apcatb.2013.09.043.

(44) Wang, N.; Li, T.; Song, Y.; Liu, J.; Wang, F. Metal-Free Nitrogen-Doped Porous Carbons Derived from Pomelo Peel Treated by Hypersaline Environments for Oxygen Reduction Reaction. *Carbon* **2018**, *130*, 692–700. https://doi.org/10.1016/j.carbon.2018.01.068.

(45) Han, H.; Chao, S.; Bai, Z.; Wang, X.; Yang, X.; Qiao, J.; Chen, Z.; Yang, L. Metal-Organic-Framework-Derived Co Nanoparticles Deposited on N-Doped Bimodal Mesoporous Carbon Nanorods as Efficient Bifunctional Catalysts for Rechargeable Zinc−Air Batteries. *ChemElectroChem* **2018**, *5* (14), 1868–1873. https://doi.org/10.1002/celc.201701289.

(46) Lv, Q.; Si, W.; Yang, Z.; Wang, N.; Tu, Z.; Yi, Y.; Huang, C.; Jiang, L.; Zhang, M.; He, J.; Long, Y. Nitrogen-Doped Porous Graphdiyne: A Highly Efficient Metal-Free Electrocatalyst for Oxygen Reduction Reaction. *ACS Appl. Mater. Interfaces* **2017**, *9* (35), 29744–29752. https://doi.org/10.1021/acsami.7b08115.

(47) Thanh, T. D.; Chuong, N. D.; Hien, H. V.; Kim, N. H.; Lee, J. H. CuAg@Ag Core–Shell Nanostructure Encapsulated by N-Doped Graphene as a High-Performance Catalyst for Oxygen Reduction Reaction. *ACS Appl. Mater. Interfaces* **2018**, *10* (5), 4672–4681. https://doi.org/10.1021/acsami.7b16294.

(48) Begum, H.; Kim, Y.-B. Improvement of Catalytic Activity of Platinum Nanoparticles Decorated Carbon Graphene Composite on Oxygen Electroreduction for Fuel Cells. *Processes* **2019**, *7* (9), 586. https://doi.org/10.3390/pr7090586.

(49) Lim, B.; Jiang, M.; Camargo, P. H. C.; Cho, E. C.; Tao, J.; Lu, X.; Zhu, Y.; Xia, Y. Pd-Pt Bimetallic Nanodendrites with High Activity for Oxygen Reduction. *Science* **2009**, *324* (5932), 1302–1305. https://doi.org/10.1126/science.1170377.

(50) Chen, T.; Cai, Z.; Yang, Z.; Li, L.; Sun, X.; Huang, T.; Yu, A.; Kia, H. G.; Peng, H. Nitrogen-Doped Carbon Nanotube Composite Fiber with a Core–Sheath Structure for Novel Electrodes. *Advanced Materials* **2011**, *23* (40), 4620–4625. https://doi.org/10.1002/adma.201102200.

(51) Wang, S.; Iyyamperumal, E.; Roy, A.; Xue, Y.; Yu, D.; Dai, L. Vertically Aligned BCN Nanotubes as Efficient Metal-Free Electrocatalysts for the Oxygen Reduction Reaction: A Synergetic Effect by Co-Doping with Boron and Nitrogen. *Angewandte Chemie International Edition* **2011**, *50* (49), 11756–11760. https://doi.org/10.1002/anie.201105204.

(52) Zhang, J.; Song, X.; Li, P.; Wang, S.; Wu, Z.; Liu, X. An Iron-Based Catalyst with Multiple Active Components Synergetically Improved Electrochemical Performance for Oxygen Reduction Reaction. *Catalysts* **2018**, *8* (6), 243. https://doi.org/10.3390/catal8060243.

(53) Hu, K.; Xiao, Z.; Cheng, Y.; Yan, D.; Chen, R.; Huo, J.; Wang, S. Iron Phosphide/N, P-Doped Carbon Nanosheets as Highly Efficient Electrocatalysts for Oxygen Reduction Reaction over the Whole PH Range. *Electrochimica Acta* **2017**, *254*, 280–286. https://doi.org/10.1016/j.electacta.2017.09.131.

(54) Wang, Z.; Peng, S.; Hu, Y.; Li, L.; Yan, T.; Yang, G.; Ji, D.; Srinivasan, M.; Pan, Z.; Ramakrishna, S. Cobalt Nanoparticles Encapsulated in Carbon Nanotube-Grafted Nitrogen and Sulfur Co-Doped Multichannel Carbon Fibers as Efficient Bifunctional Oxygen

Electrocatalysts. *J. Mater. Chem. A* **2017**, *5* (10), 4949–4961. https://doi.org/10.1039/C6TA10291C.

(55) Yang, F.; Abadia, M.; Chen, C.; Wang, W.; Li, L.; Zhang, L.; Rogero, C.; Chuvilin, A.; Knez, M. Design of Active and Stable Oxygen Reduction Reaction Catalysts by Embedding CoxOynanoparticles into Nitrogen-Doped Carbon. *Nano Res.* **2017**, *10* (1), 97–107. https://doi.org/10.1007/s12274-016-1269-5.

(56) Wei, W.; Ge, H.; Huang, L.; Kuang, M.; Al-Enizi, A. M.; Zhang, L.; Zheng, G. Hierarchically Tubular Nitrogen-Doped Carbon Structures for the Oxygen Reduction Reaction. *J. Mater. Chem. A* **2017**, *5* (26), 13634–13638. https://doi.org/10.1039/C7TA02658G.

(57) Huang, X.; Yin, X.; Yu, X.; Tian, J.; Wu, W. Preparation of Nitrogen-Doped Carbon Materials Based on Polyaniline Fiber and Their Oxygen Reduction Properties. *Colloids and Surfaces A: Physicochemical and Engineering Aspects* **2018**, *539*, 163–170. https://doi.org/10.1016/j.colsurfa.2017.12.024.

(58) Sun, X.; Song, P.; Zhang, Y.; Liu, C.; Xu, W.; Xing, W. A Class of High Performance Metal-Free Oxygen Reduction Electrocatalysts Based on Cheap Carbon Blacks. *Scientific Reports* **2013**, *3*, 2505. https://doi.org/10.1038/srep02505.

(59) Chen, R.; Yan, J.; Liu, Y.; Li, J. Three-Dimensional Nitrogen-Doped Graphene/MnO Nanoparticle Hybrids as a High-Performance Catalyst for Oxygen Reduction Reaction. *J. Phys. Chem. C* **2015**, *119* (15), 8032–8037. https://doi.org/10.1021/acs.jpcc.5b00306.

(60) Li, X.; Guan, B. Y.; Gao, S.; Lou, X. W. (David). A General Dual-Templating Approach to Biomass-Derived Hierarchically Porous Heteroatom-Doped Carbon Materials for Enhanced Electrocatalytic Oxygen Reduction. *Energy Environ. Sci.* **2019**, *12* (2), 648–655. https://doi.org/10.1039/C8EE02779J.

(61) Xue, L.; Li, Y.; Liu, X.; Liu, Q.; Shang, J.; Duan, H.; Dai, L.; Shui, J. Zigzag Carbon as Efficient and Stable Oxygen Reduction Electrocatalyst for Proton Exchange Membrane Fuel Cells. *Nature Communications* **2018**, *9* (1), 3819. https://doi.org/10.1038/s41467-018-06279-x.

(62) Zhang, P.; Sun, F.; Xiang, Z.; Shen, Z.; Yun, J.; Cao, D. ZIF-Derived in Situ Nitrogen-Doped Porous Carbons as Efficient Metal-Free Electrocatalysts for Oxygen Reduction Reaction. *Energy Environ. Sci.* **2013**, *7* (1), 442–450. https://doi.org/10.1039/C3EE42799D.

(63) Sathiskumar, C.; Ramakrishnan, S.; Vinothkannan, M.; Karthikeyan, S.; Yoo, D. J.; Rhan Kim, A. Nitrogen-Doped Porous Carbon Derived from Biomass Used as Trifunctional Electrocatalyst toward Oxygen Reduction, Oxygen Evolution and Hydrogen Evolution Reactions. *Nanomaterials (Basel)* **2019**, *10* (1). https://doi.org/10.3390/nano10010076.

(64) Gao, R.; Dai, Q.; Du, F.; Yan, D.; Dai, L. C60-Adsorbed Single-Walled Carbon Nanotubes as Metal-Free, PH-Universal, and Multifunctional Catalysts for Oxygen Reduction, Oxygen Evolution, and Hydrogen Evolution. *J. Am. Chem. Soc.* **2019**, *141* (29), 11658–11666. https://doi.org/10.1021/jacs.9b05006.

(65) Han, L.; Cui, X.; Liu, Y.; Han, G.; Wu, X.; Xu, C. (Charles); Li, B. Nitrogen and Phosphorus Modification to Enhance the Catalytic Activity of Biomass-Derived Carbon toward the Oxygen Reduction Reaction. *Sustainable Energy Fuels* **2020**, *4* (6), 2707–2717. https://doi.org/10.1039/C9SE00985J.

(66) Dumont, J. H.; Martinez, U.; Artyushkova, K.; Purdy, G. M.; Dattelbaum, A. M.; Zelenay, P.; Mohite, A.; Atanassov, P.; Gupta, G. Nitrogen-Doped Graphene Oxide Electrocatalysts for the Oxygen Reduction Reaction. *ACS Appl. Nano Mater.* **2019**, *2* (3), 1675–1682. https://doi.org/10.1021/acsanm.8b02235.

(67) Li, J.; Chen, S.; Yang, N.; Deng, M.; Ibraheem, S.; Deng, J.; Li, J.; Li, L.; Wei, Z. Ultrahigh-Loading Zinc Single-Atom Catalyst for Highly Efficient Oxygen Reduction in Both Acidic and Alkaline Media. *Angewandte Chemie International Edition* **2019**, *58* (21), 7035–7039. https://doi.org/10.1002/anie.201902109.

(68) Yang, Q.; Jia, Y.; Wei, F.; Zhuang, L.; Yang, D.; Liu, J.; Wang, X.; Lin, S.; Yuan, P.; Yao, X. Understanding the Activity of Co-N4−xCx in Atomic Metal Catalysts for Oxygen Reduction Catalysis. *Angewandte Chemie* **2020**, *132* (15), 6178–6183. https://doi.org/10.1002/ange.202000324.

(69) Gao, J.; Wang, Y.; Wu, H.; Liu, X.; Wang, L.; Yu, Q.; Li, A.; Wang, H.; Song, C.; Gao, Z.; Peng, M.; Zhang, M.; Ma, N.; Wang, J.; Zhou, W.; Wang, G.; Yin, Z.; Ma, D. Construction of a Sp3/Sp2 Carbon Interface in 3D N-Doped Nanocarbons for the Oxygen Reduction Reaction. *Angewandte Chemie International Edition* **2019**, *58* (42), 15089–15097. https://doi.org/10.1002/anie.201907915.

(70) Yang, S.; Yu, Y.; Dou, M.; Zhang, Z.; Dai, L.; Wang, F. Two-Dimensional Conjugated Aromatic Networks as High-Site-Density and Single-Atom Electrocatalysts for the Oxygen Reduction Reaction. *Angewandte Chemie International Edition* **2019**, *58* (41), 14724–14730. https://doi.org/10.1002/anie.201908023.

(71) Cui, L.; Cui, L.; Li, Z.; Zhang, J.; Wang, H.; Lu, S.; Xiang, Y. A Copper Single-Atom Catalyst towards Efficient and Durable Oxygen Reduction for Fuel Cells. *J. Mater. Chem. A* **2019**, *7* (28), 16690–16695. https://doi.org/10.1039/C9TA03518D.

(72) Guo, C.; Li, Y.; Liao, W.; Liu, Y.; Li, Z.; Sun, L.; Chen, C.; Zhang, J.; Si, Y.; Li, L. Boosting the Oxygen Reduction Activity of a Three-Dimensional Network Co–N–C Electrocatalyst via Space-Confined Control of Nitrogen-Doping Efficiency and the Molecular-Level Coordination Effect. *J. Mater. Chem. A* **2018**, *6* (27), 13050–13061. https://doi.org/10.1039/C8TA03759K.

(73) Deng, Y.; Yin, S.; Liu, Y.; Lu, Y.; Cao, X.; Wang, L.; Wang, H.; Zhao, Y.; Gu, H. Mesoporous AgPdPt Nanotubes as Electrocatalysts for the Oxygen Reduction Reaction. *ACS Appl. Nano Mater.* **2019**, *2* (4), 1876–1882. https://doi.org/10.1021/acsanm.8b02206.

(74) Song, P.; Zhang, Y.; Pan, J.; Zhuang, L.; Xu, W. Cheap Carbon Black-Based High-Performance Electrocatalysts for Oxygen Reduction Reaction. *Chem. Commun.* **2015**, *51* (10), 1972–1975. https://doi.org/10.1039/C4CC07677J.

(75) Stariha, S.; Macauley, N.; Sneed, B. T.; Langlois, D.; More, K. L.; Mukundan, R.; Borup, R. L. Recent Advances in Catalyst Accelerated Stress Tests for Polymer Electrolyte Membrane Fuel Cells. *J. Electrochem. Soc.* **2018**, *165* (7), F492–F501. https://doi.org/10.1149/2.0881807jes.

(76) Chung, H. T.; Won, J. H.; Zelenay, P. Active and Stable Carbon Nanotube/Nanoparticle Composite Electrocatalyst for Oxygen Reduction. *Nature Communications* **2013**, *4* (1), 1922. https://doi.org/10.1038/ncomms2944.

(77) Liang, H.-W.; Wu, Z.-Y.; Chen, L.-F.; Li, C.; Yu, S.-H. Bacterial Cellulose Derived Nitrogen-Doped Carbon Nanofiber Aerogel: An Efficient Metal-Free Oxygen Reduction Electrocatalyst for Zinc-Air Battery. *Nano Energy* **2015**, *11*, 366–376. https://doi.org/10.1016/j.nanoen.2014.11.008.

(78) Xin, X.; Qin, H.; Cong, H.-P.; Yu, S.-H. Templating Synthesis of Mesoporous Fe3C-Encapsulated Fe–N-Doped Carbon Hollow Nanospindles for Electrocatalysis. *Langmuir* **2018**, *34* (17), 4952–4961. https://doi.org/10.1021/acs.langmuir.8b00548.

(79) Shin, D.; Jeong, B.; Choun, M.; Ocon, J. D.; Lee, J. Diagnosis of the Measurement Inconsistencies of Carbon-Based Electrocatalysts for the Oxygen Reduction Reaction in Alkaline Media. *RSC Adv.* **2014**, *5* (2), 1571–1580. https://doi.org/10.1039/C4RA12209G.

(80) Yang, W.; Fellinger, T.-P.; Antonietti, M. Efficient Metal-Free Oxygen Reduction in Alkaline Medium on High-Surface-Area Mesoporous Nitrogen-Doped Carbons Made from Ionic Liquids and Nucleobases. *J. Am. Chem. Soc.* **2011**, *133* (2), 206–209. https://doi.org/10.1021/ja108039j.

(81) Guo, D.; Shibuya, R.; Akiba, C.; Saji, S.; Kondo, T.; Nakamura, J. Active Sites of Nitrogen-Doped Carbon Materials for Oxygen Reduction Reaction Clarified Using Model Catalysts. *Science* **2016**, *351* (6271), 361–365. https://doi.org/10.1126/science.aad0832.

(82) Huang, Z.; Liao, Z.; Yang, W.; Zhou, H.; Fu, C.; Gong, Y.; Chen, L.; Kuang, Y. Different Types of Nitrogen Species in Nitrogen-Doped Carbon Material: The Formation Mechanism and Catalytic Role on Oxygen Reduction Reaction. *Electrochimica Acta* **2017**, *245*, 957–966. https://doi.org/10.1016/j.electacta.2017.06.026.

(83) Li, B.; Sun, X.; Su, D. Calibration of the Basic Strength of the Nitrogen Groups on the Nanostructured Carbon Materials. *Phys. Chem. Chem. Phys.* **2015**, *17* (10), 6691–6694. https://doi.org/10.1039/C4CP05765A.

(84) Zhang, L.; Xia, Z. Mechanisms of Oxygen Reduction Reaction on Nitrogen-Doped Graphene for Fuel Cells. *J. Phys. Chem. C* **2011**, *115* (22), 11170–11176. https://doi.org/10.1021/jp201991j.

(85) Lv, Q.; Si, W.; He, J.; Sun, L.; Zhang, C.; Wang, N.; Yang, Z.; Li, X.; Wang, X.; Deng, W.; Long, Y.; Huang, C.; Li, Y. Selectively Nitrogen-Doped Carbon Materials as Superior Metal-Free Catalysts for Oxygen Reduction. *Nature Communications* **2018**, *9* (1), 3376. https://doi.org/10.1038/s41467-018-05878-y.

(86) Tamaki, T.; Yamauchi, A.; Ito, T.; Ohashi, H.; Yamaguchi, T. The Effect of Methanol Crossover on the Cathode Overpotential of DMFCs. *Fuel Cells* **2011**, *11* (3), 394–403. https://doi.org/10.1002/fuce.201000141.

(87) Ahmed, M.; Dincer, I. A Review on Methanol Crossover in Direct Methanol Fuel Cells: Challenges and Achievements. *International Journal of Energy Research* **2011**, *35* (14), 1213–1228. https://doi.org/10.1002/er.1889.

2.7 Supplementary Information

Particle loading study: A particle loading of 1.0 mg/cm^2 of N´-GUITAR/KB was used in this study. This loading had the highest ORR current density at -0.2V vs. Ag/AgCl relative to others shown in Figure S2.1. In general, j_p increases with higher particle loadings, however, there is a negative shift in E_p with higher particle loadings. This is possibly from increased contact resistance between the particles at higher loadings.

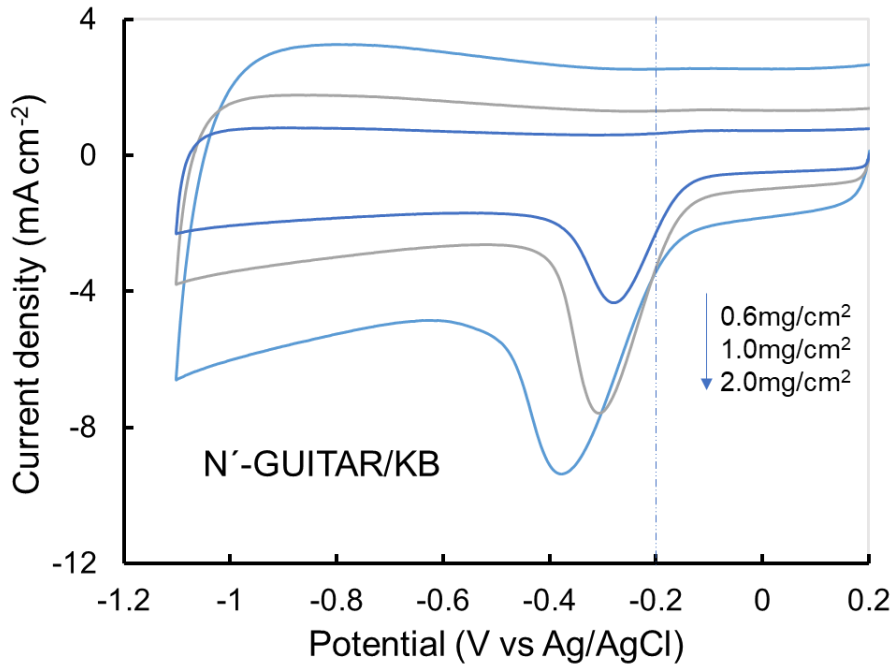

Figure S2.1: Particle loading study on N´-GUITAR/KB. Electrodes were cycled in O_2 saturated 0.1 M KOH at 50 mV/sec. The mass % of Nafion and volume of solvents were kept consistent during this experiment.

XPS study on Ketjen black (KB) substrate and Nitrogen doped Ketjen black (N'-KB): XPS results of Ketjen black substrate and nitrogen doped Ketjen black are shown in Figure S2.2. N'-KB contains 0.6 atomic % nitrogen (Figure S2.2D). The deconvoluted N1s peak of N'-KB contains 17.2% of graphitic nitrogen (Figure S2.2F), whereas N'-GUITAR/KB contains none.

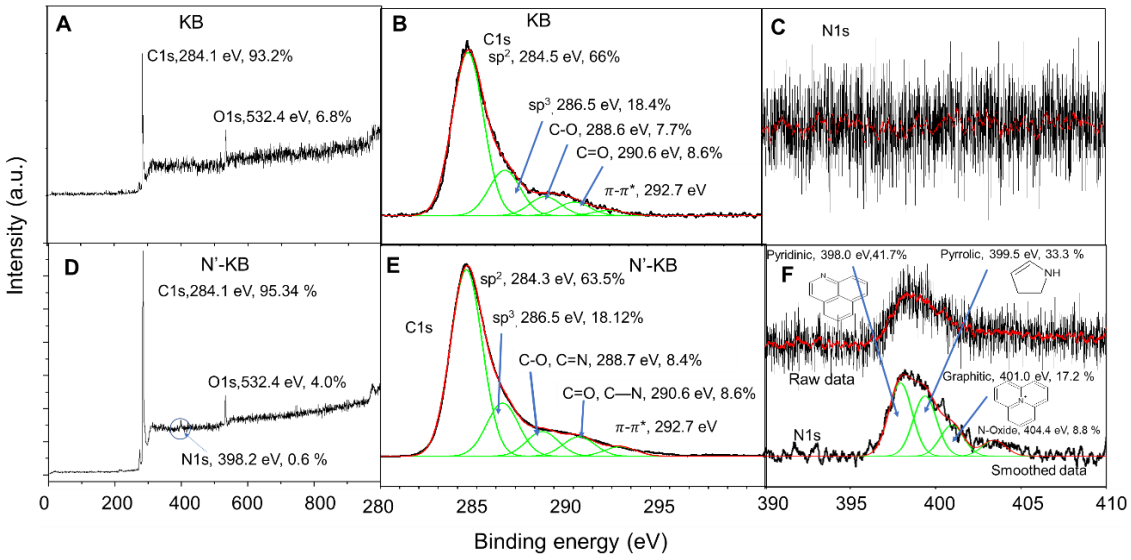

Figure S2.2: XPS comparison between KB and N'-KB. (A and D) Wide-scan XPS with the C1s, N1s, and O1s peaks highlighted. (Band E) High-resolution XPS of the C1s peak with deconvolved functional groups peaks. (C and F) High-resolution XPS of the N1s peak with the deconvoluted peaks.

The electrochemically active surface area (ECSA): ECSA for N´-GUITAR/KB is calculated from the non-faradaic capacitive current at + 0.1 V vs. Ag/AgCl.[1] This current was plotted vs. the scan rates from 5 to 300 mV/sec (Figure S2.3). The slope of this plot is the electrical double layer capacitance, which is 50.5 μF/cm^2 for flat GUITAR and 4460 μF/cm^2 for N´-GUITAR/KB. The ECSA is calculated from Equation 1, where C_{dl} is the capacitance for N´-GUITAR/KB, and $C_{dl,\ flat}$ is for the flat GUITAR electrode.

$$\left(ECSA = \frac{C_{dl,}}{C_{dl,flat}}\right) \qquad (1)$$

The ECSA for N'-GUITAR/KB is 883.16 cm^2 per cm^2 of geometric area. It is assumed that 1 cm^2 of flat GUITAR surface area equals 1 cm^2 of ECSA, assuming a surface roughness factor of 1.

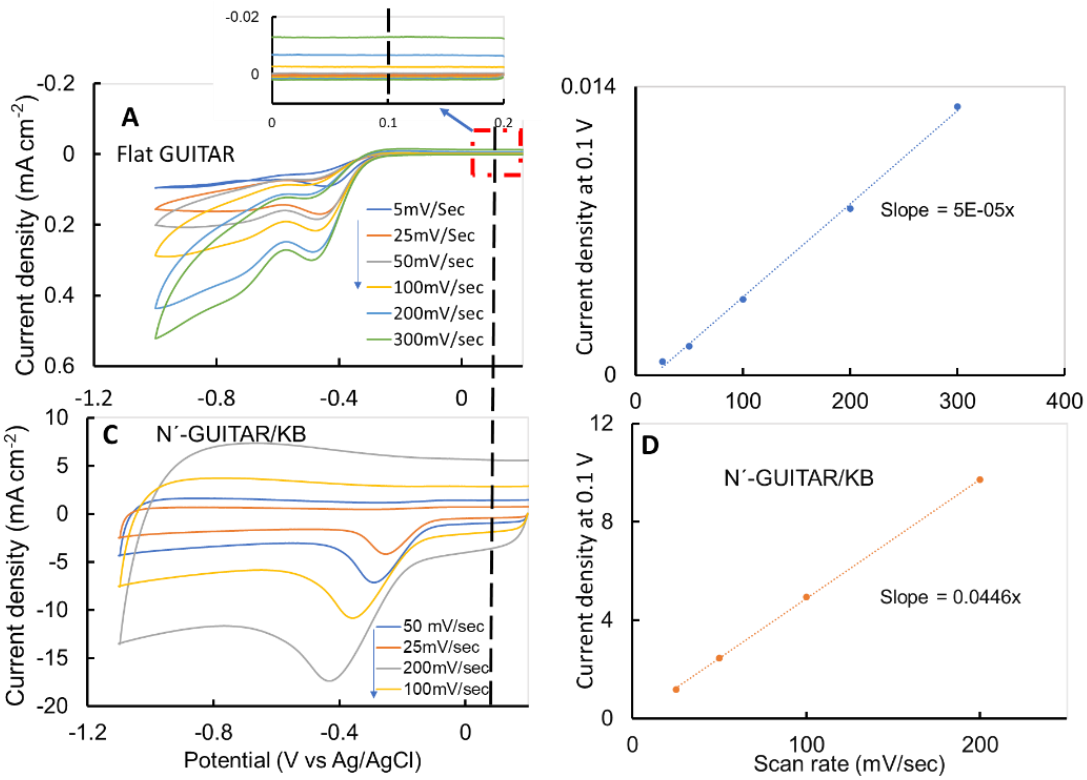

Figure S2.3: (A) and (C) include cyclic voltammograms at different scan rates on Flat GUITAR and N´-GUITAR/KB electrodes, respectively, in O_2 purged 0.1 M KOH. (B) and (D) are plots of non-faradic current density at +0.1 V vs. scan rate. The slope of these plots gives capacitive current.

The electrochemically active surface area (ECSA): ECSA for Pt/C electrocatalyst is calculated from the hydrogen desorption method using equation 2.

$$\left(ECSA = \frac{\boldsymbol{Q}\ total\ (\mu Ccm^{-2})}{\boldsymbol{Q}monolayer(\mu Ccm^{-2}) * mass\ (gm^{-2})}\right) \quad (2)$$

Where $Q_{monolayer}$ is 210 µCcm^{-2} and Q_{total} is the total charge for hydrogen desorption.[2–5] The ECSA for Pt/C is 57.9±0.3 m^{2}g^{-1} (n=2). This area is shown in Figure S2.4.

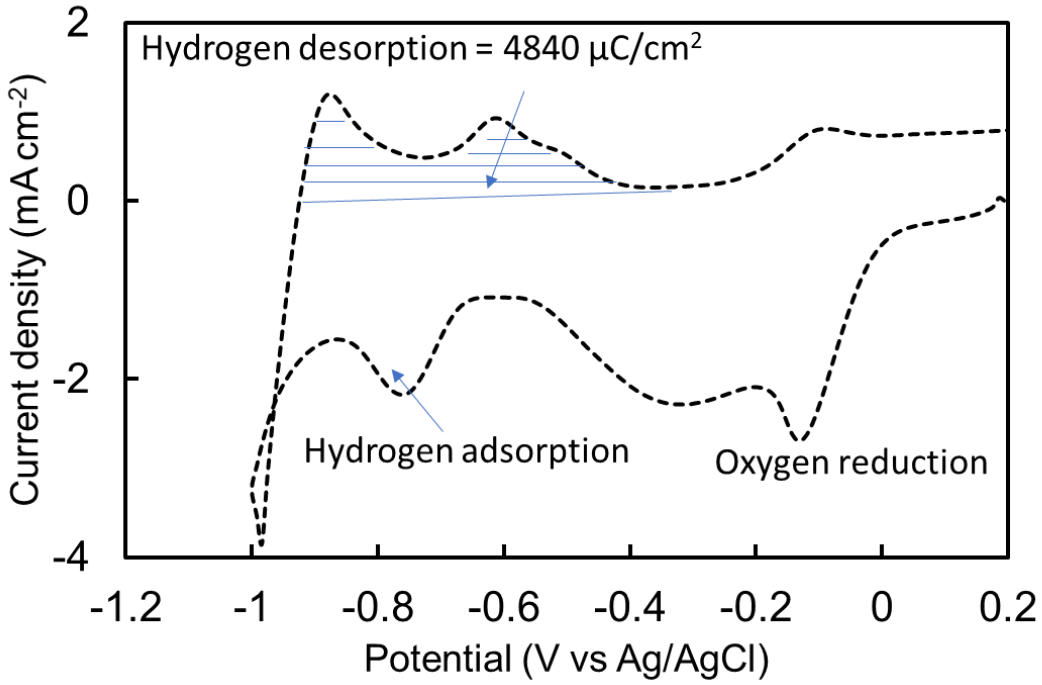

Figure S2.4: Pt/C CV in 0.1 M KOH at 50 mV/sec.

ORR performance of the control surfaces: The controls in these studies include unmodified Ketjen black and N-doped Ketjen black. These were evaluated for ORR performance under the same conditions as the N´-GUITAR/KB electrocatalyst. Figure S2.5 shows the CV's of these studies. These are included in Table 2.1 of the manuscript.

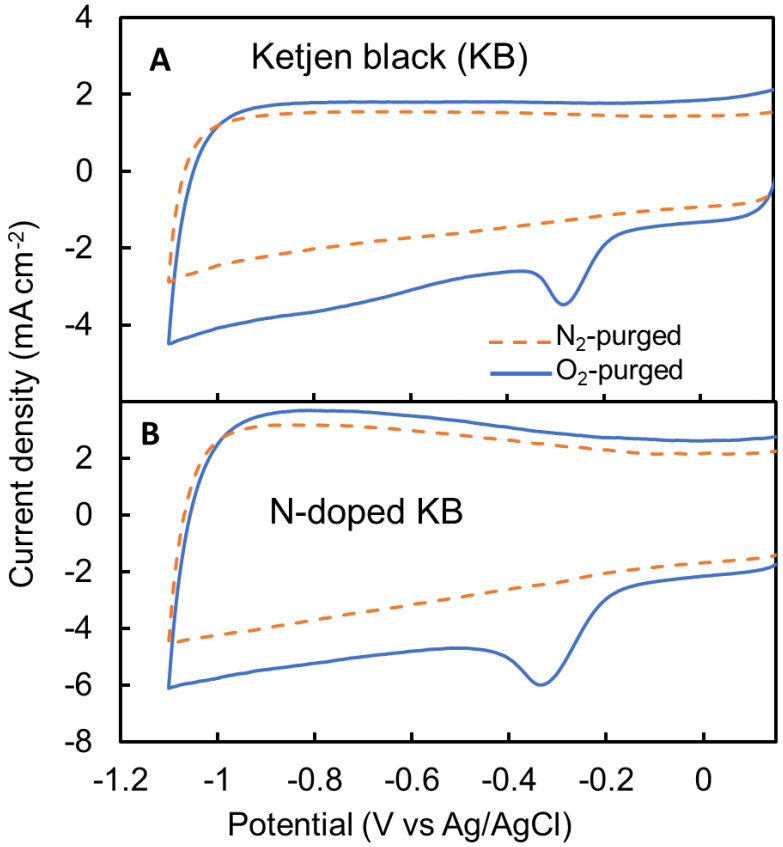

Figure S2.5: ORR CV at 50 mV/sec in O_2 and N_2 purged 0.1 M KOH. (A) Ketjen black and (B) nitrogen doped Ketjen black (N´-KB). All electrodes consisted of Nafion composites with 1.0 mg cm^{-2} particle loadings.

Table S2.1: ORR performance comparison with literature. The data for Figure 3B in the manuscript are shown in the following table with references. Table S2.1: Literature showing ORR performance at 50 mV/sec in oxygen saturated 0.1 M KOH. Note that N´-GUITAR/KB has a higher ORR current density at the peak potentials of the other electrocatalysts. Peak the current density (j_p) based on electrode geometric surface area. (Note: *indicates values estimated from their data and description.)

Reference number in manuscript- (electrocatalyst-journal- published year)	Reference in SI	Peak current density(jp) (mA cm^{-2})	Peak potential (E_p) (mV) vs Ag/AgCl
N´-GUITAR/KB	TW	6.27	-270
16- (NCNP-CNF, *ACS Appl. Mater. Interfaces*-2016)	6	3.20	-280
23-(Fe,S/NGC-900, *ACS Appl. Mater. Interfaces*-2016)	7	2.60*	-175*
30-(Co-N-OMMC 0.6, *Applied Catalysis B: Environmental*-2016)	8	2.51	-195
24- (N, F-Carbon-1000, *ACS Appl. Mater. Interfaces*-2017)	9	1.20*	-147
38-(Me/HNMK-5, *ChemElectroChem*-2018)	10	1.20*	-225*
54-(Co@NS/CNT-MCF-900, *J. of Materials Chemistry A*-2017)	11	1.00*	-146
18-(NPCS-850-J. *Phys. Chem. C* -2018)	12	1.50*	-187
56- (HT-NCTs, *J. Mater. Chem. A*- 2017)	13	1.25*	-266
57-(PCPG-900, *colloids and surfaceA*-2018)	14	1.20*	-275*
47- (CuAg@Ag/N-GNS-*ACS Appl. Mater. Interfaces*-2018)	15	2.20*	-257
58-(*BP2000-NF, Scientific Reports-2013)*	16	*2.60**	*-160*
45-(Co@N-CNR, *ChemElectrochem*-2018)	17	1.20*	-207
55-(Co_xO_y /CNT@C, *Nano Research*, 2016)	18	3.00*	-207
59-(3D-N-RGO/MnO, *The Journal of Physical Chemistry C*-2015)	19	1.00*	-350

Table S2.2: RDE-LSV comparison with literature. Comparison of half-wave potential ($E_{1/2}$) and limiting current densities (j_{lim}) are shown in Figure 4B in the manuscript (Note: *indicates values estimated from their data and description). LSV conditions are 1600 rpm at 5 mV/sec in O_2 saturated 0.1 M KOH unless otherwise mentioned.

Reference as in the manuscript. (Electrocatalyst-journal-published year)	Reference in SI	$E_{1/2}$ V vs RHE	Limiting current density, (mA cm^{-2})	Stability
N´-GUITAR/KB	TW	0.82	6.3	No loss till 30K cycle
Pt/C	TW	0.87	5.26	- 38 mV shift in $E_{1/2}$ after 30K cycle -9% current loss after 30K cycle test - 38% loss in ECSA after 30K cycle
Carbon based electrocatalysts				
60. ($N_{0.54}$–Z_3/M_1-900, *Env.Sci*-2019)	20	0.82	4.3	-0.25 mA cm^{-2} loss after 1000 CV test -2.6% current decay over 24hr at 0.565 V vs RHE
61. (N-GNr@CNT, *Nature communication* -2018)	21	0.839	5.1	N/A
62. (Porous carbon, *Energy Environ. Sci*.-2014,)	22	0.70	4.6	-25% current decay over 6.9hr at 0.4V vs RHE
63. (N-Porous carbon, *Nanomaterials* -2020)	23	0.76	3.6*	-13.5% current decay over 10 hr at 0.8V vs RHE
64. (C_{60}-SWCNT, *J. Am. Chem. Soc*.-2019)	24	0.84	1.73	-7.5% current decay over 50hr at 0.7 V vs RHE
64. (NPDC-1.09, *Sustainable Energy & Fuels*-2019)	25	0.84	6.01	-11% current decay over 22hr at 0.8V vs RHE -15mV shift after 1000 CV test

14.(N-GRW, *Science Advances* -2016)	26	0.84	3.6	-10% current decay over 12-hour test at 0.7 V vs RHE -15 mV shift in $E_{1/2}$ after 2000 cycle (35 mV $E_{1/2}$ shift for Pt/C)
24. (N, F-Carbon-1000, A*CS Appl. Mater. Interfaces*-2017)	9	0.84	5.2	-9% current decay over 5 hr use at 0.4V vs RHE - $E_{1/2}$ shift by 10 mv after 10000 CV cycle
56. (Hierarchically tubular –NCTs, *journal of materials chemistry A*-2017)	13	0.76	4.9	-20% current decay over 50 hr test at 0.65 V vs RHE
66.(NGRO, *ACS Appl. Nano Mater.* - 2019,)	27	0.84	2.5	-$E_{1/2}$ shift by 20 mV shift after 10000 cycles
78. (N-carbon nanofibers N-CN, *nano energy*-2015)	28	0.8	5.6*	-$E_{1/2}$ shift by 20 mV shift after 10000 cycles (40 mV $E_{1/2}$ shift for Pt/C)
69.(Carbon foam *Angewandte chemie*-2019)	29	0.87	4.2*	-20% current decay over 8.3 hr at 0.87 V vs RHE
39.(N-GNR8.3, *ACS Appl. Mater. Interfaces*-2014,)	30	N/A	3.5*	-4.9% current decay over 1.38 hr at -0.3 V vs Ag/AgCl
Metal-based electrocatalysts				
67. (Atomically dispersed Zn–N–C, *Angew. Chem. Int. Ed.*-2019)	31	0.87	5.0	-$E_{1/2}$ shift by 18 mV shift after 10000 cycle
68.(10Co-N@DCNF *Angew. Chem. In. Ed*.-2020)	32	0.83	6.36	-$E_{1/2}$ shift by 10 mV after 5000 cycle -5 % current decay over 8.3 hr at 0.6 V vs RHE
70.(CAN-Pc(Fe/Co), *Angewandte*- 2019)	33	0.84	5.23	-25.4% current decay over 3.3 hr at 0.85 V vs RHE
71.(Cu-based SACs, *J. Mater. Chem.* ***A***-2019)	34	0.81	5.8*	-3.5% current decay over 16 min.

				-$E_{1/2}$ shift by 9 mV shift after 5000 cycles
72.(mesoporous,3D-Co–N–C, *J. Mater. Chem. A*- 2018)	35	0.83	5.9*	-$E_{1/2}$ shift by 22 mV after 5000 cycles
54. (Co-doped with N and S, *J. Mater. Chem. A*- 2017)	11	0.837	5.35*	- $E_{1/2}$ shift by 5 mV after 2000 cycle test (55 mV $E_{1/2}$ shift for Pt/C) -8.1 % current decay over 24 hr at 0.8 V vs RHE
73. (AgPdPt Nanotubes, *ACS Appl. Nano Mater*.- 2019)	36	0.90	5.2	-$E_{1/2}$ shift by 11 mV after 5000 cycle -21.5% current decay over 5 hr at 0.5V (Pt/C 6% decrease in current and, > 11 mV shift in $E_{1/2}$)
77. (Fe_3C-Encapsulated Fe–N-Doped Carbon, *Langmuir* - 2018)	37	0.805	5.6@0.275	-$E_{1/2}$ shift by 5 mV shift after 10000 cycle -8.3% current decay over 5.5 hr test (For Pt/C 72 mV 30% i li decrease.)
30. (Cobalt-N Co-doped carbon, *Applied catalysis B; Environmental* -2016)	8	0.83	N/A	-$E_{1/2}$ shift by 3 mV after 5000 cycle (24 mV for Pt/C)
45. (Co-N-doped carbon, *Chemelectrochem*-2018)	17	N/A	N/A	-$E_{1/2}$ shift by 18 mV after 3000 cycle (45mV for Pt/C)

Tafel slope Analysis:

Figure S2.6: Shows the Tafel slopes in the region in the low potential region above -0.150 V are 0.110 and 0.098 V/decade for Pt/C and N'-GUITAR/KB, respectively. These are shown below with GUITAR/KB (0.138 V/decade).

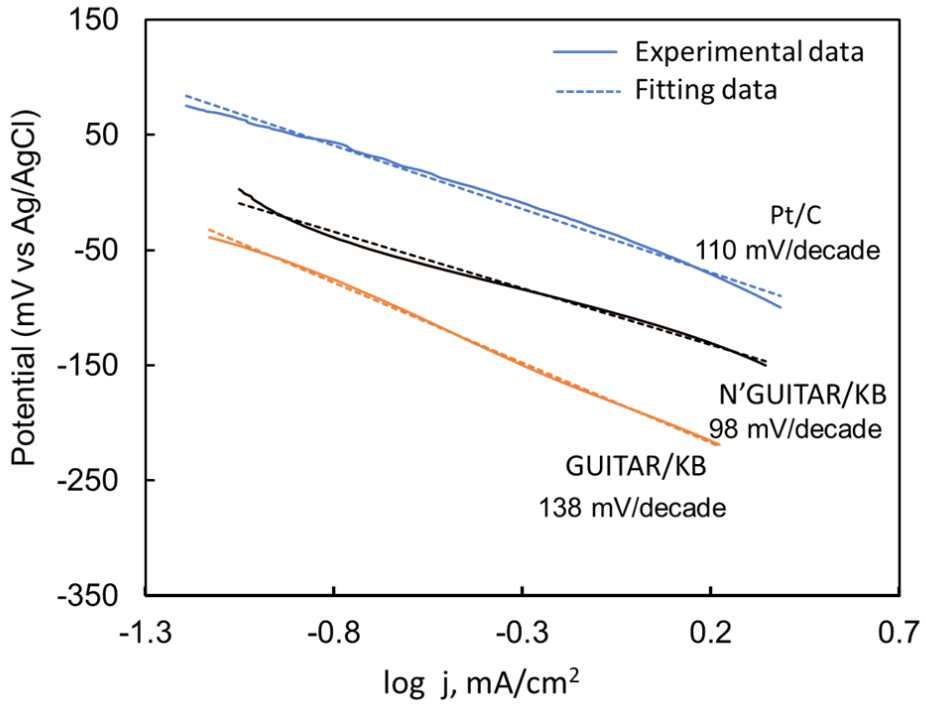

Figure S2.6: Tafel slopes for GUITAR/KB, N'-GUITAR/KB, and Pt/C. Slopes were calculated from ORR RDE LSV recorded at 1600rpm and 5 mV/sec, as shown in Figure 2.4A.

Number of electron transfer (n) studies for GUITAR/KB and Pt/C:

The number of electron transfer during ORR was estimated from rotating disk electrode linear sweep voltammetry (RDE-LSV) at 5 mV/sec in 0.1M KOH. From the slope of Koutecky-Levich (K-L) plots, n = 2.6 to 2.8 for GUITAR/KB and n = 3.6 to 3.7 (Figure S2.7, Equation 4 manuscript) for Pt/C within the potential range of -0.4 V to -0.7 V.

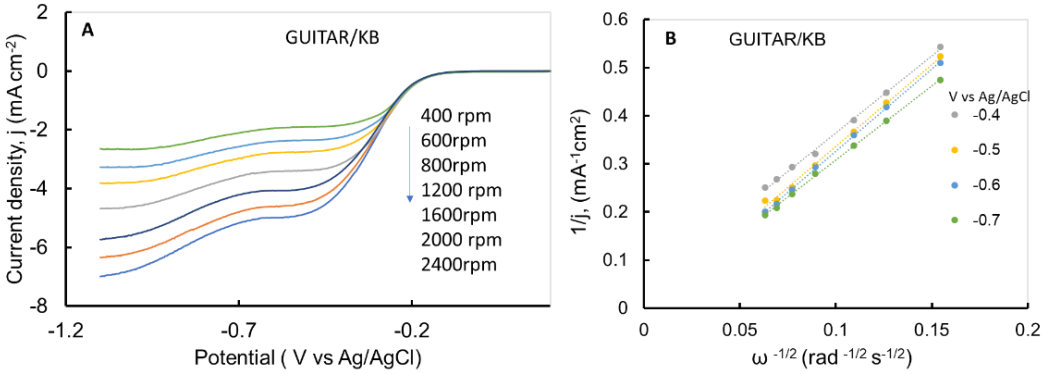

Figure S2.7: (A) Background corrected RDE-LSV in O_2 saturated 0.1 M KOH at 5 mV/sec at different rotation speeds with GUITAR/KB. (B) K-L plot for GUITAR/KB.

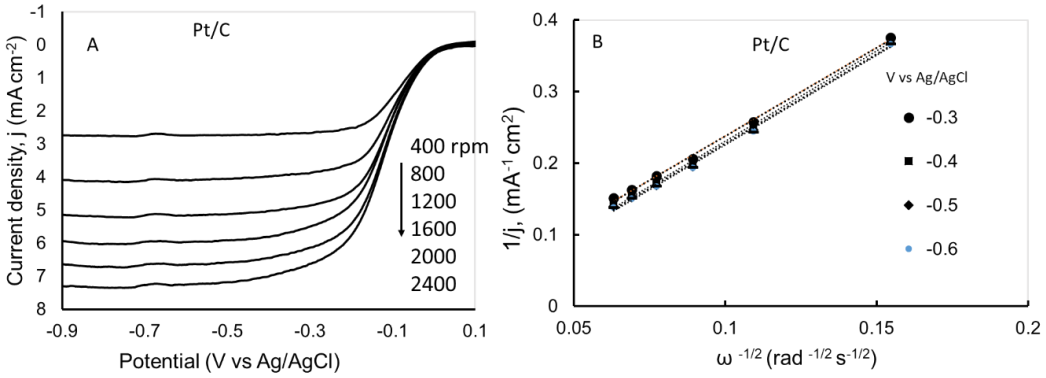

Figure S2.8: (A) Background corrected RDE-LSV in O_2 saturated 0.1 M KOH at 5 mV/sec at different rotation speeds (rpm-rotations per minute) with Pt/C. (B) K-L plot for Pt/C.

References:

(1) Voiry, D.; Chhowalla, M.; Gogotsi, Y.; Kotov, N. A.; Li, Y.; Penner, R. M.; Schaak, R. E.; Weiss, P. S. Best Practices for Reporting Electrocatalytic Performance of Nanomaterials. *ACS Nano* **2018**, *12* (10), 9635–9638. https://doi.org/10.1021/acsnano.8b07700.

(2) Garsany, Y.; Baturina, O. A.; Swider-Lyons, K. E.; Kocha, S. S. Experimental Methods for Quantifying the Activity of Platinum Electrocatalysts for the Oxygen Reduction Reaction. *Anal. Chem.* **2010**, *82* (15), 6321–6328. https://doi.org/10.1021/ac100306c.

(3) Łukaszewski, M. Electrochemical Methods of Real Surface Area Determination of Noble Metal Electrodes – an Overview. **2016**. https://doi.org/10.20964/2016.06.71.

(4) Begum, H.; Kim, Y.-B. Improvement of Catalytic Activity of Platinum Nanoparticles Decorated Carbon Graphene Composite on Oxygen Electroreduction for Fuel Cells. *Processes* **2019**, *7* (9), 586. https://doi.org/10.3390/pr7090586.

(5) Lim, B.; Jiang, M.; Camargo, P. H. C.; Cho, E. C.; Tao, J.; Lu, X.; Zhu, Y.; Xia, Y. Pd-Pt Bimetallic Nanodendrites with High Activity for Oxygen Reduction. *Science* **2009**, *324* (5932), 1302–1305. https://doi.org/10.1126/science.1170377.

(6) Panomsuwan, G.; Saito, N.; Ishizaki, T. Nitrogen-Doped Carbon Nanoparticle–Carbon Nanofiber Composite as an Efficient Metal-Free Cathode Catalyst for Oxygen Reduction Reaction. *ACS Appl. Mater. Interfaces* **2016**, *8* (11), 6962–6971. https://doi.org/10.1021/acsami.5b10493.

(7) Men, B.; Sun, Y.; Liu, J.; Tang, Y.; Chen, Y.; Wan, P.; Pan, J. Synergistically Enhanced Electrocatalytic Activity of Sandwich-like N-Doped Graphene/Carbon Nanosheets Decorated by Fe and S for Oxygen Reduction Reaction. *ACS Appl. Mater. Interfaces* **2016**, *8* (30), 19533–19541. https://doi.org/10.1021/acsami.6b06329.

(8) Sun, T.; Xu, L.; Li, S.; Chai, W.; Huang, Y.; Yan, Y.; Chen, J. Cobalt-Nitrogen-Doped Ordered Macro-/Mesoporous Carbon for Highly Efficient Oxygen Reduction Reaction. *Applied Catalysis B: Environmental* **2016**, *193*, 1–8. https://doi.org/10.1016/j.apcatb.2016.04.006.

(9) Lv, Y.; Yang, L.; Cao, D. Nitrogen and Fluorine-Codoped Porous Carbons as Efficient Metal-Free Electrocatalysts for Oxygen Reduction Reaction in Fuel Cells. *ACS Appl. Mater. Interfaces* **2017**, *9* (38), 32859–32867. https://doi.org/10.1021/acsami.7b11371.

(10) Zhong, H.; Zhang, S.; Jiang, J.; Li, D.; Tang, P.; Alonso-Vante, N.; Feng, Y. Improved Electrocatalytic Performance of Tailored Metal-Free Nitrogen-Doped Ordered Mesoporous Carbons for the Oxygen Reduction Reaction. *ChemElectroChem* **2018**, *5* (14), 1899–1904. https://doi.org/10.1002/celc.201700910.

(11) Wang, Z.; Peng, S.; Hu, Y.; Li, L.; Yan, T.; Yang, G.; Ji, D.; Srinivasan, M.; Pan, Z.; Ramakrishna, S. Cobalt Nanoparticles Encapsulated in Carbon Nanotube-Grafted Nitrogen and Sulfur Co-Doped Multichannel Carbon Fibers as Efficient Bifunctional Oxygen Electrocatalysts. *J. Mater. Chem. A* **2017**, *5* (10), 4949–4961. https://doi.org/10.1039/C6TA10291C.

(12) Qin, L.; Yuan, Y.; Wei, W.; Lv, W.; Niu, S.; He, Y.-B.; Zhai, D.; Kang, F.; Kim, J.-K.; Yang, Q.-H.; Lu, J. Graphene-Directed Formation of a Nitrogen-Doped Porous Carbon Sheet with High Catalytic Performance for the Oxygen Reduction Reaction. *J. Phys. Chem. C* **2018**, *122* (25), 13508–13514. https://doi.org/10.1021/acs.jpcc.7b12327.

(13) Wei, W.; Ge, H.; Huang, L.; Kuang, M.; Al-Enizi, A. M.; Zhang, L.; Zheng, G. Hierarchically Tubular Nitrogen-Doped Carbon Structures for the Oxygen Reduction Reaction. *J. Mater. Chem. A* **2017**, *5* (26), 13634–13638. https://doi.org/10.1039/C7TA02658G.

(14) Huang, X.; Yin, X.; Yu, X.; Tian, J.; Wu, W. Preparation of Nitrogen-Doped Carbon Materials Based on Polyaniline Fiber and Their Oxygen Reduction Properties. *Colloids and Surfaces A: Physicochemical and Engineering Aspects* **2018**, *539*, 163–170. https://doi.org/10.1016/j.colsurfa.2017.12.024.

(15) Thanh, T. D.; Chuong, N. D.; Hien, H. V.; Kim, N. H.; Lee, J. H. CuAg@Ag Core–Shell Nanostructure Encapsulated by N-Doped Graphene as a High-Performance Catalyst for Oxygen Reduction Reaction. *ACS Appl. Mater. Interfaces* **2018**, *10* (5), 4672–4681. https://doi.org/10.1021/acsami.7b16294.

(16) Sun, X.; Song, P.; Zhang, Y.; Liu, C.; Xu, W.; Xing, W. A Class of High Performance Metal-Free Oxygen Reduction Electrocatalysts Based on Cheap Carbon Blacks. *Scientific Reports* **2013**, *3*, 2505. https://doi.org/10.1038/srep02505.

(17) Han, H.; Chao, S.; Bai, Z.; Wang, X.; Yang, X.; Qiao, J.; Chen, Z.; Yang, L. Metal-Organic-Framework-Derived Co Nanoparticles Deposited on N-Doped Bimodal Mesoporous Carbon Nanorods as Efficient Bifunctional Catalysts for Rechargeable Zinc−Air Batteries. *ChemElectroChem* **2018**, *5* (14), 1868–1873. https://doi.org/10.1002/celc.201701289.

(18) Yang, F.; Abadia, M.; Chen, C.; Wang, W.; Li, L.; Zhang, L.; Rogero, C.; Chuvilin, A.; Knez, M. Design of Active and Stable Oxygen Reduction Reaction Catalysts by Embedding CoxOynanoparticles into Nitrogen-Doped Carbon. *Nano Res.* **2017**, *10* (1), 97–107. https://doi.org/10.1007/s12274-016-1269-5.

(19) Chen, R.; Yan, J.; Liu, Y.; Li, J. Three-Dimensional Nitrogen-Doped Graphene/MnO Nanoparticle Hybrids as a High-Performance Catalyst for Oxygen Reduction Reaction. *J. Phys. Chem. C* **2015**, *119* (15), 8032–8037. https://doi.org/10.1021/acs.jpcc.5b00306.

(20) Li, X.; Guan, B. Y.; Gao, S.; Lou, X. W. (David). A General Dual-Templating Approach to Biomass-Derived Hierarchically Porous Heteroatom-Doped Carbon Materials for Enhanced Electrocatalytic Oxygen Reduction. *Energy Environ. Sci.* **2019**, *12* (2), 648–655. https://doi.org/10.1039/C8EE02779J.

(21) Xue, L.; Li, Y.; Liu, X.; Liu, Q.; Shang, J.; Duan, H.; Dai, L.; Shui, J. Zigzag Carbon as Efficient and Stable Oxygen Reduction Electrocatalyst for Proton Exchange Membrane Fuel Cells. *Nature Communications* **2018**, *9* (1), 3819. https://doi.org/10.1038/s41467-018-06279-x.

(22) Zhang, P.; Sun, F.; Xiang, Z.; Shen, Z.; Yun, J.; Cao, D. ZIF-Derived in Situ Nitrogen-Doped Porous Carbons as Efficient Metal-Free Electrocatalysts for Oxygen Reduction Reaction. *Energy Environ. Sci.* **2013**, *7* (1), 442–450. https://doi.org/10.1039/C3EE42799D.

(23) Sathiskumar, C.; Ramakrishnan, S.; Vinothkannan, M.; Karthikeyan, S.; Yoo, D. J.; Rhan Kim, A. Nitrogen-Doped Porous Carbon Derived from Biomass Used as Trifunctional

Electrocatalyst toward Oxygen Reduction, Oxygen Evolution and Hydrogen Evolution Reactions. *Nanomaterials (Basel)* **2019**, *10* (1). https://doi.org/10.3390/nano10010076.

(24) Gao, R.; Dai, Q.; Du, F.; Yan, D.; Dai, L. C60-Adsorbed Single-Walled Carbon Nanotubes as Metal-Free, PH-Universal, and Multifunctional Catalysts for Oxygen Reduction, Oxygen Evolution, and Hydrogen Evolution. *J. Am. Chem. Soc.* **2019**, *141* (29), 11658–11666. https://doi.org/10.1021/jacs.9b05006.

(25) Han, L.; Cui, X.; Liu, Y.; Han, G.; Wu, X.; Xu, C. (Charles); Li, B. Nitrogen and Phosphorus Modification to Enhance the Catalytic Activity of Biomass-Derived Carbon toward the Oxygen Reduction Reaction. *Sustainable Energy Fuels* **2020**, *4* (6), 2707–2717. https://doi.org/10.1039/C9SE00985J.

(26) Yang, H. B.; Miao, J.; Hung, S.-F.; Chen, J.; Tao, H. B.; Wang, X.; Zhang, L.; Chen, R.; Gao, J.; Chen, H. M.; Dai, L.; Liu, B. Identification of Catalytic Sites for Oxygen Reduction and Oxygen Evolution in N-Doped Graphene Materials: Development of Highly Efficient Metal-Free Bifunctional Electrocatalyst. *Sci Adv* **2016**, *2* (4), e1501122. https://doi.org/10.1126/sciadv.1501122.

(27) Dumont, J. H.; Martinez, U.; Artyushkova, K.; Purdy, G. M.; Dattelbaum, A. M.; Zelenay, P.; Mohite, A.; Atanassov, P.; Gupta, G. Nitrogen-Doped Graphene Oxide Electrocatalysts for the Oxygen Reduction Reaction. *ACS Appl. Nano Mater.* **2019**, *2* (3), 1675–1682. https://doi.org/10.1021/acsanm.8b02235.

(28) Liang, H.-W.; Wu, Z.-Y.; Chen, L.-F.; Li, C.; Yu, S.-H. Bacterial Cellulose Derived Nitrogen-Doped Carbon Nanofiber Aerogel: An Efficient Metal-Free Oxygen Reduction Electrocatalyst for Zinc-Air Battery. *Nano Energy* **2015**, *11*, 366–376. https://doi.org/10.1016/j.nanoen.2014.11.008.

(29) Gao, J.; Wang, Y.; Wu, H.; Liu, X.; Wang, L.; Yu, Q.; Li, A.; Wang, H.; Song, C.; Gao, Z.; Peng, M.; Zhang, M.; Ma, N.; Wang, J.; Zhou, W.; Wang, G.; Yin, Z.; Ma, D. Construction of a Sp3/Sp2 Carbon Interface in 3D N-Doped Nanocarbons for the Oxygen Reduction Reaction. *Angewandte Chemie International Edition* **2019**, *58* (42), 15089–15097. https://doi.org/10.1002/anie.201907915.

(30) Liu, M.; Song, Y.; He, S.; Tjiu, W. W.; Pan, J.; Xia, Y.-Y.; Liu, T. Nitrogen-Doped Graphene Nanoribbons as Efficient Metal-Free Electrocatalysts for Oxygen Reduction. *ACS Appl. Mater. Interfaces* **2014**, *6* (6), 4214–4222. https://doi.org/10.1021/am405900r.

(31) Li, J.; Chen, S.; Yang, N.; Deng, M.; Ibraheem, S.; Deng, J.; Li, J.; Li, L.; Wei, Z. Ultrahigh-Loading Zinc Single-Atom Catalyst for Highly Efficient Oxygen Reduction in Both Acidic and Alkaline Media. *Angewandte Chemie International Edition* **2019**, *58* (21), 7035–7039. https://doi.org/10.1002/anie.201902109.

(32) Yang, Q.; Jia, Y.; Wei, F.; Zhuang, L.; Yang, D.; Liu, J.; Wang, X.; Lin, S.; Yuan, P.; Yao, X. Understanding the Activity of Co-N4−xCx in Atomic Metal Catalysts for Oxygen Reduction Catalysis. *Angewandte Chemie* **2020**, *132* (15), 6178–6183. https://doi.org/10.1002/ange.202000324.

(33) Yang, S.; Yu, Y.; Dou, M.; Zhang, Z.; Dai, L.; Wang, F. Two-Dimensional Conjugated Aromatic Networks as High-Site-Density and Single-Atom Electrocatalysts for the Oxygen Reduction Reaction. *Angewandte Chemie International Edition* **2019**, *58* (41), 14724–14730. https://doi.org/10.1002/anie.201908023.

(34) Cui, L.; Cui, L.; Li, Z.; Zhang, J.; Wang, H.; Lu, S.; Xiang, Y. A Copper Single-Atom Catalyst towards Efficient and Durable Oxygen Reduction for Fuel Cells. *J. Mater. Chem. A* **2019**, *7* (28), 16690–16695. https://doi.org/10.1039/C9TA03518D.

(35) Guo, C.; Li, Y.; Liao, W.; Liu, Y.; Li, Z.; Sun, L.; Chen, C.; Zhang, J.; Si, Y.; Li, L. Boosting the Oxygen Reduction Activity of a Three-Dimensional Network Co–N–C Electrocatalyst via Space-Confined Control of Nitrogen-Doping Efficiency and the Molecular-Level Coordination Effect. *J. Mater. Chem. A* **2018**, *6* (27), 13050–13061. https://doi.org/10.1039/C8TA03759K.

(36) Deng, Y.; Yin, S.; Liu, Y.; Lu, Y.; Cao, X.; Wang, L.; Wang, H.; Zhao, Y.; Gu, H. Mesoporous AgPdPt Nanotubes as Electrocatalysts for the Oxygen Reduction Reaction. *ACS Appl. Nano Mater.* **2019**, *2* (4), 1876–1882. https://doi.org/10.1021/acsanm.8b02206.

(37) Xin, X.; Qin, H.; Cong, H.-P.; Yu, S.-H. Templating Synthesis of Mesoporous Fe3C-Encapsulated Fe–N-Doped Carbon Hollow Nanospindles for Electrocatalysis. *Langmuir* **2018**, *34* (17), 4952–4961. https://doi.org/10.1021/acs.langmuir.8b00548.

Chapter 3: "Electrochemical Aspects of a Nitrogen-Doped Pseudo-Graphitic Carbon Material: Resistance to Electrode Fouling by Air-Aging and Dopamine Electro-oxidation," *Journal of Carbon Research* 2020, *6*(4), 68.

3.1 Abstract

The nitrogen-doped form of GUITAR (pseudo-Graphite from the University of Idaho Thermalized Asphalt Reaction) was examined by X-ray photoelectron, Raman, and X-ray diffraction spectroscopies and cyclic voltammetry (CV). Electrochemical studies indicate that N-GUITAR exhibits significant resistance to fouling by adsorption and by passivation. Unlike other carbon materials, it maintains fast heterogenous electron transfer (HET) kinetics with $Fe(CN)_6^{3-/4-}$ with exposure to air. The CV peak potential separation (ΔEp) of 66 mV increased to 69 mV in 3 hours vs. 67 to 221 mV for a highly oriented pyrolytic graphite (HOPG) electrode. Water contact angle measurements indicate that N-GUITAR was able to better maintain a hydrophilic state during the 3-hour exposure, going from 55.8 to 70.4° while HOPG increased from 63.8 to 80.1°. This indicates that N-GUITAR better-resisted adsorption of volatile organic compounds. CV studies of dopamine also indicate N-GUITAR is resistant to passivation. The ΔEp for the dopamine/o-dopaminoquinone couple is 83 mV indicating fast HET rates. This is reflected in the peak current ratios for the oxidation and reduction processes of 1.3, indicating that o-dopaminoquinone is not lost to passivation processes. This ratio, along with the minimal signal attenuation, is the best reported in the literature.

Keywords: Adsorption; Dopamine; Electrode fouling; Electrode kinetics; Nitrogen doping; pseudo-Graphite

3.2 Introduction

GUITAR (pseudo-Graphite from the University of Idaho Thermalized Asphalt Reaction) is a nanocrystalline graphite-like hydrogenated amorphous carbon (85% sp^2 and 15% sp^3 carbon) described in detail in recent publications [1–7]. It has morphological features similar to classical graphites but has divergent chemical and physical properties. Most prominent among these is that GUITAR has fast heterogeneous electron transfer (HET) rates at its basal plane. The defect-rich nature of GUITAR results in a high density of electronic states (DOS) near its Fermi-level. Graphitic materials have low DOS or are subject to air-aging; either effect creates sluggish HET kinetics [8–11]. Another feature is the resistance to corrosion that surpasses graphitic materials by 3 orders of magnitude in corrosion currents, and surpasses the potential windows of graphitic materials by 1 V [1,2]. In these aspects, it equals sp^3 carbon electrodes.
In summary, it has the best combination of fast HET and high corrosion resistance of any electrode [1]. Recent studies have indicated that introduction of nitrogen impurities within the carbon lattice significantly increases DOS, thus improving HET rates [12–14]. This effect has been used to improve electrochemical sensor performance, oxygen reduction reaction (ORR) catalysts in fuel cells, batteries, and ultracapacitors [12].

Electrode fouling is the process by which current signal attenuation occurs when sample matrix components undergo either passive adsorption or by redox processes which forms a polymeric film on the surface [11,15–18]. Both create a barrier to electron transfer. Recent studies indicate that fouling process of highly oriented pyrolytic graphite electrodes (HOPG) when exposed to laboratory air is through adsorption of volatile organic compounds (VOC's), which decrease HET rates with the $Fe(CN)_6^{3-/4-}$ redox probe [11,15]. The important biologic analyte, dopamine, undergoes electron transfer that gives rise to a cascade of reactions that result in an insulating layer of polydopamine [18,19]. There is a constant search for electrodes that exhibit

minimized fouling characteristics. Such materials will find eventual use in long-term sensors and implantable electrodes for in-vivo analyses and bionics [20–22]. For this investigation, we synthesized, characterized, and examined nitrogen-doped GUITAR (N-GUITAR) electrodes for its HET rates, resistance to corrosion, and fouling by air-aging and with dopamine voltammetry.

3.3 Methods and Materials

Materials and Chemicals: The reagents consisted of N_2(g) (>99.5 %, Oxarc, WA, USA), acetonitrile (Fisher Scientific, Fair Lawn, NJ, USA), dopamine hydrochloride (Sigma-Aldrich, St. Louis, MO, USA). Potassium monophosphate (99.6%), potassium diphosphate (99.8%), potassium chloride (99.7%) (Fisher Scientific, Waltham, NJ, USA), and potassium ferricyanide (Acros Organics, Morris Plains, NJ, USA). All were used as received. The quartz tube was obtained from Technical Glass Products, Inc. (Painesville Twp., OH, USA), cut into small wafers (~2cm x 0.5 cm), and used as a deposition substrate.

Synthesis of nitrogen-doped pseudo-graphite (N-GUITAR): N-GUITAR samples were prepared via a chemical vapor deposition (CVD) method. This apparatus is shown in Figure 3.1. The target substrate was loaded into a quartz boat, and the tube furnace was heated to 900°C with N_2 gas for 10 min prior to the addition of acetonitrile vapor. This system was sealed with ceramic wool to minimize air back flow. Deposition commenced by stopping the N_2 flow and allowing the passage of acetonitrile vapor from a round bottom flask at >80 °C for 25 minutes. The N_2 flow was resumed, and the tube furnace was cooled to room temperature before coated samples were removed.

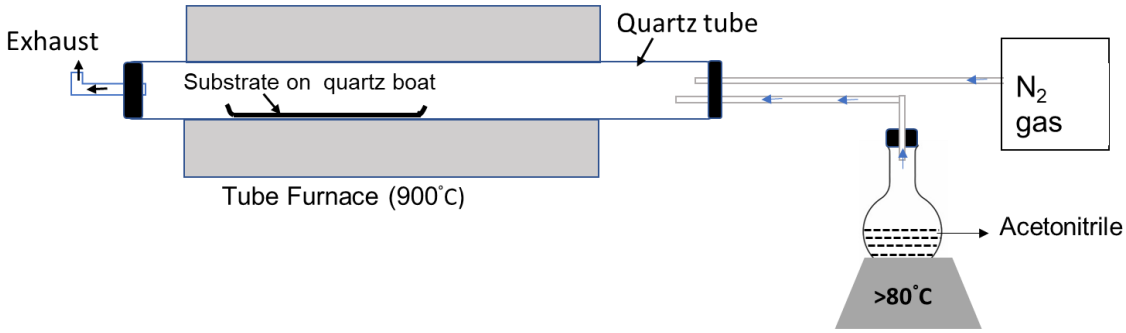

Figure 3.1. Schematic for the synthesis of N-doped pseudo-graphite using a modified CVD technique.

Scanning electron microscopy (SEM): These images were recorded with a FEI Teneo field emission microscope operating at an accelerating voltage of 2 kV, a spot size of 25-50 pA, with a secondary electron detector. Peeled HOPG thin sheet, GUITAR, and N-GUITAR flakes were attached to a mounting disk with double-sided carbon tape.

X-ray photoelectron spectroscopy (XPS): Spectra were recorded at Oklahoma State University in a custom-built vacuum chamber with a base pressure of 5×10^{-9} torr. Measurements were acquired with the Al Kα emission line (1486.6 eV) and a hemispherical energy analyzer with a resolution of 25 meV. Spectra were acquired at room temperature. Deconvolved C1s and N1s XPS peaks were fitted to Gaussian curves with Shirley background subtraction and with the full width at half maximum kept constant.

Raman: The Raman spectra were collected using a WITec™ alpha300 R Raman instrument (Germany), UHT-300 spectrometer with an Andor™ DU970N-BV CCD detector. The excitation source was a 532.5 nm, 100-mW frequency-doubled Nd:YAG laser.

Powder X-ray diffraction (XRD): XRD was conducted on a Siemens D5000 Diffractometer (Germany). The spectra were taken with Cu K-alpha radiation (0.154 nm) at 40 kV, and 30 mA in the range of 2θ = 2-80° and step size of 0.05° at room temperature.

Water contact angle measurement (WCA): Contact angle measurements were conducted with a PG-2 Pocket Goniometer (Thwing-Albert) under ambient conditions in dynamic mode using the sessile water drop (4-9 µL) method on the carbon surfaces. Contact angle was measured by capturing images over a 6 second period using Pocket Goniometer v.3.3 software [23]. The GUITAR and N-GUITAR samples were prepared by peeling them from the quartz substrate using double-sided tape (GUITAR was removed all at once, leaving a bare substrate behind), and testing was done on the freshly exposed underside. The HOPG was prepared in a similar manner using double-sided tape (HOPG can be readily exfoliated a few layers at a time), and testing was carried out on the freshly exposed underside. Each measurement was carried out at 5 different spots at each time interval, and the values were averaged.

Electrode fabrication and Electrochemistry: The GUITAR and N-GUITAR working electrodes were prepared as described in previous study [1]. Freshly exfoliated HOPG electrode was prepared by using adhesive tape, copper tape was used as a current collector, and this surface was used within 30 seconds of cleavage. All electrochemical experiments were performed in an undivided three-electrode cell, with an Ag/AgCl (3 M KCl, aq) reference electrode and a graphite rod as a counter electrode. Electrochemical analyses were conducted with either a Bioanalytical Systems CV-50W (West Lafayette, IN, USA) or a Gamry Instruments 1000 (Warminster, PA, USA) potentiostat. All solutions were prepared using house deionized water with further purification through an activated carbon cartridge (Barnstead, model D8922, Dubuque, IA). The cyclic voltammograms were modeled for standard rate constants (k^0) using Digisim 3.03b software (Bioanalytical Systems, Inc. West Lafayette, IN, USA). Dopamine oxidation peak current and peak separation values for literature was estimated by using graph grabber v2.0.2.

3.4 Results and Discussion

3.4.1 X-ray Photoelectron Spectroscopy (XPS) Analysis:

All XPS peak assignments are based on recent literature [24–27]. The wide scan XPS of N-GUITAR in Figure 3.2A reveals an atomic percentage of 86.4% C, 9.7% N, and 3.9% O based on the 284.1, 398.2, and 532.4 eV binding energy peaks, respectively. The based on deconvolved peaks the assignments for C1s (Figure 3.2B) peaks follow as 68.4% sp^2 C (284.6 eV), 21.1% sp^3 (286.1 eV), 7.8% C-N and C=N (287.6 eV), 2.7% C=O and COOH (289.4 eV). The material of this investigation is in line with other CVD-grown nitrogen-doped carbon materials that have N atomic content from 1 to 16% [14,28–31]. Also, the sp^2/sp^3 atomic ratio of this N-GUITAR is similar to undoped GUITAR in a previous investigation [1]. The O1s peak (Figure 3.2C) deconvolves to 55.8% N-O and C-O (532.1 eV) and 44.2% N=O and C=O (533.0 3 eV). For the N species in the N1s peaks (Figure 3.2D) the assignments are 23.7% pyridinic N (398.2 eV), 60.5% graphitic N-center (400.98 eV), 11.8% graphitic N- valley (403.0 eV) and 4% N-oxides (405.3 eV).

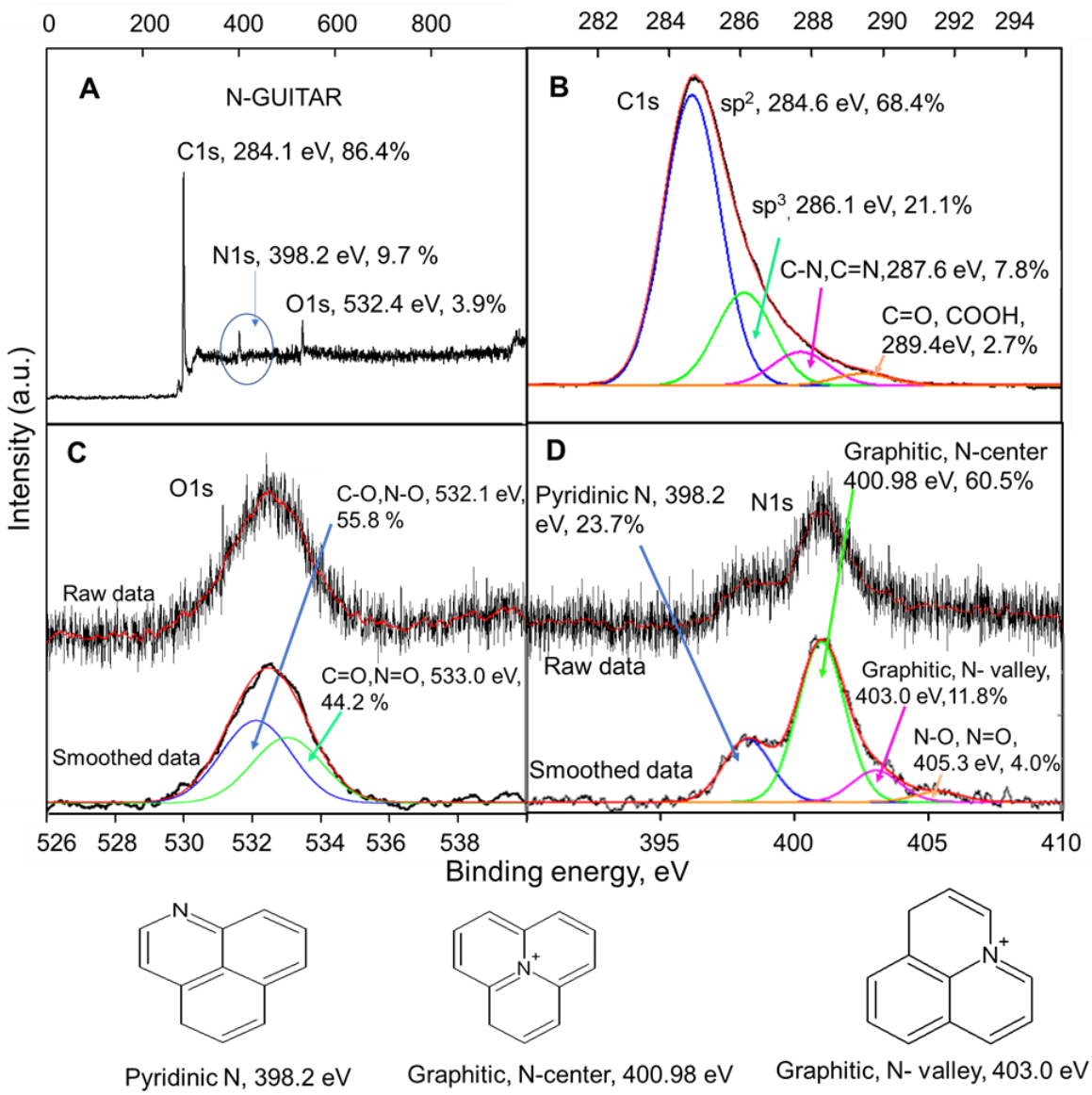

Figure 3.2. XPS analysis of N-doped pseudo graphite with the respective peak assignments and abundances. (A) the wide scan spectrum. The C1s (B), O1s (C), and N1s (D) peak with deconvolved components. The N1s and O1s spectra are presented with the raw and smoothed data using the Savitzky-Golay method. The structures of the nitrogen species are shown at the bottom.

3.4.2 Micrographs

Figure 3.3 shows the visual and microscopic features of GUITAR and N-GUITAR. The flakes

from both forms are undisguisable from each other and resemble high-quality graphite. From

the scanning electron micrographs (SEM), both a layered basal (BP) and edge plane (EP) morphology are evident. The thickness of the carbon films is 1.3-1.9 µm which increases with deposition time.

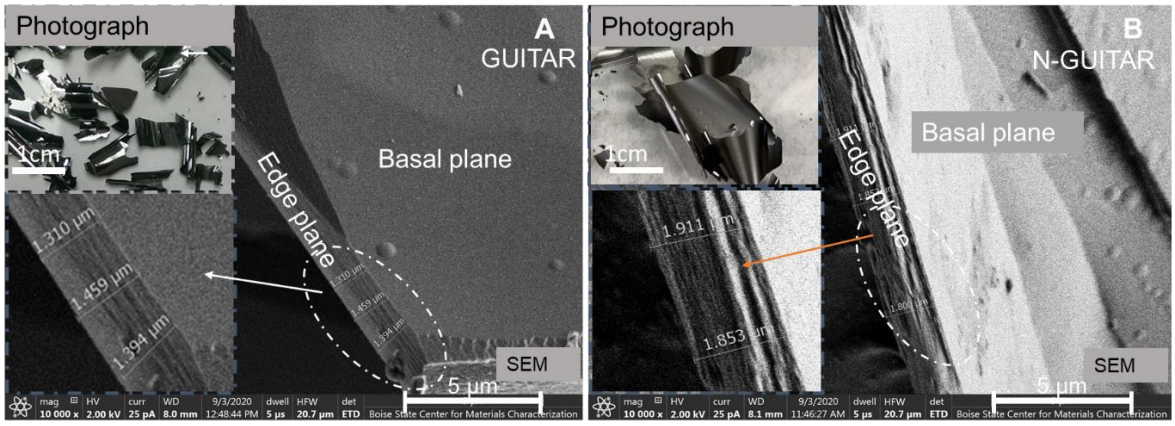

Figure 3.3. Scanning electron micrographs (SEM) of GUITAR (A) and N-GUITAR (B) with photographs of the flakes in the upper left insets. Both materials exhibit layered morphologies with edge and basal planes. The lower left insets show the SEMs of edge planes in more detail.

3.4.3 Raman Analysis

Raman spectra of N-GUITAR, GUITAR, and HOPG are shown in Figure 3.4. The D-band is related to the structural defects, while the G-band describes the degree of graphitization [32]. The HOPG spectrum is used as a reference standard for a low defect material. The GUITAR and N-GUITAR spectra indicate an upshift in the D-band to 1350 from 1340 cm^{-1} and downshift in G- band to 1566 from 1578 cm^{-1} after nitrogen doping. This is consistent with the trends observed in literature [33–35]. The increase in I_D/I_G from 1.15 to 1.66 follows the trends observed in the literature, which indicates that more defects are introduced with N-doping [33].

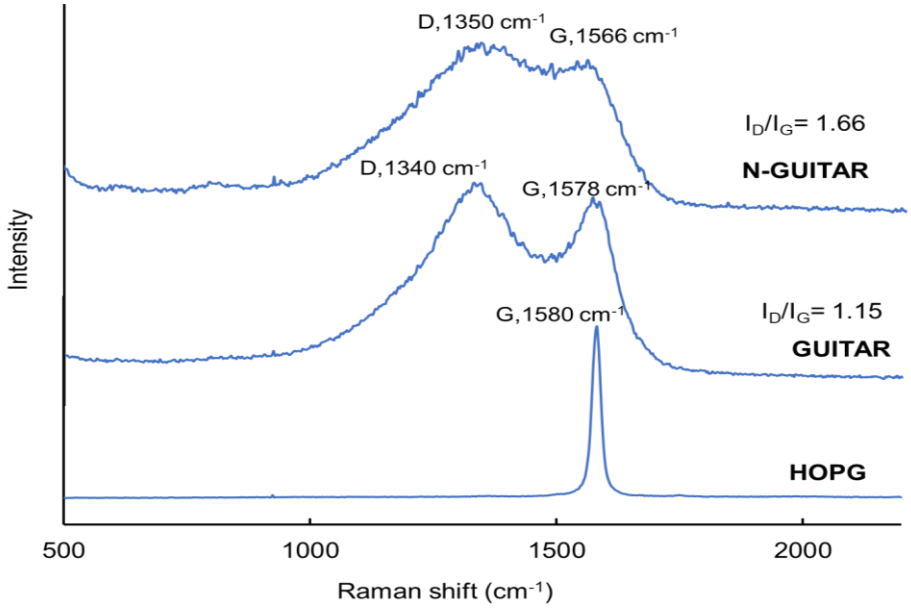

Figure 3.4. Raman spectra for N-GUITAR, GUITAR, and HOPG taken with a 532 nm laser.

3.4.4 X-ray Diffraction (XRD) Studies

Figure 3.5 shows the XRD spectra of N-GUITAR, GUITAR, and HOPG. The GUITAR XRD spectra are consistent with previous publications [1]. N-GUITAR shows a basal reflection (002) peak at $2\theta = 26.1°$, which is intermediate of GUITAR and HOPG (25.4° and 26.65°, respectively). The d-spacing, or average interlayer distance, for N-GUITAR, was found to be 341 pm, smaller than that of GUITAR (350 pm) but larger than that of HOPG (334 pm). The d-spacing was calculated from Bragg's law, $n\lambda = 2d\sin(\theta)$, where $n = 1$ and λ is the X-ray wavelength (0.154 nm). The average lateral grain size (La) for N-GUITAR and GUITAR were very similar, at 3.3 and 2.9 nm, respectively, making them both nano-crystalline. This is in contrast to HOPG, which will typically range from 30 nm to the low mm range, with the larger grain sizes indicating higher quality [36]. The grain size is calculated from Scherrer's law, $La = K\lambda/\beta\cos(\theta)$, where K = is the crystallite shape factor (1.84), β is the peak broadening at the half

maximum (FWHM), and θ is the Bragg angle [37]. This indicates that there are no major structural differences between GUITAR and N-GUITAR.

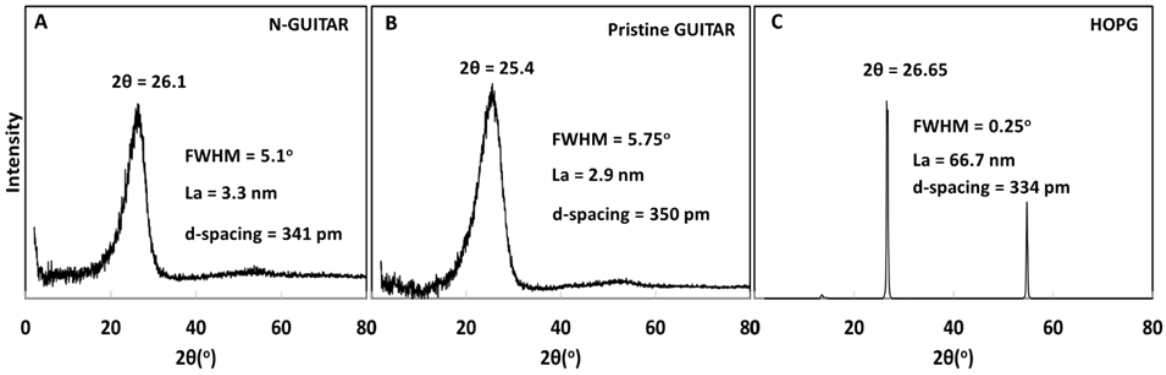

Figure 3.5. Powder XRD spectra of (A) N-GUITAR, (B) Pristine GUITAR, and (C) HOPG.

3.4.5 Aqueous Potential Windows.

The cyclic voltammograms of GUITAR and N-doped GUITAR in 1M H_2SO_4 at 50 mV/s are presented in Figure 3.6. Based on the cathodic and anodic limits at 200 μA/cm^2 the potential windows for GUITAR and N-doped GUITAR are 3.0 and 2.7 V, respectively. A decrease in potential window is commonly observed in N-doped materials when compared with their corresponding undoped analogs [38]. This is attributed to faster heterogeneous electron transfer kinetics of the N-doped carbon for hydrogen and oxygen evolution [38,39]. However, both N-GUITAR and GUITAR have aqueous potential windows that are 1 V greater than sp^2-hybridized carbon electrodes and match amorphous carbon (a-C) and boron-doped diamond (BDD) materials in this aspect [2,40]. Literature trends suggest that increasing sp^3-C content increases the potential window; however, at the cost of lowering the HET rate with the $Fe(CN)_6^{4-/3-}$ redox probe [1,41]. The GUITAR electrode counters this trend with a wide potential window and fast HET kinetics [1].

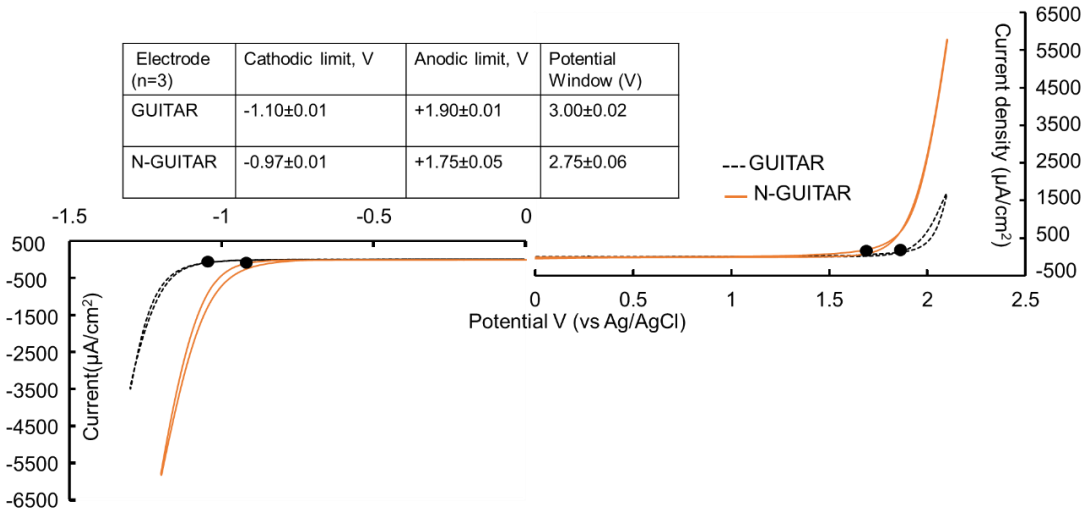

Figure 3.6 Cyclic voltammetric behavior of GUITAR (dashed line) and N-doped GUITAR (solid line) in 1 M H_2SO_4 taken at 50 mV/s. The starting potential for both anodic (right) and cathodic (left) sweeps is 0.0 V. The 200 µA/cm^2 potential limits are indicted with black dots, and the potential windows are listed in the table inset.

3.4.6 Tafel Corrosion Studies

Tafel polarization measurements were carried out in Ar saturated 1.0 M H_2SO_4 using a single compartment 1.0 L volume cell under vigorously stirred conditions (see Figure 3.7). The working electrodes were allowed to equilibrate in electrolyte solutions for ≥ 1 hour to attain an equilibrium prior to the start of polarization. The working electrodes were scanned from -0.5 to +0.5 V vs. Ag/AgCl at a scan rate of 1 mV/s. Corrosion current (i_{corr}) and corrosion potential (E_{corr}) were estimated by extrapolations of the respective Tafel plots[1]. The average i_{corr} of N-GUITAR is $7.3\times10^{-9} \pm 3.2\times10^{-9}$ A/cm^2, a very similar anodic stability to GUITAR ($2.07\times10^{-9} \pm 0.7\times10^{-9}$ A/cm^2). This is three orders of magnitude lower than a graphite rod ($1.82\times10^{-6} \pm 1.06\times10^{-6}$ A/cm^2), which falls into the typical range of other sp^2-C electrodes [1,42,43]. It is significant that both N-GUITAR and its undoped counterpart have anodic stability in the range of a-C and BDD electrodes (i_{corr} typically ranging from 10^{-9} to 10^{-8} A/cm^2) [44,45]. The corrosion resistance of GUITAR is based on lack of electrolyte intercalation through interplanar, and

basal plane defects [2,46,47]. The N-doped form apparently maintains this feature. The anodic limit of Figure 3.6 indicates that there is no intercalation of electrolyte through the BP of either GUITAR or N-GUITAR [2].

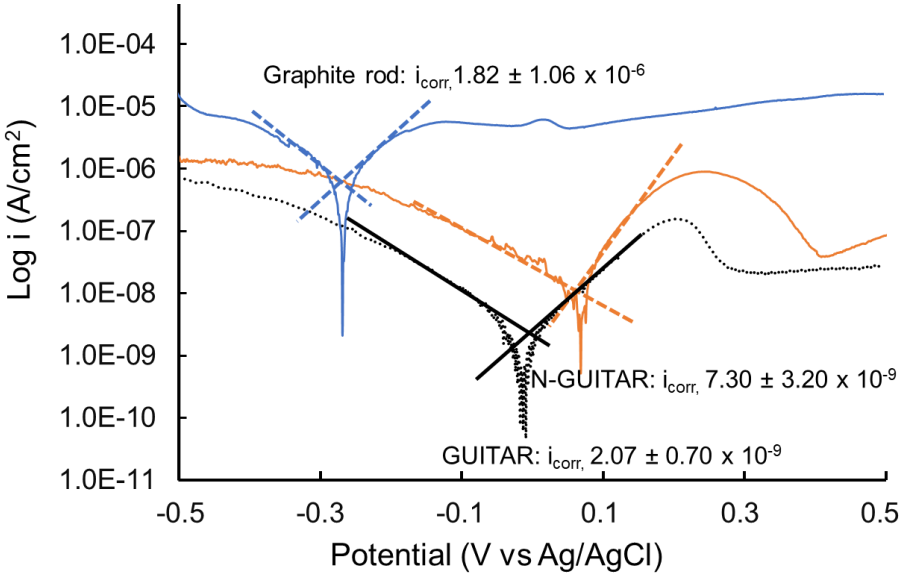

Figure 3.7. Tafel Plots with extrapolated corrosion currents (i_{corr}, A/cm^2) were indicated for each. The average and one standard deviation interval (n = 3) are reported for electrode material.

3.4.7 Heterogeneous Electron Transfer (HET) characteristics of N-GUITAR with $Fe(CN)_6^{3-/4-}$

The $Fe(CN)_6^{3-/4-}$ species is a common probe for measuring HET rates across the electrode-electrolyte interface. It is considered an inner-sphere redox couple and is strongly influenced by the density of electronic states (DOS) near the Fermi level, adsorbed contaminants, and surface chemistry [48–50]. With graphitic materials, there is a clear difference in $Fe(CN)_6^{3-/4-}$ HET rates between basal (BP) and edge planes (EP). The standard rate constant (k^0) for the EP and BP range from 10^{-5} to 10^{-1} and from 10^{-10} to 10^{-6} cm s^{-1}, respectively [2,51]. Sluggish HET kinetics of graphitic materials at the BP is attributed to low DOS near the Fermi-level or from aging in laboratory air which creates an adsorbed layer of volatile organic compounds [9–11,52]. Figure 3.8

shows the CV recorded for 1 mM $Fe(CN)_6^{3-/4-}$ in 0.1 M KCl at 50 mV/sec. Basal plane GUITAR electrodes are unusual in that there is a fast calculated k^0 of 1.2 x 10^{-2} cm/s and 1.6 x 10^{-2} cm/s for N-GUITAR [1,2]. This lies in the upper range of other N-doped and undoped carbon electrodes (1.02 x 10^{-4} to- 1.5 x 10^{-2}cm/s) [39,40,53,54]. Both materials have fast HET kinetics due to the rich density of structural defects, which increase DOS [55].

3.4.8 N-GUITAR is Resistant to Air-Aging

Several investigators have examined the air-aging effects of HOPG with the Fe $(CN)_6^{3-/4-}$ probe [2,11,15,56]. Unwin et al. have examined freshly cleaved surfaces of HOPG electrodes which have a CV peak separation (ΔEp) of 58 mV. After 3 hours of exposure to air, that surface exhibited a decrease in HET rates with a ΔEp of 450 mV [11]. Liu et al. also conducted a study of HOPG air aging. By storing their electrodes at -15° C, they were able to slow the aging effect. The ΔEp increased at a slower rate from 59 mV on a fresh surface to 95 mV at 8 hours [15]. Compton and coworkers show that ΔEp increases from 227 to 596mV at 2 hours [56]. A recent body of literature indicates that this effect is from the adsorption of volatile organic compounds (VOCs) onto the surface of HOPG, which creates a barrier to HET. Ellipsometry indicates that this layer is about 0.6 nm thick [15]. Water droplet contact angle (WCA) measurements also support the adsorption hypothesis. Generally, other investigators have found that HOPG and graphene surfaces become more hydrophobic with exposure time, increasing in contact angle from 59-70°to 90-95° [15,16,57,58].

In this investigation, a freshly cleaved surface of HOPG gave $Fe(CN)_6^{3-/4-}$ ΔEp of 67 mV with a standard deviation of 4 mV over three measurements at 50 mV/s. The ΔEp increases to 165 ± 60 and 221 ± 30 mV at the 1- and 3-hour intervals, respectively (Figure 3.8C). This trend follows literature observations. During that interval, the WCA increased from 63.8° ± 5.2° to 80.1° ± 10.8°, again matching literature trends. GUITAR electrodes (Figure 3.8B) gave

increases in ΔEp from 71 ± 2 to 102 ± 5 mV and WCA from 62.6° ± 5.5° to 78.4° ± 7.2° from the 0 to 3-hour time interval. These CV trends match that of a previous investigation. [2] A demonstrates that N-GUITAR is the most resistant to air-aging effects when compared to literature and GUITAR. The CV exhibited a minimal increase from 66 ± 5 to 69 ± 3 mV for ΔEp from the fresh surface to 3 hours of air exposure. The change in WCA for N-GUITAR again exhibited a minimal increase from 55.8° ± 7.1° to 70.4° ± 5.0° after aging. No other material has been observed in the literature that has such resistance to air-aging. This remarkable property indicates excellent prospects for durable electrochemical sensors [4–7,59].

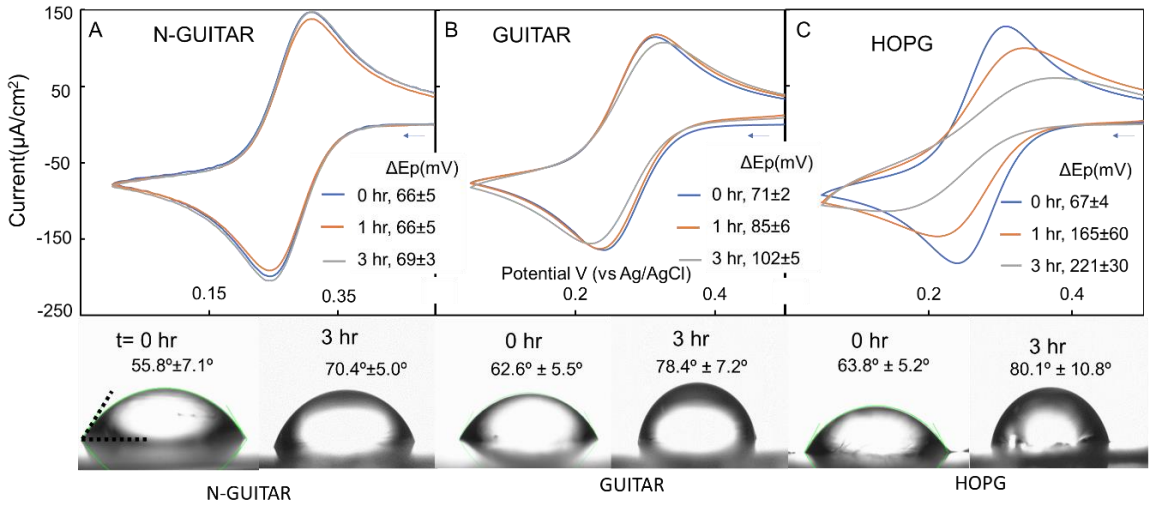

Figure 3.8 Cyclic Voltammetric (CV) studies for the N-GUITAR (A), GUITAR (B), and (HOPG) electrode with 1 mM Fe $(CN)_6^{3-/4-}$ in 0.1 M KCl at 50 mV/sec. CV was recorded in the freshly exfoliated surface at 0, 1, and 3 hours of air exposure (n=3). Water contact angle measurement (WCA) on N-GUITAR, GUITAR, and HOPG are also shown on their respective positions. WCA measurements were also carried out on freshly exfoliated surfaces at 0, 1, and 3 hrs of air exposure.

3.4.9 N-doped GUITAR is Tolerant to Dopamine Fouling because of Fast HET Kinetics.

Figure 3.9A shows the CV response of N-GUITAR at relatively high (1mM) and low concentration (1μM) of dopamine (DA) in 0.1 M phosphate buffer (pH 7.0). The CV waves

are assigned the process seen in step 1. The ΔEp for 1 mM DA (CV wave seen in Figure 3.9A) is 85 mV at 100 mV/s. Decreasing ΔEp is associated with faster HET rates [19]. This is the narrowest ΔEp for DA reported in the literature, with the exception of EP-pyrolytic graphite with 59 mV [17]. The ΔEp for GUITAR is 174 mV. Generally, ΔEp varies from 100 to 350 mV for most carbon electrodes [17,19].

Due to their biocompatibility and chemical inertness, carbon electrodes are favored for in-vivo voltammetric detection of dopamine [60]. However, they are highly susceptible to fouling from the dopamine polymerization process described in the introduction and the scheme seen in Figure 10. Generally, carbon electrodes tend to lose 20 to 75% of CV current signal after 10 cycles with 1 mM DA [17,19]. Figure 3.9B plots the peak current with each CV cycle for three trial runs. One standard deviation error bar is expressed with each point. For N-GUITAR at 1 μM DA, there is no loss of peak current over 10 CV cycles. At the higher concentration of 1 mM, there is a 10% loss in peak current. The GUITAR electrode experienced a 25% loss in peak current which is in the range of other carbon materials [17,19]. By maintaining the DA peak current, it is apparent that the N-GUITAR surface provides less favorable conditions for the formation of polydopamine.

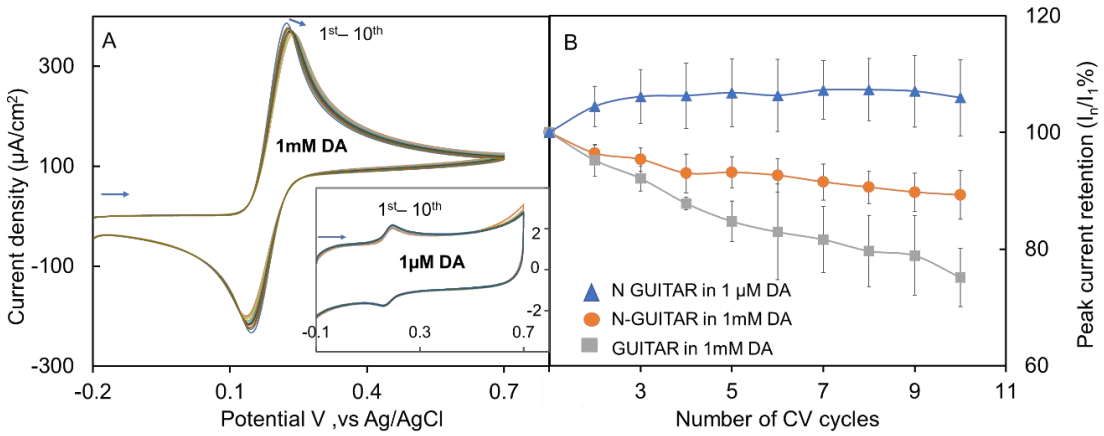

Figure 3.9 (A) 10 CV cycles recorded in 1 mM and (inset) 1 μM dopamine in 0.1 M phosphate buffer system (PBS) at pH 7.0 at 100 mV/sec for N-GUITAR electrode. (B) A plot of relative oxidative peak current density vs. number of CV runs. The one standard deviation interval for three CV runs are shown with each data point.

The reaction scheme for electrode fouling is shown below in Figure 3.10. The CV waves of Figure 3.9A are associated with DA and its oxidized product, o-dopaminoquinone (Step 1). It is the latter that undergoes processes with further electro-oxidation that result in electrode fouling through Steps 2-4 [19,22]. The fraction of o-dopaminoquinone that contributes to fouling can be described by the ratio of CV peak anodic and cathodic currents, $i_{p,a}/i_{p,c}$. A quantity close to one is associated with a lower fraction of o-dopaminoquinone, contributing to Steps 2-4. Higher values of $i_{p,a}/i_{p,c}$ indicate that the electrode fouling processes are more facile.

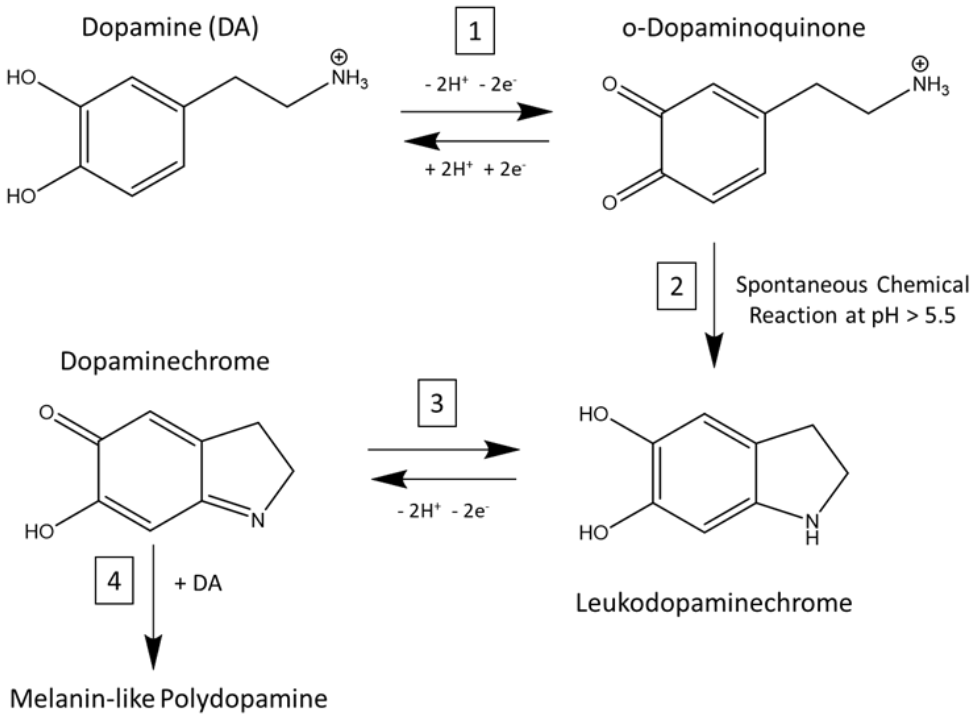

Figure 3.10. Reaction scheme for electrode fouling by electrochemical dopamine oxidation [17,61]. Step 1) The electrode oxidation and reduction assigned to the cyclic voltammetric (CV) waves of Figure 3.9A. Steps 2-4 are the spontaneous series of reactions that result in the formation of the insulating layer of melanin-like polydopamine.

For the N-GUITAR electrode, the $i_{p,a}/i_{p,c}$ ratio is 1.3, and this is the lowest value reported in the literature. For GUITAR, this value is 1.7. This indicates that o-dopaminoquinone is least likely to contribute to fouling using the N-GUITAR material. Figure 3.11 illustrates the performance of N-GUITAR with literature. A plot of $i_{p,a}/i_{p,c}$ vs. ΔEp for DA is shown in Figure 3.11A with a clear trend of fast HET rates associated with a lower $i_{p,a}/i_{p,c}$ ratio. Rapid consumption of o-dopaminoquinone reduces the probability of electrode fouling by Steps 2-4. This effect may be attributed to the HET rate for o-dopaminoquinone reduction back to DA (inverse Step 1). Figure 3.11B illustrates that low $i_{p,a}/i_{p,c}$ is associated with less $i_{p,a}$ signal loss over 10 CV cycles. Fast HET rates with a variety of redox species on GUITAR electrodes have been discussed in previous publications[2,4,7,57]. This effect is associated with a high DOS

arising from structural defects. It is apparent that this effect is enhanced by nitrogen doping GUITAR.

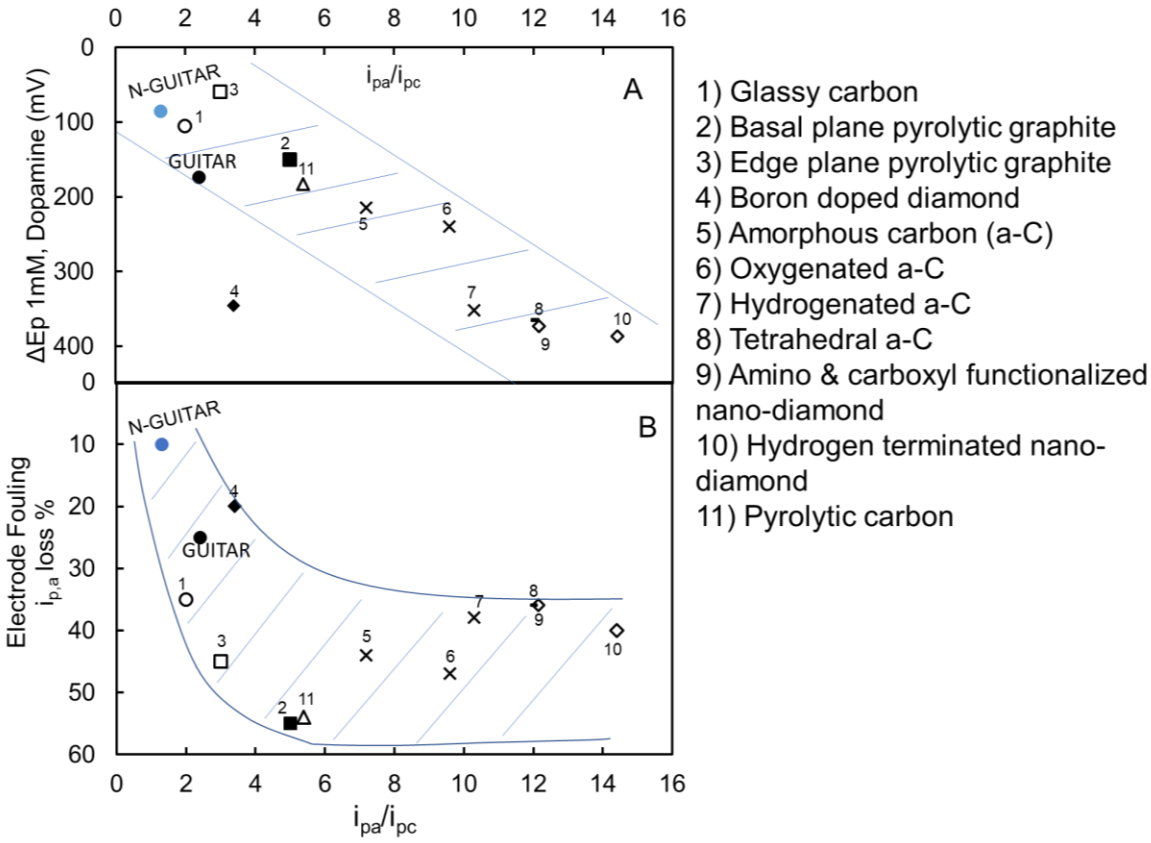

Figure 3.11. The cyclic voltammetric trends regarding HET kinetics of Step 1 in Figure 10. N-GUITAR and GUITAR, as well as literature data, were recorded in 1 mM DA at pH 7 phosphate buffer solutions [17–19]. The $i_{p,a}/i_{p,c}$ ratio indicates the reversibility of Step 1 and electrode fouling through loss of $i_{p,\,a.}$ (A) plot of $i_{p,a}/i_{p,c}$ vs. Δ Ep for N-GUITAR, GUITAR, and literature carbon. It is clear that a trend forms with fast HET kinetics (narrow ΔEp) and lower $i_{p,a}/i_{p,c.}$ (B) Electrode fouling through $i_{p,a}$ loss vs. $i_{p,a}/i_{p,c}$. The trends are in the shaded region and show that N-GUITAR has the fastest HET rate (A) with the least amount of electrode fouling (B).

3.5 Conclusions

The N-GUITAR material maintains the features of GUITAR electrodes, e.g., fast HET rates, wide aqueous potential window, and resistance to corrosion. However, it deviates from GUITAR in that it exhibits more resistance to fouling than GUITAR and other carbon electrodes. The two studies representing the predominant mechanisms of fouling; physical adsorption, and polymerization of matrix components were both observed to be less severe on the surface of N-GUITAR over GUITAR and literature carbon electrodes. In air-aging studies, the WCA measurements indicate that N-GUITAR is less susceptible to VOC physical adsorption than GUITAR or other literature carbon electrodes. In fouling by DA electro-oxidation, N-GUITAR also shows less susceptibility than GUITAR or literature carbons. This is mainly attributed to fast HET kinetics for the DA/o-dopaminoquinone redox couple on the N-GUITAR electrode. The combination of fast HET and resistance to signal attenuation indicates much promise for N-GUITAR electrodes for DA sensing.

3.6 References

(1) Kabir, H.; Zhu, H.; May, J.; Hamal, K.; Kan, Y.; Williams, T.; Echeverria, E.; McIlroy, D. N.; Estrada, D.; Davis, P. H.; Pandhi, T.; Yocham, K.; Higginbotham, K.; Clearfield, A.; Cheng, I. F. The Sp2-Sp3 Carbon Hybridization Content of Nanocrystalline Graphite from Pyrolyzed Vegetable Oil, Comparison of Electrochemistry and Physical Properties with Other Carbon Forms and Allotropes. *Carbon* **2019**, *144*, 831–840. https://doi.org/10.1016/j.carbon.2018.12.058.

(2) Gyan, I. O.; Wojcik, P. M.; Aston, D. E.; McIlroy, D. N.; Cheng, I. F. A Study of the Electrochemical Properties of a New Graphitic Material: GUITAR. *ChemElectroChem* **2015**, *2* (5), 700–706. https://doi.org/10.1002/celc.201402433.

(3) Cheng, I. F.; Xie, Y.; Allen Gonzales, R.; Brejna, P. R.; Sundararajan, J. P.; Fouetio Kengne, B. A.; Eric Aston, D.; McIlroy, D. N.; Foutch, J. D.; Griffiths, P. R. Synthesis of Graphene Paper from Pyrolyzed Asphalt. *Carbon* **2011**, *49* (8), 2852–2861. https://doi.org/10.1016/j.carbon.2011.03.020.

(4) Gyan, I. O.; Cheng, I. F. Electrochemical Study of Biologically Relevant Molecules at Electrodes Constructed from GUITAR, a New Carbon Allotrope. *Microchemical Journal* **2015**, *122*, 39–44. https://doi.org/10.1016/j.microc.2015.04.002.

(5) Kabir, H.; Ma, P. Y.; Renn, N.; Nicholas, N. W.; Cheng, I. F. Electrochemical Determination of Free Chlorine on Pseudo-Graphite Electrode. *Talanta* **2019**, *205*, 120101. https://doi.org/10.1016/j.talanta.2019.06.101.

(6) Kabir, H.; Zhu, H.; Lopez, R.; Nicholas, N. W.; McIlroy, D. N.; Echeverria, E.; May, J.; Cheng, I. F. Electrochemical Determination of Chemical Oxygen Demand on Functionalized Pseudo-Graphite Electrode. *Journal of Electroanalytical Chemistry* **2019**, 113448. https://doi.org/10.1016/j.jelechem.2019.113448.

(7) Zhu, H.; Hassan, T.; Kabir, H.; May, J.; Hamal, K.; Lopez, R.; J. Smith, H.; W. Nicholas, N.; Sankaran, P.; N. McIlroy, D.; Francis Cheng, I. Voltammetric PH Sensor Based on Electrochemically Modified Pseudo-Graphite. *Analyst* **2020**. https://doi.org/10.1039/D0AN01405B.

(8) Slate, A. J.; Brownson, D. A. C.; Dena, A. S. A.; Smith, G. C.; Whitehead, K. A.; Banks, C. E. Exploring the Electrochemical Performance of Graphite and Graphene Paste Electrodes Composed of Varying Lateral Flake Sizes. *Phys. Chem. Chem. Phys.* **2018**, *20* (30), 20010–20022. https://doi.org/10.1039/C8CP02196A.

(9) McCreery, R. L.; McDermott, M. T. Comment on Electrochemical Kinetics at Ordered Graphite Electrodes. *Anal. Chem.* **2012**, *84* (5), 2602–2605. https://doi.org/10.1021/ac2031578.

(10) Davies, T. J.; Hyde, M. E.; Compton, R. G. Nanotrench Arrays Reveal Insight into Graphite Electrochemistry. *Angewandte Chemie International Edition* **2005**, *44* (32), 5121–5126. https://doi.org/10.1002/anie.200462750.

(11) Patel, A. N.; Collignon, M. G.; O'Connell, M. A.; Hung, W. O. Y.; McKelvey, K.; Macpherson, J. V.; Unwin, P. R. A New View of Electrochemistry at Highly Oriented Pyrolytic Graphite. *J. Am. Chem. Soc.* **2012**, *134* (49), 20117–20130. https://doi.org/10.1021/ja308615h.

(12) Wang, H.; Maiyalagan, T.; Wang, X. Review on Recent Progress in Nitrogen-Doped Graphene: Synthesis, Characterization, and Its Potential Applications. *ACS Catal.* **2012**, *2* (5), 781–794. https://doi.org/10.1021/cs200652y.

(13) Inagaki, M.; Toyoda, M.; Soneda, Y.; Morishita, T. Nitrogen-Doped Carbon Materials. *Carbon* **2018**, *132*, 104–140. https://doi.org/10.1016/j.carbon.2018.02.024.

(14) Wei, D.; Liu, Y.; Wang, Y.; Zhang, H.; Huang, L.; Yu, G. Synthesis of N-Doped Graphene by Chemical Vapor Deposition and Its Electrical Properties. *Nano Lett.* **2009**, *9* (5), 1752–1758. https://doi.org/10.1021/nl803279t.

(15) Li, Z.; Kozbial, A.; Nioradze, N.; Parobek, D.; Shenoy, G. J.; Salim, M.; Amemiya, S.; Li, L.; Liu, H. Water Protects Graphitic Surface from Airborne Hydrocarbon Contamination. *ACS Nano* **2016**, *10* (1), 349–359. https://doi.org/10.1021/acsnano.5b04843.

(16) Salim, M.; Hurst, J.; Montgomery, M.; Tolman, N.; Liu, H. Airborne Contamination of Graphite as Analyzed by Ultra-Violet Photoelectron Spectroscopy. *Journal of Electron*

Spectroscopy and Related Phenomena **2019**, *235*, 8–15. https://doi.org/10.1016/j.elspec.2019.06.001.

(17) Patel, A. N.; Tan, S.; Miller, T. S.; Macpherson, J. V.; Unwin, P. R. Comparison and Reappraisal of Carbon Electrodes for the Voltammetric Detection of Dopamine. *Anal. Chem.* **2013**, *85* (24), 11755–11764. https://doi.org/10.1021/ac401969q.

(18) Trouillon, R.; O'Hare, D. Comparison of Glassy Carbon and Boron Doped Diamond Electrodes: Resistance to Biofouling. *Electrochimica Acta* **2010**, *55* (22), 6586–6595. https://doi.org/10.1016/j.electacta.2010.06.016.

(19) Peltola, E.; Sainio, S.; Holt, K. B.; Palomäki, T.; Koskinen, J.; Laurila, T. Electrochemical Fouling of Dopamine and Recovery of Carbon Electrodes. *Anal. Chem.* **2018**, *90* (2), 1408–1416. https://doi.org/10.1021/acs.analchem.7b04793.

(20) Puthongkham, P.; Venton, B. J. Nanodiamond Coating Improves the Sensitivity and Antifouling Properties of Carbon Fiber Microelectrodes. *ACS Sens.* **2019**, *4* (9), 2403–2411. https://doi.org/10.1021/acssensors.9b00994.

(21) Bennet, K. E.; Tomshine, J. R.; Min, H.-K.; Manciu, F. S.; Marsh, M. P.; Paek, S. B.; Settell, M. L.; Nicolai, E. N.; Blaha, C. D.; Kouzani, A. Z.; Chang, S.-Y.; Lee, K. H. A Diamond-Based Electrode for Detection of Neurochemicals in the Human Brain. *Front Hum Neurosci* **2016**, *10*. https://doi.org/10.3389/fnhum.2016.00102.

(22) Hanssen, B. L.; Siraj, S.; Wong, D. K. Y. Recent Strategies to Minimise Fouling in Electrochemical Detection Systems. *Reviews in Analytical Chemistry* **2016**, *35* (1), 1–28. https://doi.org/10.1515/revac-2015-0008.

(23) Luo, S.; Cao, J.; McDonald, A. G. Esterification of Industrial Lignin and Its Effect on the Resulting Poly(3-Hydroxybutyrate-Co-3-Hydroxyvalerate) or Polypropylene Blends. *Industrial Crops and Products* **2017**, *97*, 281–291. https://doi.org/10.1016/j.indcrop.2016.12.024.

(24) Ouyang, W.; Zeng, D.; Yu, X.; Xie, F.; Zhang, W.; Chen, J.; Yan, J.; Xie, F.; Wang, L.; Meng, H.; Yuan, D. Exploring the Active Sites of Nitrogen-Doped Graphene as Catalysts

for the Oxygen Reduction Reaction. *International Journal of Hydrogen Energy* **2014**, *39* (28), 15996–16005. https://doi.org/10.1016/j.ijhydene.2014.01.045.

(25) Ratso, S.; Kruusenberg, I.; Vikkisk, M.; Joost, U.; Shulga, E.; Kink, I.; Kallio, T.; Tammeveski, K. Highly Active Nitrogen-Doped Few-Layer Graphene/Carbon Nanotube Composite Electrocatalyst for Oxygen Reduction Reaction in Alkaline Media. *Carbon* **2014**, *73*, 361–370. https://doi.org/10.1016/j.carbon.2014.02.076.

(26) Guo, D.; Shibuya, R.; Akiba, C.; Saji, S.; Kondo, T.; Nakamura, J. Active Sites of Nitrogen-Doped Carbon Materials for Oxygen Reduction Reaction Clarified Using Model Catalysts. *Science* **2016**, *351* (6271), 361–365. https://doi.org/10.1126/science.aad0832.

(27) Wu, J.; Ma, L.; Yadav, R. M.; Yang, Y.; Zhang, X.; Vajtai, R.; Lou, J.; Ajayan, P. M. Nitrogen-Doped Graphene with Pyridinic Dominance as a Highly Active and Stable Electrocatalyst for Oxygen Reduction. *ACS Appl. Mater. Interfaces* **2015**, *7* (27), 14763–14769. https://doi.org/10.1021/acsami.5b02902.

(28) Wu, T.; Shen, H.; Sun, L.; Cheng, B.; Liu, B.; Shen, J. Nitrogen and Boron Doped Monolayer Graphene by Chemical Vapor Deposition Using Polystyrene, Urea and Boric Acid. *New J. Chem.* **2012**, *36* (6), 1385–1391. https://doi.org/10.1039/C2NJ40068E.

(29) Luo, Z.; Lim, S.; Tian, Z.; Shang, J.; Lai, L.; MacDonald, B.; Fu, C.; Shen, Z.; Yu, T.; Lin, J. Pyridinic N Doped Graphene: Synthesis, Electronic Structure, and Electrocatalytic Property. *J. Mater. Chem.* **2011**, *21* (22), 8038–8044. https://doi.org/10.1039/C1JM10845J.

(30) Zan, R.; Altuntepe, A. Nitrogen Doping of Graphene by CVD. *Journal of Molecular Structure* **2020**, *1199*, 127026. https://doi.org/10.1016/j.molstruc.2019.127026.

(31) Chen, H.; Yang, Y.; Hu, Z.; Huo, K.; Ma, Y.; Chen, Y.; Wang, X.; Lu, Y. Synergism of C5N Six-Membered Ring and Vapor−Liquid−Solid Growth of CNx Nanotubes with Pyridine Precursor. *J. Phys. Chem. B* **2006**, *110* (33), 16422–16427. https://doi.org/10.1021/jp062216e.

(32) Couzi, M.; Bruneel, J.-L.; Talaga, D.; Bokobza, L. A Multi Wavelength Raman Scattering Study of Defective Graphitic Carbon Materials: The First Order Raman Spectra Revisited. *Carbon* **2016**, *107*, 388–394. https://doi.org/10.1016/j.carbon.2016.06.017.

(33) Yang, Q.-H.; Hou, P.-X.; Unno, M.; Yamauchi, S.; Saito, R.; Kyotani, T. Dual Raman Features of Double Coaxial Carbon Nanotubes with N-Doped and B-Doped Multiwalls. *Nano Lett.* **2005**, *5* (12), 2465–2469. https://doi.org/10.1021/nl051779j.

(34) Sheng, Z.-H.; Shao, L.; Chen, J.-J.; Bao, W.-J.; Wang, F.-B.; Xia, X.-H. Catalyst-Free Synthesis of Nitrogen-Doped Graphene via Thermal Annealing Graphite Oxide with Melamine and Its Excellent Electrocatalysis. *ACS Nano* **2011**, *5* (6), 4350–4358. https://doi.org/10.1021/nn103584t.

(35) Panchakarla, L. S.; Govindaraj, A.; Rao, C. N. R. Nitrogen- and Boron-Doped Double-Walled Carbon Nanotubes. *ACS Nano* **2007**, *1* (5), 494–500. https://doi.org/10.1021/nn700230n.

(36) Andonovic, B.; Temkov, M.; Ademi, A.; Petrovski, A. Laue Functions Model vs Scherrer Equation in Determination of Graphene Layers Number on The Ground of Xrd Data. **2014**, 6.

(37) Warren, B. E. X-Ray Diffraction in Random Layer Lattices. *Phys. Rev.* **1941**, *59* (9), 693–698. https://doi.org/10.1103/PhysRev.59.693.

(38) Kamata, T.; Kato, D.; Niwa, O. Electrochemical Performance at Sputter-Deposited Nanocarbon Film with Different Surface Nitrogen-Containing Groups. *Nanoscale* **2019**, *11* (21), 10239–10246. https://doi.org/10.1039/C9NR01569H.

(39) Tanaka, Y.; Furuta, M.; Kuriyama, K.; Kuwabara, R.; Katsuki, Y.; Kondo, T.; Fujishima, A.; Honda, K. Electrochemical Properties of N-Doped Hydrogenated Amorphous Carbon Films Fabricated by Plasma-Enhanced Chemical Vapor Deposition Methods. *Electrochimica Acta* **2011**, *56* (3), 1172–1181. https://doi.org/10.1016/j.electacta.2010.11.006.

(40) Yang, X.; Haubold, L.; DeVivo, G.; Swain, G. M. Electroanalytical Performance of Nitrogen-Containing Tetrahedral Amorphous Carbon Thin-Film Electrodes. *Anal. Chem.* **2012**, *84* (14), 6240–6248. https://doi.org/10.1021/ac301124r.

(41) Kamata, T.; Kato, D.; Ida, H.; Niwa, O. Structure and Electrochemical Characterization of Carbon Films Formed by Unbalanced Magnetron (UBM) Sputtering Method. *Diamond and Related Materials* **2014**, *49*, 25–32. https://doi.org/10.1016/j.diamond.2014.07.007.

(42) Wang, W.; Wei, Z.; Su, W.; Fan, X.; Liu, J.; Yan, C.; Zeng, C. Kinetic Investigation of Vanadium (V)/(IV) Redox Couple on Electrochemically Oxidized Graphite Electrodes. *Electrochimica Acta* **2016**, *205*, 102–112. https://doi.org/10.1016/j.electacta.2016.04.109.

(43) Chorbadzhiyska, E.; Bardarov, I.; Hubenova, Y.; Mitov, M. Graphite–Metal Oxide Composites as Potential Anodic Catalysts for Microbial Fuel Cells. *Catalysts* **2020**, *10* (7), 796. https://doi.org/10.3390/catal10070796.

(44) Kapałka, A.; Fóti, G.; Comninellis, C. Determination of the Tafel Slope for Oxygen Evolution on Boron-Doped Diamond Electrodes. *Electrochemistry Communications* **2008**, *10* (4), 607–610. https://doi.org/10.1016/j.elecom.2008.02.003.

(45) Suffredini, H. B.; Machado, S. A. S.; Avaca, L. A. The Water Decomposition Reactions on Boron-Doped Diamond Electrodes. *Journal of the Brazilian Chemical Society* **2004**, *15* (1), 16–21. https://doi.org/10.1590/S0103-50532004000100004.

(46) Goss, C. A.; Brumfield, J. C.; Irene, E. A.; Murray, R. W. Imaging the Incipient Electrochemical Oxidation of Highly Oriented Pyrolytic Graphite. *Anal. Chem.* **1993**, *65* (10), 1378–1389. https://doi.org/10.1021/ac00058a014.

(47) Alliata, D.; Kötz, R.; Haas, O.; Siegenthaler, H. In Situ AFM Study of Interlayer Spacing during Anion Intercalation into HOPG in Aqueous Electrolyte. *Langmuir* **1999**, *15* (24), 8483–8489. https://doi.org/10.1021/la990402o.

(48) McCreery, R. L. Advanced Carbon Electrode Materials for Molecular Electrochemistry. *Chem. Rev.* **2008**, *108* (7), 2646–2687. https://doi.org/10.1021/cr068076m.

(49) Huang, L.; Cao, Y.; Diao, D. Nanosized Graphene Sheets Induced High Electrochemical Activity in Pure Carbon Film. *Electrochimica Acta* **2018**, *262*, 173–181. https://doi.org/10.1016/j.electacta.2018.01.027.

(50) Chen, P.; McCreery, R. L. Control of Electron Transfer Kinetics at Glassy Carbon Electrodes by Specific Surface Modification. *Anal. Chem.* **1996**, *68* (22), 3958–3965. https://doi.org/10.1021/ac960492r.

(51) Villarreal, C. C.; Pham, T.; Ramnani, P.; Mulchandani, A. Carbon Allotropes as Sensors for Environmental Monitoring. *Current Opinion in Electrochemistry* **2017**, *3* (1), 106–113. https://doi.org/10.1016/j.coelec.2017.07.004.

(52) Kislenko, V. A.; Pavlov, S. V.; Kislenko, S. A. Influence of Defects in Graphene on Electron Transfer Kinetics: The Role of the Surface Electronic Structure. *Electrochimica Acta* **2020**, *341*, 136011. https://doi.org/10.1016/j.electacta.2020.136011.

(53) Kamata, T.; Kato, D.; Hirono, S.; Niwa, O. Structure and Electrochemical Performance of Nitrogen-Doped Carbon Film Formed by Electron Cyclotron Resonance Sputtering. *Anal. Chem.* **2013**, *85* (20), 9845–9851. https://doi.org/10.1021/ac402385q.

(54) Lagrini, A.; Deslouis, C.; Cachet, H.; Benlahsen, M.; Charvet, S. Elaboration and Electrochemical Characterization of Nitrogenated Amorphous Carbon Films. *Electrochemistry Communications* **2004**, *6* (3), 245–248. https://doi.org/10.1016/j.elecom.2003.12.009.

(55) Zhong, J.-H.; Zhang, J.; Jin, X.; Liu, J.-Y.; Li, Q.; Li, M.-H.; Cai, W.; Wu, D.-Y.; Zhan, D.; Ren, B. Quantitative Correlation between Defect Density and Heterogeneous Electron Transfer Rate of Single Layer Graphene. *J. Am. Chem. Soc.* **2014**, *136* (47), 16609–16617. https://doi.org/10.1021/ja508965w.

(56) Ji, X.; Banks, C. E.; Crossley, A.; Compton, R. G. Oxygenated Edge Plane Sites Slow the Electron Transfer of the Ferro-/Ferricyanide Redox Couple at Graphite Electrodes. *ChemPhysChem* **2006**, *7* (6), 1337–1344. https://doi.org/10.1002/cphc.200600098.

(57) Li, Z.; Wang, Y.; Kozbial, A.; Shenoy, G.; Zhou, F.; McGinley, R.; Ireland, P.; Morganstein, B.; Kunkel, A.; Surwade, S. P.; Li, L.; Liu, H. Effect of Airborne Contaminants on the Wettability of Supported Graphene and Graphite. *Nature Materials* **2013**, *12* (10), 925–931. https://doi.org/10.1038/nmat3709.

(58) Kozbial, A.; Li, Z.; Sun, J.; Gong, X.; Zhou, F.; Wang, Y.; Xu, H.; Liu, H.; Li, L. Understanding the Intrinsic Water Wettability of Graphite. *Carbon* **2014**, *74*, 218–225. https://doi.org/10.1016/j.carbon.2014.03.025.

(59) Kabir, H.; Lopez, R.; May, J.; Hamal, K.; Nicholas, N. W.; Cheng, I. F. Salicylic Acid Detection Using a Pseudo-Graphite Electrode. 9.

(60) Kamal Eddin, F. B.; Wing Fen, Y. Recent Advances in Electrochemical and Optical Sensing of Dopamine. *Sensors* **2020**, *20* (4), 1039. https://doi.org/10.3390/s20041039.

(61) Harreither, W.; Trouillon, R.; Poulin, P.; Neri, W.; Ewing, A. G.; Safina, G. Carbon Nanotube Fiber Microelectrodes Show a Higher Resistance to Dopamine Fouling. *Anal. Chem.* **2013**, *85* (15), 7447–7453. https://doi.org/10.1021/ac401399s.

(62) Kabir, H.; Gyan, I. O.; Foutch, J. D.; Zhu, H.; Cheng, I. F. Application of GUITAR on the Negative Electrode of the Vanadium Redox Flow Battery: Improved V3+/2+ Heterogeneous Electron Transfer with Reduced Hydrogen Gassing. *C—Journal of Carbon Research* **2016**, *2* (2), 13. https://doi.org/10.3390/c2020013.

Chapter 4: "An Oxygen Reduction Reaction Electrocatalyst Tuned for Hydrogen Peroxide Generation Based on a Pseudo-Graphite Doped with Graphitic Nitrogen". (*To be Submitted*)

4.1 Abstract

The carbon material GUITAR (pseudo-graphite from the University of Idaho thermolyzed asphalt reaction) can be doped with nitrogen in two prevalent forms. In a previous study, N'-GUITAR had a predominance of pyridinic and pyrrolic moieties with no graphitic nitrogen. In this study, N-GUITAR contains a 9.7% N atomic abundance, with that fraction consisting of 72.3 % graphitic, 23.7% pyridinic, and 0% pyrrolic nitrogen. The two materials allow for the examination of hypotheses regarding the importance of the three different nitrogen moieties in the oxygen reduction reaction (ORR). In the previous investigation, the lack of graphitic nitrogen of N'-GUITAR gave a preferred pathway of $4e^-$ ORR to H_2O. In this investigation, N-GUITAR gave a $2e^-$ ORR pathway to H_2O_2. This was elucidated by current efficiency and hydrodynamic voltammetry studies. The high predominance of graphitic nitrogen confirms the hypothesis regarding 2 vs. $4e^-$ ORR pathways with N-doped carbon materials. N-GUITAR was also evaluated for parasitic pathways for H_2O_2 production. At -0.95 V vs Ag/AgCl the current efficiency for H_2O_2 is 96% in 0.05 M Na_2SO_4 with a production rate of 4.9 mg cm^{-2} hr^{-1}. This indicates possibilities for water purification and treatment applications, which require 10 to 250 mg/L depending on conditions.

Keywords: Hydrogen Peroxide, Oxygen Reduction Reaction

4.2 Introduction

Hydrogen peroxide (H_2O_2) is a relatively eco-friendly and widely used oxidant in the water purification, chemical, and medical industries.[1,2] It is a greener oxidizing agent than chlorine in that it leaves no halogenated by-products such as trihalomethanes and haloacetic acids and is effective over a wider pH range.[3,4] A partial barrier to wider implementation is that the predominant method of H_2O_2 production, the anthraquinone process, is highly energy-intensive and requires large quantities of extraction solvents.[2,3] Furthermore, transportation issues also hinder its widespread application in water treatment. Onsite generation through the electrochemical process offers minimization of environmental impact as it can be conducted under aqueous and ambient conditions with no hazardous materials or waste.[5-7] This process proceeds by a $2e^-$ electrochemical process outlined in Equation 1.

(1) $O_2 + 2H^+ + 2e^- \rightarrow H_2O_2$ $\quad E^0 = 0.695$ V, $E^{0'}$ (pH 7) = 0.282 V

The challenges in the electrochemical production of H_2O_2 are improving slow kinetics and minimizing competing reactions. Slow electrode kinetics gives significant overpotentials for Equation 1 that require electrode potentials from -0.5 to -1.5 V vs Ag/AgCl.[8-9] At these potentials, three other parasitic electrochemical reactions are possible. These include the $4e^-$ oxygen reduction reactions (ORR) to water (Equation 2), the hydrogen evolution reaction (HER, Equation 3), and the 2e- reduction of H_2O_2 to H_2O (Equation 4).[8-10]

(2) $O_2 + 4H^+ + 4e^- \rightarrow 2H_2O$ $\quad E^0 = 1.23$ V, $E^{0'}$ (pH 7) = 0.817 V

(3) $2H^+ + 2e^- \rightarrow H_2$ $\quad E^0 = 0.00$, $E^{0'}$ (pH 7) = -0.413 V

(4) $H_2O_2 + 2H^+ + 2e^- \rightarrow 2H_2O$ $\quad E^0 = 1.763$ V, $E^{0'}$ (pH 7) = 1.35 V

It is therefore incumbent that any electrocatalyst for Equation 1 must be selective for this process. This has been noted by several investigators.[9,11] For this contribution, we demonstrate an electrocatalyst that is preferential for the reaction in Equation 1 based on GUITAR (graphite from the University of Idaho thermolyzed asphalt reaction). This carbon material consists of an 85/15 mole ratio of sp^2/sp^3 carbon with a crystallite grain size of 1.5 nm.[12,13] The interlayer d-spacing of 350 pm is slightly expanded over graphite's 335 pm. It is a pseudo-graphite in that it has visual and microscopic features that resemble graphite but has differing properties. Distinguishing characteristics over graphite and other carbon allotropes is that GUITAR has fast heterogeneous electron transfer (HET) kinetics with the $Fe(CN)_6^{4-/3-}$ probe at the basal and edge planes while maintaining excellent corrosion resistance.[12-14] The 3-volt aqueous potential window is among the largest reported. GUITAR is grown using a chemical vapor deposition process, which allows the fabrication of electrodes ranging from the nano- to macro-sizes, depending on the substrate.[12,15,16]

A significant consideration is the tunability of the electrocatalyst for performance and selectively between the reactions of Equations 1-4. Nitrogen doping of carbon materials is associated with the enhancement of electrocatalysis of ORR.[17,18] This is attributed to the polarized C-N bond facilitating the adsorption of O_2.[19,20] Predominate forms of N in sp^2 carbon

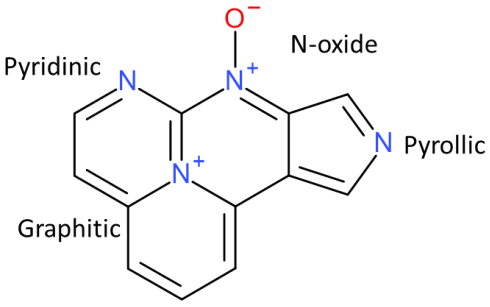

Figure 4.1. Nitrogen moieties in the graphite lattice.

lattices are pyridinic, pyrrolic, N-oxides, and graphitic moieties shown in **Figure** 4.1.

In computational studies, graphitic N is hypothesized to drive the $2e^-$ process of Equation 1.[21] However, experimental investigations have only been conducted on mixed nitrogen moiety carbon materials; therefore, definitive experimental evidence has yet to be gathered.[21-23] Pyridinic and pyrrolic moieties have been associated with the $4e^-$ transfer ORR (Equation 2) useful in fuel cell applications.[18] The N-oxide moiety is not associated with any specific ORR pathway. In a previous investigation, a specific nitrogen doping method led to a GUITAR variant with a 0.9% total nitrogen atomic abundance giving fractions of 0% graphitic N, 46.0% pyridinic, 41.3 % pyrrolic, and 12.4% N-oxide. This electrocatalyst, N'-GUITAR, proved to be durable and efficient for the $4e^-$ transfer ORR to H_2O.[15] An alternative doping method produced a nitrogen-doped pseudo-graphite which contains 9.7% N.[13] This material, called N-GUITAR, contains 72.3% graphitic N, 23.7%, pyridinic, 0.0% pyrrolic, and 4.0% N-oxide.[13] It is noteworthy that GUITAR is the only known carbon material that can be selectively synthesized for predominantly pyridinic/pyrrolic or graphitic nitrogen moieties. This provides an opportunity to examine the role of these functionalities in the pathway outlined in Equations 1 and 2.

4.3 Methods and Materials

4.3.1 Materials and Chemicals:

KFD graphite felt (SLG Carbon Company, St. Marys, PA, USA) was used as received. The reagents in this investigation were compressed Ar(g) and O_2(g) (>99.5 %, Oxarc, WA, USA), soybean oil (Walmart), paraffin (Gulf Wax), sulfuric acid (96.3%, J.T Baker Chemical Co, Phillipsburg, NJ, USA). Potassium chloride was obtained from Fisher Scientific (Waltham, NJ, USA), and potassium ferricyanide was obtained from Acros Organics (Morris Plains, NJ, USA). Sodium sulfate (EMD Chemicals, Germany), 30% H_2O_2 (Fisher Scientific, Belgium),

and ethanol (99.5%, Pharmaco, CT, USA) were used without further purification. All aqueous solutions were prepared with deionized water passed through an activated carbon purification cartridge (Barnstead, model D8922, Dubuque, IA).

4.3.2 Electrode Fabrication and Electrochemical Setup.

N-GUITAR samples were synthesized as described in previous studies.[13] Briefly, N-GUITAR films were prepared via a chemical vapor deposition (CVD) technique with a tube furnace at 900°C using acetonitrile precursor. Quartz wafers, KFD graphite felts, and Ketjen black were used as a substrate. Working electrode areas were isolated as described in the previous study. (16) Complete wetting of the electrode was conducted by washing with isopropanol followed with deionized water prior to use.[24] All electrochemical studies were conducted in a three-electrode set up cell with Ag/AgCl/ 3M KCl reference electrode using either a Bioanalytical System CV-50 W (West Lafayette, IN, USA) or a Gamry Instruments Interface 1000 potentiostat. The cell design is shown in Figure 4.2. The cell consisted of anodic and cathodic chambers with a separator membrane composed of cellulose acetate on cellulose paper.[25] This design allows for the formation of H_2O_2 via Reaction 1 without consumption at the anode through Reaction 4.

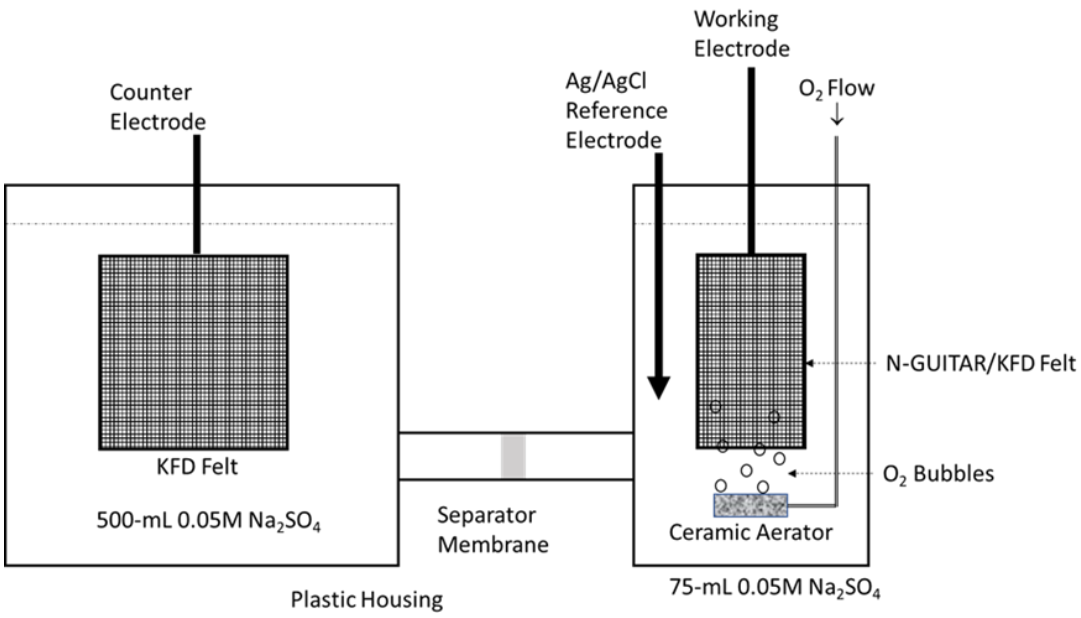

Figure 4.2 Electrochemical cell design for H_2O_2 generation.

Hydrodynamic experiments were carried out with a Pine Instrument glassy carbon rotating electrode (RDE) (Grove City, PA, USA). For that study, N-GUITAR was deposited on Ketjen black particles and drop-cast onto the RDE disks. This follows a procedure developed in a previous investigation.[15]

4.3.3 H_2O_2 Analysis

This was conducted by a colorimetric method.[26] Potassium titanium oxide oxalate dihydrate (Sigma-Aldrich) forms an aqueous complex with H_2O_2, which has an optical absorbance maximum at 400 nm. A Beer's Law based calibration curve was established with H_2O_2 (Pharmaco, CT, USA) standardized with $KMnO_4$ (J.T Baker Chemical Co, Phillipsburg, NJ, USA) and sodium oxalate (Fisher Scientific, Waltham, NJ, USA).

4.4 Results and Discussion

4.4.1 Formation of the Electrocatalyst and Surface Area.

The N-GUITAR electrocatalyst was formed by CVD onto a KFD graphite felt substrate, as demonstrated in a previous study.[13] SEM micrographs of bare KFD fiber and N-GUITAR/KFD are shown in Figure 4.3. The fiber diameter of KFD (7.4 ± 0.9μm (n=10)) is within the range reported in literature.[16,27] Deposition of N-GUITAR increases this diameter to 10.0.4 ± 0.9μm (n=10). The surface area of 62.2 cm^2 per cm^2 of geometric area for N-GUITAR/KFD was calculated assuming the electrode comprises cylindrical fibers.[16,24] This value agrees with cyclic voltammetric (CV) studies of $Fe(CN)_6^{4-/3-}$ using the Randles-Sevcik equation below where i_p, n, A, C (1×10^{-6} mol/cm^3), D (7.26×10^{-6} cm^2/s) and n are peak current, number of electrons transferred, area, concentration, diffusion coefficient, and potential sweep rate, respectively.[16]

(5) $i_p = 268{,}600\ n^{3/2}AC\sqrt{(D\nu)}$

The CV's are shown in Figure 2A. A plot of i_p vs. $\nu^{1/2}$ in Figure 4.4B indicates semi-infinite linear diffusion, and the slope gives an electrochemically active surface area (ECSA) of 59.0 cm^2 per cm^2 of geometric area. ECSA for GUITAR/KFD and bare KFD are 50.6 cm^2 and 61.5 cm^2 per cm^2 of geometric area, respectively.[16]

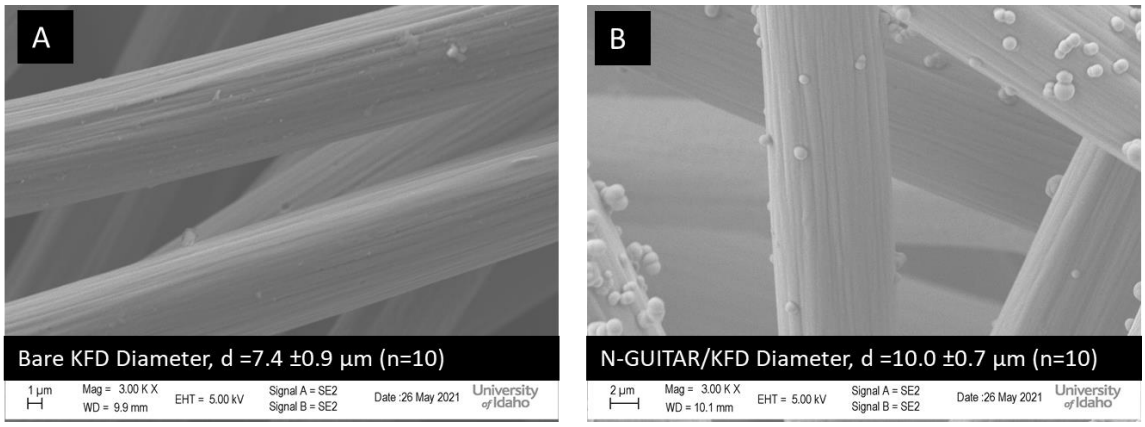

Figure 4.3. (A) Scanning electron micrographs (SEM) micrographs of as obtained KFD felt. (B) N-GUITAR coated KFD. The average diameter KFD fiber is 7.4± 0.9 µm (n=10) and for N-GUITAR/KFD is 10.0 ± 0.7 µm (n=10). These measurements were estimated with ImageJ software.

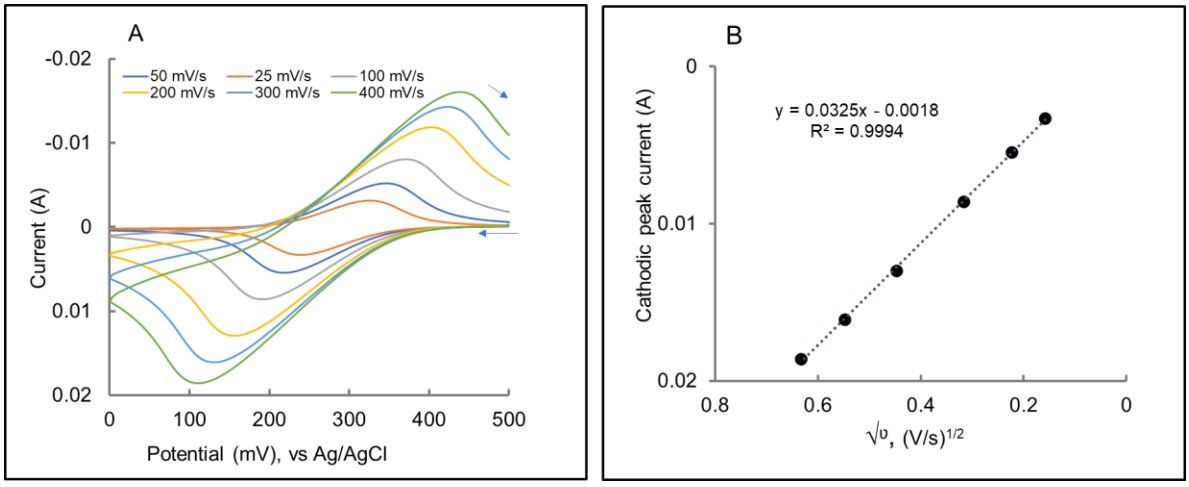

Figure 4.4. (A) Cyclic voltammograms (CV) obtained at various scan rates of 1mM $Fe(CN)_6^{3-/4-}$, 1 M KCl. (B) Cathodic peak current (i_p) vs. square root of scan rate for the estimation of the electrochemically active surface area (ECSA) from the Randles-Sevcik equation. The best fit line indicates semi-infinite linear diffusion.

4.4.2 Cyclic Voltammetric Studies.

The electrocatalysts were examined for ORR activity by cyclic voltammetry (CV) in 0.05M Na_2SO_4 at 50mV/sec under O_2 and Ar purged conditions. These are shown in Figure 4.5. Under O_2 purge, GUITAR/KFD exhibits two peak potentials (E_p's) of -0.65 and -1.10 V. Based on literature, this is an indication of the $2e^-$ process ORR through Equation (1) and the subsequent consumption of H_2O_2 through the reaction of Equation 4.[28,29,30] In case of N-GUITAR/KFD, there is only a single E_p at -0.77 V, which qualitatively indicates $2e^-$ transfer giving H_2O_2 in the ORR of Equation 1 without the consumption of H_2O_2 through Equation 4, This will be examined in detail below. Also notable is the relatively large peak current (i_p) of 7.0 mA/cm^2 at 50mV/sec, which is the highest reported in the literature (0.7- 4.5 mA/cm^2).[27-29,31] The i_p based on ECSA is 0.12 mA/cm^2. The CV's for both electrode materials under Ar purge indicate an overpotential of about 1 V for the HER (Equation 3).

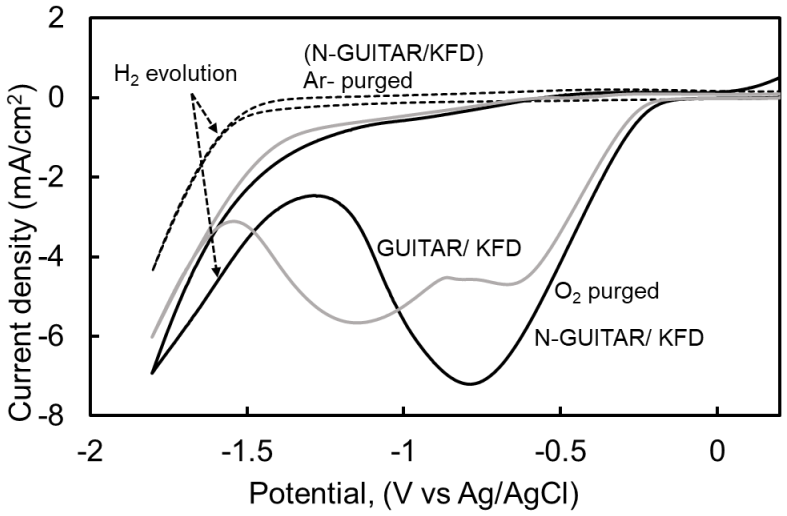

Figure 4.5. CVs at 50 mV/s in 0.05 M Na_2SO_4 under O_2 and Ar saturated conditions for N-GUITAR/KFD and KFD electrode. The peak potentials (E_p's) for GUITAR/KFD are -0.65 and -1.10 V and for N-GUITAR is -0.77 V. The hydrogen evolution reaction (HER) for the scans are also indicated.

4.4.3 H_2O_2 production is the major pathway for the N-GUITAR electrocatalyst.

The electrocatalyst was evaluated for generation of H_2O_2 by controlled potential electrolysis (CPE) at potentials ranging from -0.35 to -1.50 V vs. Ag/AgCl for 30 min in O_2 saturated 0.050 M Na_2SO_4 (aq). The saturation is ensured by bubbling O_2 across the electrode surface, which also aids in mass transport. The N-GUITAR cathode ECSA is 260 cm^2, corresponding to a geometric area of 4.4 cm^2. Control electrodes of the same geometric areas include GUITAR/KFD (ESCA 223 cm^2) and KFD (ECSA 270 cm^2). Selected current-time profiles with the N-GUITAR/KFD cathode are shown in Figure 4.6A. These remained at a steady state during the electrolysis for each potential. This is an indication of constant mass transport of O_2 to the electrode and stable electrocatalyst performance. Figure 4.6C shows the time profile for H_2O_2 concentration at the applied potential of -1.5 V for N-GUITAR/KFD. The data was obtained by taking 0.5 ml aliquots every 5 minutes for H_2O_2 analysis. This system obeys zero-order kinetics with the observed linear increase in H_2O_2 concentration, which is similar to other electrochemical H_2O_2 generation studies in the literature.[32,33] Performance of the control electrodes, GUITAR/KFD, and KFD are also shown in Figure 4.6C. As can be seen through the slopes, the N-doped material is a much more efficient electrocatalyst than either of the control electrodes. Figure 4.6B illustrates the effect of driving potential on the rates of H_2O_2 production (μmoles/cm^2-hour). The N-GUITAR/KFD electrode increased H_2O_2 with driving potential from the range -0.3 to -1.5V. Both control electrodes decreased in production rate from -0.95 V. It is surprising that GUITAR/KFD is much less efficient than bare KFD. This may be from the consumption of H_2O_2 through Reaction 4 and may be observed in the 2nd CV wave at E_p -1.1 V for GUITAR/KFD in Figure 4.5. Further evidence is presented in the current efficiency studies below.

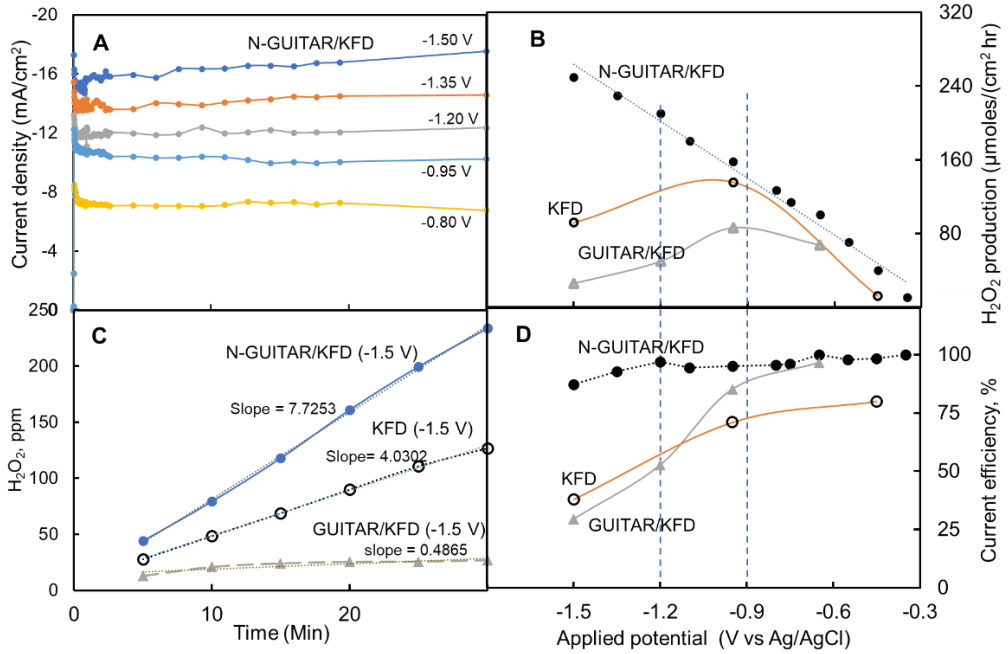

Figure 4.6. (A) Current-time curves recorded in O_2 saturated 0.05 M Na_2SO_4 at various constant electrode potentials. (B) Amount of H_2O_2 generated during constant potential analysis and normalized for geometric area (C) Concentration of measured H_2O_2 with time (D) Plot of current efficiency for H_2O_2 production at different applied potential.

Under O_2 purge, the controlled potential electrolysis gave pH shifts from pH 7.0 to approximately pH 12. The final pH is expected from the reactions of Equations 1, 2, and 4. A Pourbaix diagram in Figure 4.7 illustrates that this shift in pH does not affect the spontaneity of reactions from electrode potentials from -0.35 V to -1.50 V vs. Ag/AgCl.

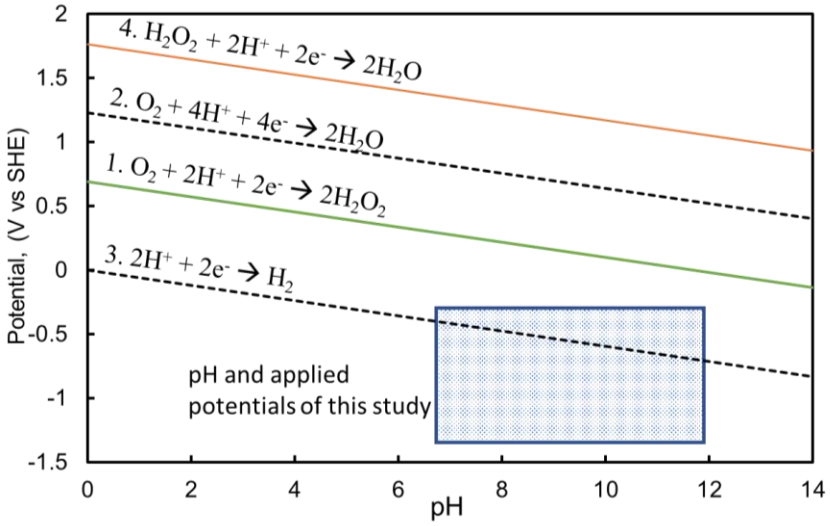

Figure 4.7 Pourbaix diagram for the reactions in Equations 1-4. The shaded region is the pH and potential conditions of this study

The current efficiency ($CE_{H_2O_2/O_2}$) was examined for H_2O_2 production through Equation 1 for each of the three electrode systems of this study. This is described in Equation 6, where n is number of electrons transferred in the balanced half-reaction, F is a Faraday's constant, V is volume of the cell, and i is the current. [34]

$$(6)\quad CE_{H_2O_2/O_2} = \frac{nFV\,[H_2O_2]}{\int_0^t i\,dt} \times 100$$

Figure 4.6 D demonstrates that N-GUITAR/KFD maintains excellent CE $_{H_2O_2/O_2}$ at all potentials. At the highest driving potential of -1.5 V, it has a $CE_{H_2O_2/O_2}$ of 88%, at -1.2 V it is 97% (also see Table 1, Column D). The CE $_{H_2O_2/O_2}$ for both KFD and GUITAR/KFD are notably lower, at 38 % and 29%, respectively at -1.5 V vs. Ag/AgCl. Figure 4.6 D shows that both control electrodes increase H_2O_2 production rates from -0.35 to 0.95 V with noticeable drops

at higher driving potentials. This may be from the consumption of H_2O_2 via Reaction 4. That problem is absent for the N-GUITAR/KFD electrocatalyst as it increases H_2O_2 production with increasing cathodic potential.

In general, N-GUITAR operates at a higher CE relative to literature electrocatalysts. Figure 4.8 illustrates the competitiveness of this electrocatalyst at the various applied potentials relative to literature non-metal electrocatalysts. Also included are the control surfaces of GUITAR and bare KFD at their maximum CE and production rate. This N-doped pseudo-graphite electrode operates at 95 to 100% CE $_{H_2O_2/O_2}$ at potentials of -0.35 to -0.95 V, while literature electrodes are at 45 to 95% at similar potentials. [32,33,35-37] This effect gives N-GUITAR the ability to operate at higher driving potentials without CE penalties effectively. At the highest potential of this study, -1.5 V vs. Ag/AgCl, this electrocatalyst operates at 88 % CE $_{H_2O_2/O_2}$ with a production rate of 250 μmoles/h/cm^2 (8.5 mg hr^{-1}cm^{-2}). This is the highest CE reported for this relatively high rate. A report at a higher rate had a CE $_{H_2O_2/O_2}$ of 40.5 %.[38] Considering these values (CE $_{H_2O_2/O_2}$ and H_2O_2 production rate) N-GUITAR electrode has the best combination of high current efficiency and H_2O_2 production rate. [32,33,35-37]

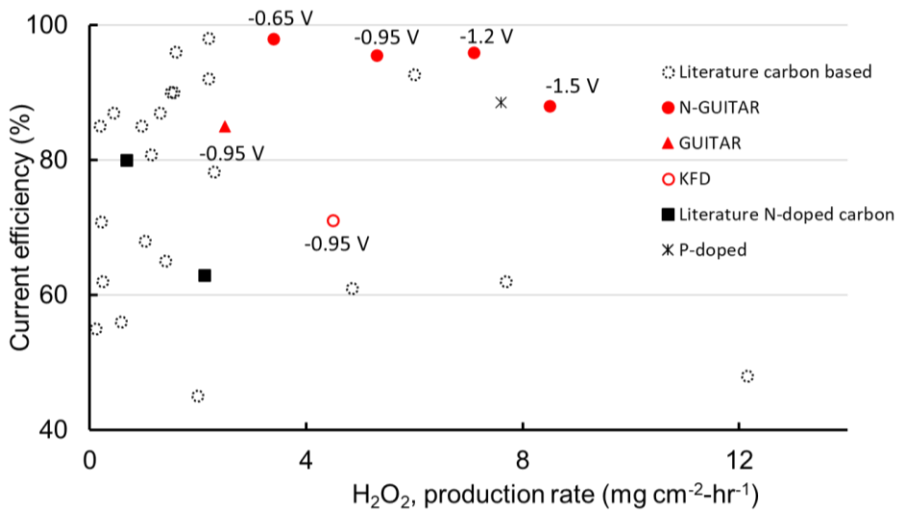

Figure 4.8. A plot of H_2O_2 production rate and current efficiency for the N-GUITAR ORR electrocatalyst. The applied potentials are indicated. The highest rates for H_2O_2 production rate GUITAR and KFD are included along with literature electrocatalysts.[32,35,37-49]

4.4.4 The Hydrogen Evolution Reaction is a Minor Pathway for the Electrocatalyst.

The high CE $_{H_2O_2/O_2}$ indicates that the major pathway for the electrocatalyst is through Reaction 1. The extent of the competing pathways, Reactions 2 through 4, were investigated with chronoamperometric and rotated disk electrode methods. Reaction 3 is the hydrogen evolution reaction (HER). Previous studies of GUITAR and its variants showed that these materials are kinetically slow for HER. Generally, the overpotential is 1 to 1.5 V and is among the highest of all electrode materials.[12-14] The N-GUITAR/KFD cathode was examined for the HER by chronoamperometry in Ar-purged 0.050 M Na_2SO_4 at -0.95, -1.20 and -1.50 V vs. Ag/AgCl. Figure 4.9 shows the respective chronoamperograms for this study. In the absence of O_2 the charge from those currents is proportional to total H_2 production. These charges are summarized in Table 1, Column A. When compared to the charge obtained under saturated O_2 conditions in Figure 5A and summarized in Table 1 Column B, the HER is a minor component of overall cathodic current ranging from 0.2% at -0.95V to 7.8% at -1.5V (Table 1 Column C).

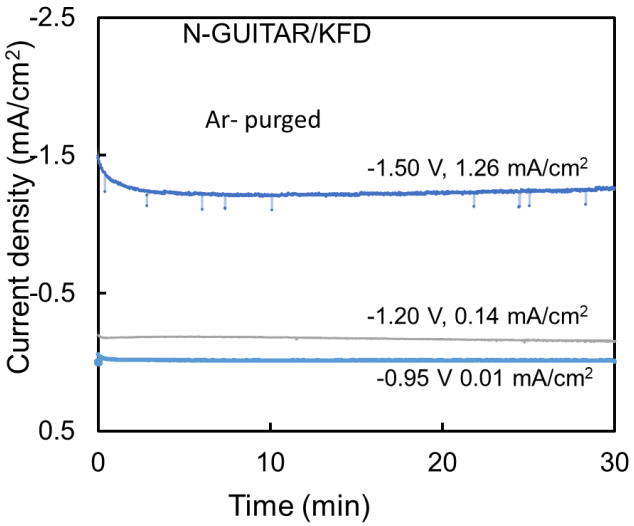

Figure 4.9. Chronoamperograms recorded in Ar purged 0.05M Na_2SO_4. The potentials and steady-state currents for the N-GUITAR/KFD electrodes are described in the diagram.

4.4.5 Assessment of the Contribution of the 4e$^-$ ORR (Reaction 2) Pathway to the Overall Cathodic Current: Rotating Disk Electrode (RDE) Hydrodynamic Studies.

The contribution of Reaction 2 to the overall cathodic current was estimated through the measurement of n, the number of electrons transferred in the half-reaction. As n is 2 for Reaction 1, increases over that quantity indicate possible contributions by Reaction 2 where n = 4. To assess this characteristic, rotating disk electrode (RDE) experiments were conducted for n (Figure 4.10A). The RDE gives n through the Koutecky-Levich (K-L) relationship in Equation 7. The symbols J, $J_{k'}$ and ω are the current density, kinetic current density, and angular velocity, respectively. In the K-L Equation, **B** is $0.62nFv^{1/6}\ C_{O_2}D_{O_2}{}^{2/3}$ where F is Faraday's constant, ν is the kinematic viscosity of the electrolyte (0.01 $cm^2\ s^{-1}$), C_{O_2} is the bulk concentration of oxygen (1.20×10^{-6} mol cm^{-3}), and D_{O_2} is the diffusion coefficient of O_2 in 0.050 M Na_2SO_4 ($1.90 \times 10^{-5}\ cm^2\ s^{-1}$). (15,37)

$$(7)\ \frac{1}{J} = \frac{1}{J_k} + \frac{1}{B\omega^{1/2}}$$

For the RDE study, the graphitic nitrogen-rich N-GUITAR electrocatalysts was deposited on Ketjen black particles as described in the Experimental and in previous studies.[15] In those investigations, pristine GUITAR had n = 2.6 to 2.8. A variant of an N-doped GUITAR (N´-GUITAR) which had a predominance of pyridinic and pyrrolic moieties, was found to have n = 3.6 to 3.7.[15] The background-corrected linear sweep voltammetric (5 mV/s) RDE at rotation rates from 400 to 2400 rpm are shown in Figure 7A. Between the potential range of -0.7 to -1.5V vs. Ag/AgCl, this electrocatalyst was found to have n = 1.99 (see Figure 4.10B). This, along with CE data of Section 3.3, strongly indicate that this electrocatalyst has a strong preference for Reaction 1, with Reaction 2 being a negligible pathway.

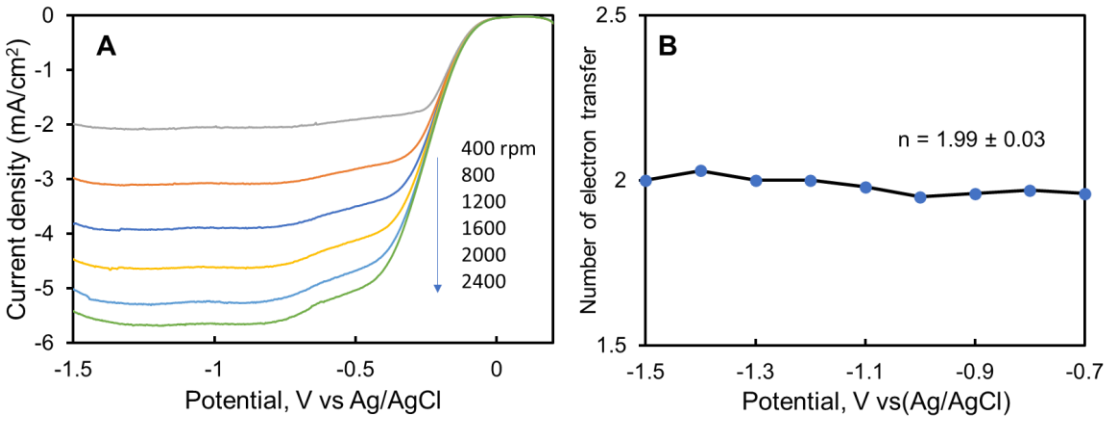

Figure 4.10 (A) Rotating disk electrode (RDE) linear sweep voltammograms recorded at different rotating rates in 0.05 M Na_2SO_4. (B) The number of electrons transferred from the Koutecky-Levich Equation over the potential range of -0.7 to -1.5 V. The average n with one standard deviation is shown.

4.4.6 Other Pathways that Lead to the Loss of H_2O_2.

The pathways that lead to the loss of H_2O_2 are the electrochemical processes of $4e^-$ ORR of Equation 2 discussed above, electroreduction of H_2O_2 giving H_2O (Equation 4), and disproportionation through the reaction in Equation 8. (10)

(8) $2\ H_2O_2 \rightarrow O_2 + 2H_2O$

The three reactions cannot be distinguished from one another and therefore are treated together. The contribution to pathways that lead to the loss of H_2O_2 is outlined in Equations 2, 4, and 8 and can be inferred from the Equation 9 and summarized in Table 1 Column E.

(9) Pathways for H_2O_2 consumption (%) = $100 - CE_{H_2} - CE_{H_2O_2/O_2}$

The 3 values in Column E are not statistically different from each other, it is possible that the disappearance of H_2O_2 is invariant to the applied potentials.

Table 4-1 : Breakdown of major pathways during oxygen electrolysis in 0.050M Na_2SO_4 (aq) for 30 minutes with n = 3. One standard deviation intervals are included.

	A	B	C	D	E
Potential V vs. Ag/AgCl	Charge obtained under Ar purge. (Fig 6)	Charge obtained under O_2 purge (Fig. 5A)	Current Efficiency for H_2 Production Via Equation 3	Current Efficiency for H_2O_2 Production via Equation 6	Pathway for H_2O_2 degradation pathways (Equations 2, 4, and 7)
-0.95 V	0.17 ± 0.04 coulombs	87.4 ± 5.3 coulombs	0.2% ± 0.06%	96 .0% ± 1.0%	3.8% ± 1.0%
-1.20	1.42 ± 0.10	100.0 ± 4.5	1.4 ± 0.2	95.0 ± 2.0	3.6 ± 2.0
-1.50	10.5 ± 0.5	134.0 ± 3.6	7.8 ± 0.5	87.8 ± 1.8	4.4 ± 1.8

4.4.7 The N-GUITAR Electrocatalyst is Stable.

The electrocatalyst stability is demonstrated in the sequence of experiments outlined in Figure 4.11. The electrode was subjected to a constant potential of -1.5 V for five 30-minute cycles under O_2 purge. The H_2O_2 production rate (Figure 4.11A) and current efficiencies (Figure 4.11B) indicate stability.

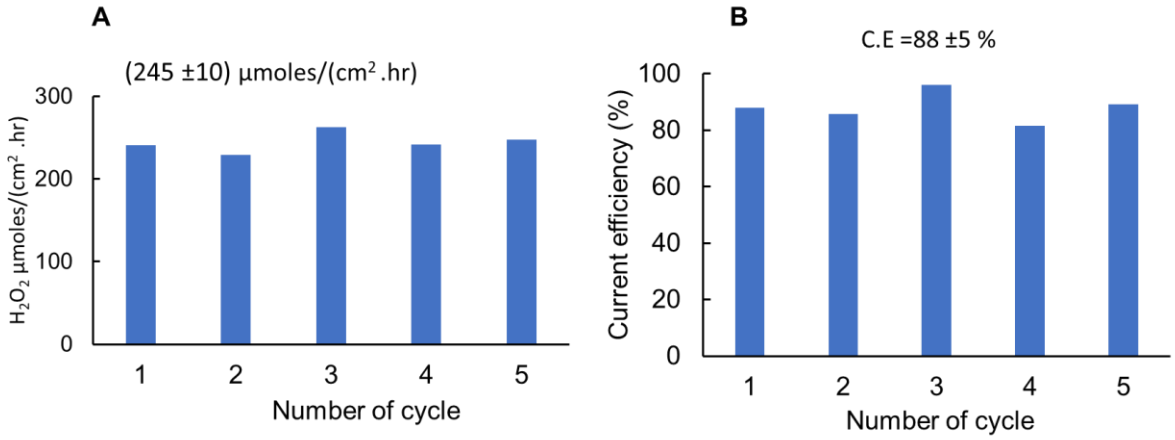

Figure 4.11: Stress tests of the N-GUITAR electrode for H_2O_2 production. Average values and one standard deviation are indicated on each graph. (A) Rates of hydrogen peroxide generation at -1.5 V of applied potential in 0.05 M Na_2SO_4. (B) Current efficiencies as calculated using Equation 6.

4.5 Summary and Conclusion

The ability to selectively dope GUITAR with different nitrogen moieties is unique to this pseudo-graphitic material. Our previous form of nitrogen-doped material, N´-GUITAR, contains 0.9 % nitrogen by the atomic abundance with the division in those species as 0.0 % graphitic-N, 46.0 % pyridinic, 41.6 % pyrrolic, and 12.4 % N-oxide.[15] That electrocatalyst gave an ORR pathway through a $4e^-$ mechanism giving H_2O (Equation 2). In this study, another form of nitrogen-doped pseudo-graphite, N-GUITAR (9.7% N atomic abundance). Those N species have a division of 72.3 % graphitic N, 23.7 % pyridinic, 0.0 % pyrrolic and 4.0 % N-oxide.[13] Based on the rotating disk electrode and chronoamperometric studies, N-GUITAR

shows a strong preference for the $2e^-$ route to H_2O_2 production (Equation 1). This result agrees with the literature indicates the importance of the graphitic N for this pathway. (21,23) While N-GUITAR has a relatively high abundance of pyridinic nitrogen (23.7%), it was observed that this moiety did not significantly contribute to the $4e^-$ pathway. This runs contra to literature hypotheses.[18] However, this result must be viewed in the context that GUITAR is a pseudo-graphite with a plethora of structural defects. The preference for the 2e- ORR pathway, along with significant overpotentials for the HER (Equation 3) and H_2O_2 consumption (Equation 4), gives an electrocatalyst with the highest combination of H_2O_2 production and current efficiency in literature. The H_2O_2 production rate from Figure 5C is 466 mg/L-hour at -1.5 V and 285 mg/L-hour at -0.95 V. This indicates applications in water treatment and wastewater remediation, which require17-68 mg/L H_2O_2 in conjunction with UV light, and 50-250 mg/L H_2O_2 for Fenton Reaction processes.[50,51] It also can be used directly as a disinfectant which requires 10-100 mg/L of H_2O_2.[52] It should be expected that higher production H_2O_2 rates can be obtained with optimized cell and electrode configurations.

4.6 References

(1) Ciriminna, R.; Albanese, L.; Meneguzzo, F.; Pagliaro, M. Hydrogen Peroxide: A Key Chemical for Today's Sustainable Development. *ChemSusChem* **2016**, *9* (24), 3374–3381.

(2) Campos-Martin, J. M.; Blanco-Brieva, G.; Fierro, J. L. G. Hydrogen Peroxide Synthesis: An Outlook beyond the Anthraquinone Process. *Angewandte Chemie International Edition* **2006**, *45* (42), 6962–6984.

(3) Siahrostami, S.; Villegas, S. J.; Bagherzadeh Mostaghimi, A. H.; Back, S.; Farimani, A. B.; Wang, H.; Persson, K. A.; Montoya, J. A Review on Challenges and Successes in Atomic-Scale Design of Catalysts for Electrochemical Synthesis of Hydrogen Peroxide. *ACS Catal.* **2020**, *10* (14), 7495–7511.

(4) Gopal, K.; Tripathy, S. S.; Bersillon, J. L.; Dubey, S. P. Chlorination Byproducts, Their Toxicodynamics and Removal from Drinking Water. *Journal of Hazardous Materials* **2007**, *140* (1), 1–6.

(5) Yang, S.; Verdaguer-Casadevall, A.; Arnarson, L.; Silvioli, L.; Čolić, V.; Frydendal, R.; Rossmeisl, J.; Chorkendorff, I.; Stephens, I. E. L. Toward the Decentralized Electrochemical Production of H2O2: A Focus on the Catalysis. *ACS Catal.* **2018**, *8* (5), 4064–4081.

(6) Jung, E.; Shin, H.; Hooch Antink, W.; Sung, Y.-E.; Hyeon, T. Recent Advances in Electrochemical Oxygen Reduction to H_2O_2: Catalyst and Cell Design. *ACS Energy Lett.* **2020**, *5* (6), 1881–1892.

(7) Gao, J.; Liu, B. Progress of Electrochemical Hydrogen Peroxide Synthesis over Single Atom Catalysts. *ACS Materials Lett.* **2020**, *2* (8), 1008–1024.

(8) Badellino, C.; Rodrigues, C. A.; Bertazzoli, R. Oxidation of Pesticides by in Situ Electrogenerated Hydrogen Peroxide: Study for the Degradation of 2,4-Dichlorophenoxyacetic Acid. *J Hazard Mater* **2006**, *137* (2), 856–864.

(9) Zhou, W.; Meng, X.; Gao, J.; Alshawabkeh, A. N. Hydrogen Peroxide Generation from O2 Electroreduction for Environmental Remediation: A State-of-the-Art Review. *Chemosphere* **2019**, *225*, 588–607.

(10) Xia, G.; Lu, Y.; Xu, H. Electrogeneration of Hydrogen Peroxide for Electro-Fenton via Oxygen Reduction Using Polyacrylonitrile-Based Carbon Fiber Brush Cathode. *Electrochimica Acta* **2015**, *158*, 390–396.

(11) Song, J.; Cho, S. Catalytic Materials for Efficient Electrochemical Production of Hydrogen Peroxide. *APL Materials* **2020**, *8* (5), 050701.

(12) Kabir, H.; Zhu, H.; May, J.; Hamal, K.; Kan, Y.; Williams, T.; Echeverria, E.; McIlroy, D. N.; Estrada, D.; Davis, P. H.; Pandhi, T.; Yocham, K.; Higginbotham, K.; Clearfield, A.; Cheng, I. F. The Sp2-Sp3 Carbon Hybridization Content of Nanocrystalline Graphite from Pyrolyzed Vegetable Oil, Comparison of Electrochemistry and Physical Properties with Other Carbon Forms and Allotropes. *Carbon* **2019**, *144*, 831–840.

(13) Hamal, K.; May, J.; Zhu, H.; Dalbec, F.; Echeverria, E.; McIlroy, D. N.; Aston, E.; Cheng, I. F. Electrochemical Aspects of a Nitrogen-Doped Pseudo-Graphitic Carbon Material: Resistance to Electrode Fouling by Air-Aging and Dopamine Electro-Oxidation. *C* **2020**, *6* (4), 68.

(14) Gyan, I. O.; Wojcik, P. M.; Aston, D. E.; McIlroy, D. N.; Cheng, I. F. A Study of the Electrochemical Properties of a New Graphitic Material: GUITAR. *ChemElectroChem* **2015**, *2* (5), 700–706.

(15) Hamal, K.; May, J.; Koirala, D.; Zhu, H.; Kabir, H.; Echeverria, E.; McIlroy, D. N.; Nicholas, N.; Cheng, I. F. Highly Stable, Low-Cost Metal-Free Oxygen Reduction Reaction Electrocatalyst Based on Nitrogen-Doped Pseudo-Graphite. *Energy & Fuels* **2021**.

(16) Kabir, H.; Gyan, I. O.; Foutch, J. D.; Zhu, H.; Cheng, I. F. Application of GUITAR on the Negative Electrode of the Vanadium Redox Flow Battery: Improved V3+/2+ Heterogeneous Electron Transfer with Reduced Hydrogen Gassing. *C* **2016**, *2* (2), 13.

(17) Guo, D.; Shibuya, R.; Akiba, C.; Saji, S.; Kondo, T.; Nakamura, J. Active Sites of Nitrogen-Doped Carbon Materials for Oxygen Reduction Reaction Clarified Using Model Catalysts. *Science* **2016**, *351* (6271), 361–365.

(18) Gong, K.; Du, F.; Xia, Z.; Durstock, M.; Dai, L. Nitrogen-Doped Carbon Nanotube Arrays with High Electrocatalytic Activity for Oxygen Reduction. *Science* **2009**, *323* (5915), 760–764.

(19) Ma, R.; Lin, G.; Zhou, Y.; Liu, Q.; Zhang, T.; Shan, G.; Yang, M.; Wang, J. A Review of Oxygen Reduction Mechanisms for Metal-Free Carbon-Based Electrocatalysts. *npj Comput Mater* **2019**, *5* (1), 1–15.

(20) Subramanian, N. P.; Li, X.; Nallathambi, V.; Kumaraguru, S. P.; Colon-Mercado, H.; Wu, G.; Lee, J.-W.; Popov, B. N. Nitrogen-Modified Carbon-Based Catalysts for Oxygen Reduction Reaction in Polymer Electrolyte Membrane Fuel Cells. *Journal of Power Sources* **2009**, *188* (1), 38–44.

(21) Zhang, J.; Zhang, G.; Jin, S.; Zhou, Y.; Ji, Q.; Lan, H.; Liu, H.; Qu, J. Graphitic N in Nitrogen-Doped Carbon Promotes Hydrogen Peroxide Synthesis from Electrocatalytic Oxygen Reduction. *Carbon* **2020**, *163*, 154–161.

(22) Lai, L.; Potts, J. R.; Zhan, D.; Wang, L.; Poh, C. K.; Tang, C.; Gong, H.; Shen, Z.; Lin, J.; Ruoff, R. S. Exploration of the Active Center Structure of Nitrogen-Doped Graphene-Based Catalysts for Oxygen Reduction Reaction. *Energy Environ. Sci.* **2012**, *5* (7), 7936–7942.

(23) Contreras, E.; Dominguez, D.; Tiznado, H.; Guerrero-Sanchez, J.; Takeuchi, N.; Alonso-Nunez, G.; Contreras, O. E.; Oropeza-Guzmán, M. T.; Romo-Herrera, J. M. N-Doped Carbon Nanotubes Enriched with Graphitic Nitrogen in a Buckypaper Configuration as Efficient 3D Electrodes for Oxygen Reduction to H2O2. *Nanoscale* **2019**, *11* (6), 2829–2839.

(24) Smith, R. E. G.; Davies, T. J.; Baynes, N. de B.; Nichols, R. J. The Electrochemical Characterisation of Graphite Felts. *Journal of Electroanalytical Chemistry* **2015**, *747*, 29–38.

(25) Koirala, D.; Yensen, N.; Allen, P. B. Open Source All-Iron Battery 2.0. *HardwareX* **2021**, *9*, e00171.

(26) Sellers, R. M. Spectrophotometric Determination of Hydrogen Peroxide Using Potassium Titanium(IV) Oxalate. *Analyst* **1980**, *105* (1255), 950.

(27) Huang, X. Fabrication and Properties of Carbon Fibers. *Materials* **2009**, *2* (4), 2369–2403.

(**28)** Panomsuwan, G.; Saito, N.; Ishizaki, T. Nitrogen-Doped Carbon Nanoparticle–Carbon Nanofiber Composite as an Efficient Metal-Free Cathode Catalyst for Oxygen Reduction Reaction. *ACS Appl. Mater. Interfaces* **2016**, *8* (11), 6962–6971.

(29) Chen, T.; Cai, Z.; Yang, Z.; Li, L.; Sun, X.; Huang, T.; Yu, A.; Kia, H. G.; Peng, H. Nitrogen-Doped Carbon Nanotube Composite Fiber with a Core–Sheath Structure for Novel Electrodes. *Advanced Materials* **2011**, *23* (40), 4620–4625.

(30) Sheng, Z.-H.; Shao, L.; Chen, J.-J.; Bao, W.-J.; Wang, F.-B.; Xia, X.-H. Catalyst-Free Synthesis of Nitrogen-Doped Graphene via Thermal Annealing Graphite Oxide with Melamine and Its Excellent Electrocatalysis. *ACS Nano* **2011**, *5* (6), 4350–4358.

(31) Chen, Z.; Chen, S.; Siahrostami, S.; Chakthranont, P.; Hahn, C.; Nordlund, D.; Dimosthenis, S.; Nørskov, J. K.; Bao, Z.; Jaramillo, T. F. Development of a Reactor with Carbon Catalysts for Modular-Scale, Low-Cost Electrochemical Generation of H2O2. *React. Chem. Eng.* **2017**, *2* (2), 239–245.

(32) Liu, Y.; Quan, X.; Fan, X.; Wang, H.; Chen, S. High-Yield Electrosynthesis of Hydrogen Peroxide from Oxygen Reduction by Hierarchically Porous Carbon. *Angewandte Chemie* **2015**, *127* (23), 6941–6945.

(33) Yang, W.; Zhou, M.; Cai, J.; Liang, L.; Ren, G.; Jiang, L. Ultrahigh Yield of Hydrogen Peroxide on Graphite Felt Cathode Modified with Electrochemically Exfoliated Graphene. *J. Mater. Chem. A* **2017**, *5* (17), 8070–8080.

(34) Bonakdarpour, A.; Esau, D.; Cheng, H.; Wang, A.; Gyenge, E.; Wilkinson, D. P. Preparation and Electrochemical Studies of Metal–Carbon Composite Catalysts for Small-Scale Electrosynthesis of H2O2. *Electrochimica Acta* **2011**, *56* (25), 9074–9081.

(35) Zhou, L.; Zhou, M.; Zhang, C.; Jiang, Y.; Bi, Z.; Yang, J. Electro-Fenton Degradation of p-Nitrophenol Using the Anodized Graphite Felts. *Chemical Engineering Journal* **2013**, *233*, 185–192.

(36) Zhou, L.; Zhou, M.; Hu, Z.; Bi, Z.; Serrano, K. Chemically Modified Graphite Felt as an Efficient Cathode in Electro-Fenton for p-Nitrophenol Degradation. *Electrochimica Acta* **2014**, *140*, 376–383.

(37) Xia, Y.; Shang, H.; Zhang, Q.; Zhou, Y.; Hu, X. Electrogeneration of Hydrogen Peroxide Using Phosphorus-Doped Carbon Nanotubes Gas Diffusion Electrodes and Its Application in Electro-Fenton. **2019**.

(38) Yu, X.; Zhou, M.; Ren, G.; Ma, L. A Novel Dual Gas Diffusion Electrodes System for Efficient Hydrogen Peroxide Generation Used in Electro-Fenton. *Chemical Engineering Journal* **2015**, *263*, 92–100.

(39) Sheng, Y.; Song, S.; Wang, X.; Song, L.; Wang, C.; Sun, H.; Niu, X. Electrogeneration of Hydrogen Peroxide on a Novel Highly Effective Acetylene Black-PTFE Cathode with PTFE Film. Electrochimica Acta **2011**, 56 (24), 8651–8656.

(40) Yang, W.; Zhou, M.; Cai, J.; Liang, L.; Ren, G.; Jiang, L. Ultrahigh Yield of Hydrogen Peroxide on Graphite Felt Cathode Modified with Electrochemically Exfoliated Graphene. J. Mater. Chem. A **2017**, 5 (17), 8070–8080.

(41) Pozzo, A. D.; Palma, L. D.; Merli, C.; Petrucci, E. An Experimental Comparison of a Graphite Electrode and a Gas Diffusion Electrode for the Cathodic Production of Hydrogen Peroxide. J Appl Electrochem **2005**, 35 (4), 413–419

(42) Yu, F.; Zhou, M.; Yu, X. Cost-Effective Electro-Fenton Using Modified Graphite Felt That Dramatically Enhanced on H2O2 Electro-Generation without External Aeration. Electrochimica Acta **2015**, 163, 182–189.

(43) Xu, X.; Chen, J.; Zhang, G.; Song, Y.; Yang, F. Homogeneous Electro-Fenton Oxidative Degradation of Reactive Brilliant Blue Using a Graphene Doped Gas-Diffusion Cathode. Int. J. Electrochem. Sci. **2014**, 9, 569 – 579.

(44) Zhou, W.; Ding, Y.; Gao, J.; Kou, K.; Wang, Y.; Meng, X.; Wu, S.; Qin, Y. Green Electrochemical Modification of RVC Foam Electrode and Improved H2O2 Electrogeneration by Applying Pulsed Current for Pollutant Removal. Environ Sci Pollut Res **2018**, 25 (6), 6015–6025.

(45) Zhou, W.; Rajic, L.; Zhao, Y.; Gao, J.; Qin, Y.; Alshawabkeh, A. N. Rates of H2O2 Electrogeneration by Reduction of Anodic O2 at RVC Foam Cathodes in Batch and Flow-through Cells. Electrochimica Acta **2018**, 277, 185–196.

(46) Zarei, M.; Salari, D.; Niaei, A.; Khataee, A. Peroxi-Coagulation Degradation of C.I. Basic Yellow 2 Based on Carbon-PTFE and Carbon Nanotube-PTFE Electrodes as Cathode. Electrochimica Acta **2009**, 54 (26), 6651–6660.

(47) Choi, J.; Hwang, S. H.; Jang, J.; Yoon, J. High Yield Hydrogen Peroxide Production in a Solid Polymer Electrolyte Electrolyzer with a Carbon Fiber Coated Mesh Substrate. Electrochemistry Communications **2013**, 30, 95–98.

(48) Zhou, L.; Zhou, M.; Hu, Z.; Bi, Z.; Serrano, K. Chemically Modified Graphite Felt as an Efficient Cathode in Electro-Fenton for p-Nitrophenol Degradation. Electrochimica Acta **2014**, 140, 376–383.

(49) Zhou, L.; Hu, Z.; Zhang, C.; Bi, Z.; Jin, T.; Zhou, M. Electrogeneration of Hydrogen Peroxide for Electro-Fenton System by Oxygen Reduction Using Chemically Modified Graphite Felt Cathode. Separation and Purification Technology **2013**, Complete (111), 131–136.

(50) J. C. Crittenden, R. R. Trussell, D. W. Hand, K. J. Howe, and G. Tchobanoglous, 'Hydrogen Peroxide/ UV Light Process', in MWH's Water Treatment: Principles and Design, 3rd ed., Hoboken, NJ: John Wiley and Sons, **2012**, pp. 1455–1472.

(51) G. R. Agladze, G. S. Tsurtsumia, B.-I. Jung, J.-S. Kim, and G. Gorelishvili, 'Comparative study of chemical and electrochemical Fenton treatment of organic pollutants in wastewater', J. Appl. Electrochem, **2007**, 37, 985–990.

(52) J. B. A. Arends, S. Van Denhouwe, W. Verstraete, N. Boon, and K. Rabaey, 'Enhanced disinfection of wastewater by combining wetland treatment with bioelectrochemical H2O2 production', Bioresour. Technol, **2014**, 155, 352–358.

Chapter 5: Conclusion and Future Prospective

In this dissertation work, a low-cost metal-free pseudo graphite (GUITAR) based electrocatalyst was synthesized and characterized for selective oxygen reduction reaction (ORR). A highly defective GUITAR surface was used as a base material to tune its properties by nitrogen doping. This material benefits from the low cost of synthesis, fast HET rate, higher corrosion resistance, and the ability to coat on different templates. Two different selective nitrogen doping techniques were explored for their applications in the ORR. Emphasis was placed on selective nitrogen doping and their preferences towards 4 electrons or 2 electron ORR pathways, improved stability, performance, and scalability.

Selectively doped GUITAR with predominantly pyridinic and pyrrolic moieties (0.0 % graphitic-N moieties) preferred ORR through 4 electron pathways: This form of nitrogen-doped GUITAR (N´-GUITAR) was synthesized using melamine as the nitrogen precursor. This N´-GUITAR contains 46.0 %- pyridinic, 41.6 %- pyrrolic nitrogen, 12.4 % N-oxide and with a notable absence of graphitic nitrogen (0.0 %). The total abundance of nitrogen in N´-GUITAR was 0.9 atomic %. This electrocatalyst proved to be durable and efficient (up to 85%) for the $4e^-$ ORR to H_2O. The electrochemical characterization was carried out based on the Department of Energy (DOE) stress test protocol. Based on the exceptional stability and low cost of synthesis, N´-GUITAR stands as a practical candidate for widespread use in fuel cell technology.

Selectively doped GUITAR with predominantly graphitic-N (72.3%) moieties preferred ORR through 2 electron pathways: A second attempt to increase N content on GUITAR surface

resulted in selectively doped graphitic N moieties (72.6 %) with 23.7 % pyridinic, 4.0% N-oxide, and 0.0% pyrrolic nitrogen (as shown in Figure 5.1). This form of nitrogen-doped GUITAR, named N-GUITAR, was synthesized using acetonitrile as a precursor and contained a 9.7 atomic % nitrogen. N-GUITAR showed a strong preference for the $2e^-$ route to H_2O_2 with a current efficiency of up to 95%. Higher selectively for the $2e^-$ ORR pathway and significant overpotentials for the hydrogen evolution (HER) give this electrocatalyst the highest combination of H_2O_2 production and current efficiency in literature.

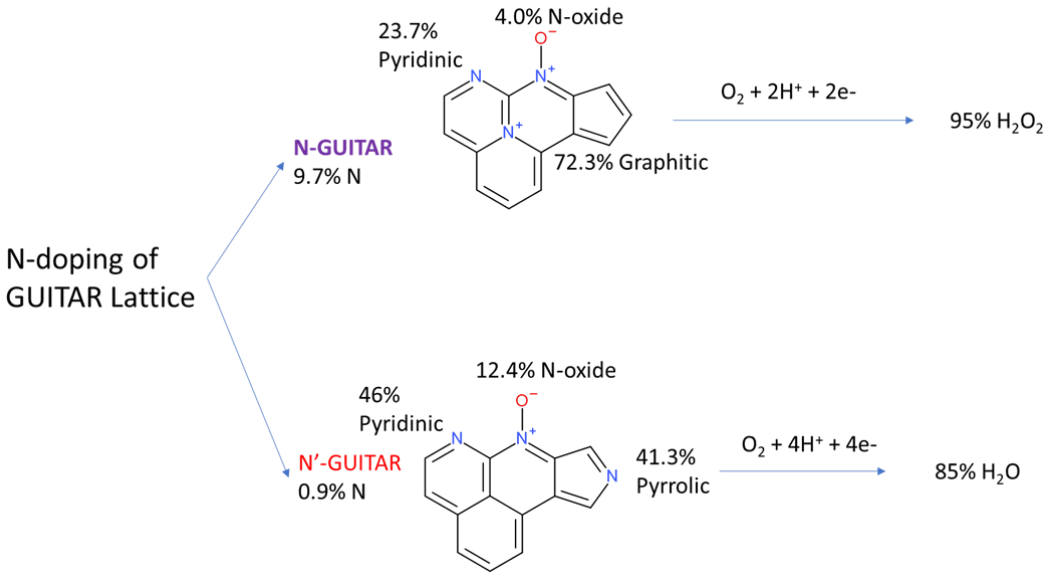

Figure 5.1 Nitrogen moieties on GUITAR surface and their preferences towards ORR.

The ability to selectively dope different nitrogen moieties is unique to this pseudo-graphitic material, GUITAR. It is expected that two different forms of a selectively nitrogen-doped GUITAR will help elucidate the roles of the different N-species for ORR. This experimental

study suggests that pyridinic and pyrrolic groups are responsible for ORR through the $4e^-$ pathway while graphitic N is responsible for ORR through the $2e^-$ pathways. Future work will focus on computational modeling for guidance on the optimal dopant concentration and ratios of the pyrrolic, pyridinic, and graphitic moieties to reduce the ORR overpotential for both 2 and 4 electron ORR pathways while maintaining reaction specificity.

N-GUITAR as a robust electrochemical sensor: Apart from ORR, N-GUITAR was also tested for electrochemical sensor applications. Nitrogen-modified GUITAR electrode was tested for electrode passivation by volatile organic compounds (VOCs) and detection of dopamine via electro-oxidation. Cyclic voltametric studies along with the water contact angle measurement showed that N-GUITAR exhibits significant resistance to fouling by VOCs adsorption. Electrode passivation by adsorbed VOCs is common in literature for other graphitic carbon materials, which decreases the heterogeneous electron transfer rate. GUITAR and N-GUITAR electrodes showed less prone to this effect, which might be due to the nanocrystalline and highly defective nature of GUITAR (with a high density of electronic state). It is also expected that polarized C-N bond on N-GUITAR hinders VOC adsorption. N-GUITAR electrode also shows better kinetics for dopamine electro-oxidation and resistance towards electrode fouling by dopamine polymerization. With the combination of these results and the easy synthesis process, N-GUITAR has much promise for implantable dopamine sensor for longer-term applications. Ongoing investigation with this material also showed encouraging results towards electrochemical detection of uric acid and electrochemical nitrogen reduction reaction.